NOTICE

The quality of this microform is heavily dependent upon the quality of the original thesis submitted for microfilming. Every effort has been made to ensure the highest quality of reproduction possible.

If pages are missing, contact the university which granted the degree.

Some pages may have indistinct print especially if the original pages were typed with a poor typewriter ribbon or if the university sent us an inferior photocopy.

Previously copyrighted materials (journal articles, published tests, etc.) are not filmed.

Reproduction in full or in part of this microform is governed by the Canadian Copyright Act, R.S.C. 1970, c. C-30.

AVIS

La qualité de cette microforme dépend grandement de la qualité de la thèse soumise au microfilmage. Nous avons tout fait pour assurer une qualité supérieure de reproduction.

S'il manque des pages, veuillez communiquer avec l'université qui a conféré le grade.

La qualité d'impression de certaines pages peut laisser à désirer, surtout si les pages originales ont été dactylographiées à l'aide d'un ruban usé ou si l'université nous a fait parvenir une photocopie de qualité inférieure.

Les documents qui font déjà l'objet d'un droit d'auteur (articles de revue, tests publiés, etc.) ne sont pas microfilmés.

La reproduction, même partielle, de cette microforme est soumise à la Loi canadienne sur le droit d'auteur, SRC 1970, c. C-30.

THE UNIVERSITY OF ALBERTA

SOIL-GEOGRID INTERFACIAL SHEAR STRENGTH

by

© LINDA WAI MAN BOBEY

A THESIS

SUBMITTED TO THE FACULTY OF GRADUATE STUDIES AND RESEARCH

IN PARTIAL FULFILMENT OF THE REQUIREMENTS FOR THE DEGREE

OF MASTER OF SCIENCE

DEPARTMENT OF CIVIL ENGINEERING

EDMONTON, ALBERTA

SPRING 1988

ISBN 0-315-42719-1

THE UNIVERSITY OF ALBERTA

RELEASE FORM

NAME OF AUTHOR LINDA WAI MAN BOBEY

TITLE OF THESIS SOIL-GEOGRID INTERFACIAL SHEAR STRENGTH

DEGREE FOR WHICH THESIS WAS PRESENTED MASTER OF SCIENCE

YEAR THIS DEGREE GRANTED SPRING 1988

Permission is hereby granted to THE UNIVERSITY OF ALBERTA LIBRARY to reproduce single copies of this thesis and to lend or sell such copies for private, scholarly or scientific research purposes only.

The author reserves other publication rights, and neither the thesis nor extensive extracts from it may be printed or otherwise reproduced without the author's written permission.

(SIGNED) Linda Bobey

PERMANENT ADDRESS:

6004 - 186 STREET

EDMONTON, ALBERTA

CANADA

DATED December 2, 1987

THE UNIVERSITY OF ALBERTA

FACULTY OF GRADUATE STUDIES AND RESEARCH

The undersigned certify that they have read, and recommend to the Faculty of Graduate Studies and Research, for acceptance, a thesis entitled SOIL-GEOGRID INTERFACIAL SHEAR STRENGTH submitted by LINDA WAI MAN BOBEY in partial fulfilment of the requirements for the degree of MASTER OF SCIENCE.

.....
Co-Supervisor

.....
Co-Supervisor

.....

.....

.....

Date October 29, 1987

ABSTRACT

High strength geotextiles and geogrids have been developed and used as reinforcement in soil-reinforcement applications. Few studies have been made on the interface strength properties of cohesive soils with geotextiles or geogrids. At the present time no standard test apparatus or procedure exists to measure the interfacial strength parameters for the design of geogrid reinforced slopes.

The main objective of this research program is to determine the influence of the construction and geometry of four geogrids and a geotextile on the interfacial shear strength of a granular and a cohesive soil. In addition, a modification to the standard direct shear testing apparatus is presented and a testing procedure for measuring the interfacial shear strength is developed.

The test results show that the interfacial shear strength of reinforced soil is less than the shear strength of the unreinforced soil. The percent of open area and the aperture dimensions of geogrids are found to have an influence on the interfacial friction of reinforced sand. Geogrids with large apertures permit a greater degree of soil to soil interaction and exhibit higher interfacial friction than woven geotextiles. It is found that geogrids do not represent significant planes of weakness within a compacted granular fill. Geotextiles may represent a more potential sliding plane within a granular embankment than geogrids. For cohesive soil, geogrids with a high percent of

open area and geotextiles with a rough surface texture can generate shearing strength approaching that of the unreinforced clay.

ACKNOWLEDGEMENTS

This research was performed under the guidance of Dr. J. D. Scott and Professor E.A. Richards. The advice and assistance provided by Dr. Scott and Professor Richards are greatly appreciated.

I would like to thank Steve Gamble, Christine Hurley, Jay Khajuria, and Jan Radziszewski for their technical assistance during the experimental study.

Appreciation is expressed to the Alberta Transportation and Utilities Research and Development Department and the Department of Civil Engineering for providing financial support for this study.

The geogrids supplied by Mirafi Inc., Signode Corp., and Tensar Corp. and the geotextile from Nilex Inc. are appreciated.

Finally I would like to thank my grandmother, my parent, and my husband for their love, support, and encouragement.

Table of Contents

List of Tables

List of Figures

List of Plates

List of Symbols

In the following list of symbols, a prime on an angle or stress represents effective stress:

a', a_T	Intercept of the line joining the failure stresses on the p-q diagram
c'	Effective cohesion intercept
c_G	Interfacial adhesion intercept of the solid reinforcement
c_T, c_u	Apparent or undrained cohesion intercept
c_{TP}	Total interfacial cohesion intercept
C_v	Coefficient of consolidation
$(dv/dh)_p$	Dilation rate corresponding to the peak shear stress
D_{50}	Grain diameter for 50% finer by weight
E	Efficiency
E_ϕ	Efficiency of friction angle
E_c	Efficiency of cohesion or adhesion
G	Specific gravity
S_r	Degree of saturation
a	Ratio of solid area of the reinforcement to the

total area of the reinforcement

δ_G Angle of interfacial friction of the solid reinforcement

δ'_{GP} Peak total angle of interfacial friction of the solid reinforcement

δ'_{GR} Residual total angle of interfacial friction of the solid reinforcement

δ'_T, δ_T Total angle of interfacial fricton between the reinforcement and the sand

$\delta'_{TP}, \delta_{TP}$ Peak total angle of interfacial friction

δ'_{TR} Residual total angle of interfacial friction

σ'_n, σ_n Normal stress

θ Angle between the plane of the reinforcement and the horizontal shear surface

τ_P Peak shear strength

τ_{TP} Total interfacial shear strength

ϕ, ϕ' Effective angle of internal friction

ϕ'_P Peak angle of internal friction

ϕ'_R, ϕ'_{CV} Friction angle measured at constant volume condition

ϕ_u Apparent or undrained angle of friction

ψ', ψ_T Slope of the line joining the failure stresses on the p-q diagram

1. INTRODUCTION

1.1 Statement of Problem

In the early 1970's high tensile strength geotextiles were developed and used as reinforcement in the design of slopes, embankments, and retaining structures. The role of geotextiles is to improve the stability of these structures against shear failure. The potential for the shear failure of a slope can be analyzed by the limit equilibrium method. A circular arc failure surface is assumed to pass through an embankment and tangent to the surface of the competent foundation (Figure 1.1). The soil mass is divided into a series of vertical slices and the equilibrium of each of these slices is considered. As shown in Figure 1.1 the resisting forces and the driving forces of each slice are summed at the bottom of the slice. The factor of safety against shear failure is the ratio of the resisting moment to the driving moment. Similar stability analysis can be performed on a slope reinforced with geotextiles. Figure 1.2 shows that the driving force of the reinforced slope is the same as that of the unreinforced slope, but the resisting forces against shear failure of the reinforced slope are increased by the tensile force in the geotextile. Therefore, the inclusion of high strength geotextiles increases the stability of the slopes by increasing the resisting moment against shear failure. A higher factor of safety results.

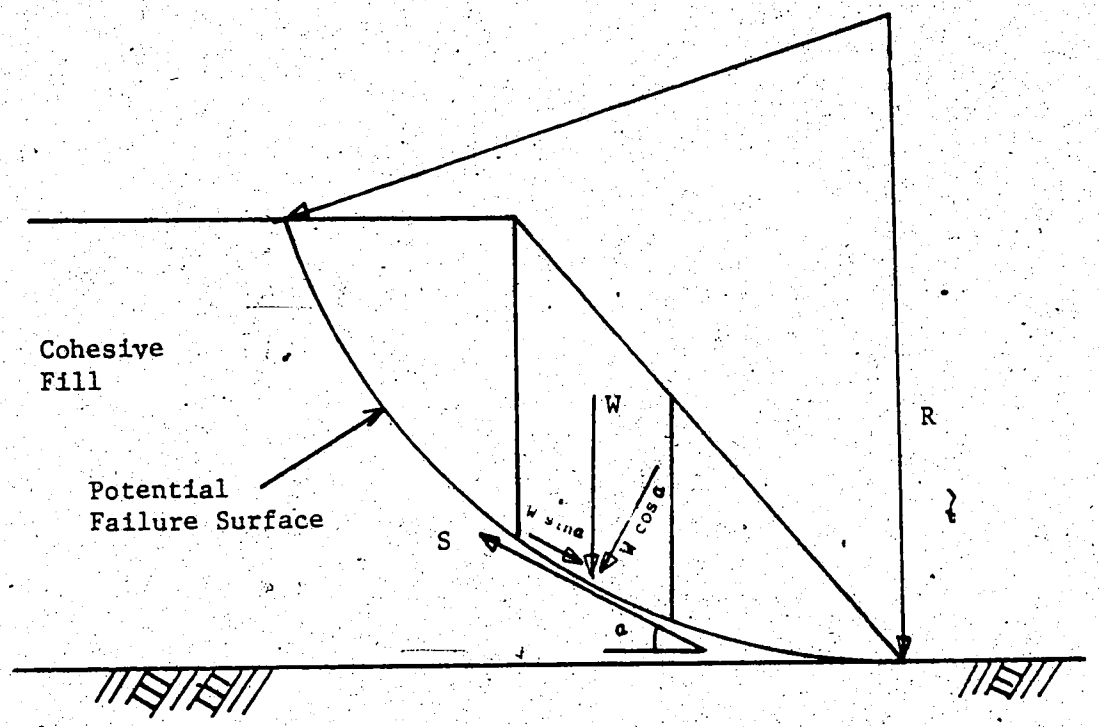

Competent Foundation

$$\text{Factor of Safety (FS)} = \frac{\text{Resisting Moment } (M_R)}{\text{Driving Moment } (M_D)}$$

$$FS = \frac{R\,S}{R\,W\,\sin\alpha}$$

$$FS = \frac{R\,(c\,l + W\cos\alpha\tan\phi)}{W\sin\alpha}$$

c = cohesion of soil
l = Arc length of slice.
N = Total normal stress across the base of slice.
R = Radius of the failure circle.
S = Shear force on the base of slice.
W = Total weight of slice.
ϕ = Internal friction angle of soil.
α = Angle of intersection of horizontal to tangent at center of slice.

Figure 1.1 Slope Stability Analysis of an Unreinforced Embankment

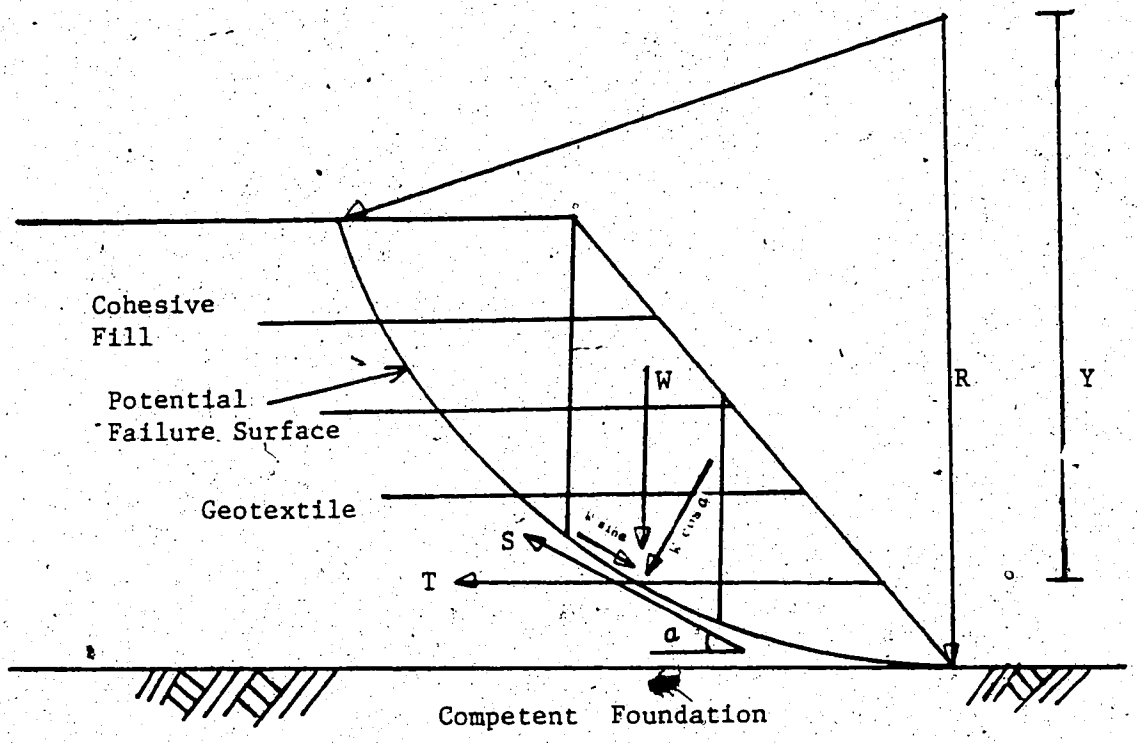

$$\text{Factor of Safety (FS)} = \frac{\text{Resisting Moment } (M_R)}{\text{Driving Moment } (M_D)}$$

$$FS = \frac{R\ S}{R\ W \sin\alpha}$$

$$FS = \frac{R\ (cl + (W \cos\alpha \tan\phi)) + Ty}{W \sin\alpha}$$

c = cohesion of soil
l = Arc length of slice.
N = Total normal stress across the base of slice.
R = Radius of the failure circle.
S = Shear force on the base of slice.
T = Geotextile tensile strength.
W = Total weight of slice.
y = Moment arm for geotextile.
ϕ = Internal friction angle of soil.
α = Angle of intersection of horizontal to tangent at center of slice.

Figure 1.2 Slope Stability Analysis of an Unreinforced Embankment

The other possible modes of failure of the reinforced slope are: sliding failure of the soil mass along a geotextile surface and pullout failure of a geotextile. The resistance to a sliding failure and to a pullout failure is a function of the soil and geotextile interfacial friction. Design consideration of either failure mechanism requires a knowledge of the soil and geotextile interfacial shear strength. The magnitude of the interfacial strength is primarily a function of the physical properties of the soil, the normal stress acting on the reinforcement, and the construction or the geometry of the reinforcement. This interfacial shear strength can be determined experimentally in the direct shear test.

Recently, a new type of high strength polymer reinforcement called geogrid has emerged. Geogrids are used frequently in a variety of soil reinforcement applications. The mechanism of interaction between a soil and a geogrid is similar to that of a soil and a geotextile with the addition of interlocking of coarse grained particles within the geogrid apertures.

Numerous studies have been made on the interface strength properties of non-cohesive soils and geotextiles. There has been little research studying the interface interaction between soil and geogrids. The design engineer lacks information for selecting the appropriate geogrid for a particular soil-reinforcement application. At the present time no standard test apparatus or procedure exists to

measure the appropriate material parameters for the design of geogrid reinforced slopes.

1.2 Objectives of Thesis

The main objective of this research is to determine the influence of the construction and geometry of four geogrids and a geotextile on the interfacial shear strength of a granular and a cohesive soil. In addition, a modification to the standard direct shear testing apparatus is presented and a testing procedure for measuring the interfacial shear strength is developed.

1.3 Scope of Thesis

This research program is funded by Alberta Transportation and forms part of a comprehensive study of geogrid reinforced slopes. A 12 m high testfill is presently under construction in Devon, Alberta. Cohesive fill material from a nearby borrow is used for the embankment and will be used in this research. Three different types of high strength geogrids are used as primarily reinforcement for this embankment. Hence, the interactions between the Devon soil and the three geogrids are of interest and will be studied in this testing program. A fourth geogrid and a geotextile also will be tested to form a comparative study. A uniformly graded sand supplied by the laboratory of Alberta Transportation will be tested as a typical granular soil for embankment construction.

To assess the influence of the properties of the reinforcement on the interfacial interaction, the laboratory study will be conducted in two parts. In the first part, the soil properties which appear necessary for the design of soil-reinforcement will be determined. The stress, strain, and shear strength of the soil will be measured in a standard triaxial or a direct shear apparatus. In the second part, the soil and reinforcement interfacial stress and deformation properties will be measured. These interface properties will be measured in the modified wide width direct shear apparatus to model the plane strain conditions which exist in the field. The results will be analyzed in terms of total and effective stress conditions. The properties of the reinforcement which may influence the interface interaction will be examined, and factors that may affect the interacial strength will be discussed.

1.4 Organization of Thesis

Published information concerning direct shear box test methods, advantages and disadvantages of the direct shear test, test assumptions, and compaction methods are reviewed in Chapter 2. The mechanisms of soil and reinforcement interaction and published studies on soil-geosynthetic interfacial shear strength are also presented.

Chapter 3 contains index properties and strength properties of a cohesive and a non-cohesive soil. The construction and the geometry of four geogrids and one

goetextile are also given. A description of the laboratory apparatus and test procedure employed in the experimental program are presented in Chapter 4.

The experimental results and discussion of the reinforced sand are presented in Chapter 5. The analysis and discussion of the reinforced clay test results are included in Chapter 6. The conclusions drawn from this research are summarized in Chapter 7 and recommendations for future research are presented.

2. LITERATURE REVIEW

2.1 Introduction

This chapter will present a summary of the published literature on the various types of direct shear box test methods and the limitations and advantages of the shear test. Test assumptions and in-place compaction methods are described. The mechanisms of soil-reinforcement interaction based on interface friction and cohesion or adhesion are presented. Factors that affect the interface friction between soil and reinforcement are discussed. Direct shear test results that have been published on both granular and cohesive soils reinforced with geotextiles, geogrids, and geomembranes are summarized.

2.2 Direct Shear Box Tests

The friction or adhesion between soil and reinforcement is commonly evaluated in a direct shear box. Richards and Scott (1985) discussed the five modified direct shear box test methods that are used by many researchers. These five methods are the fixed, partially fixed, completely free, the Myles' large base, and the central base shear mode (Figure 2.1). The advantages and disadvantages of each test method are also summarized in their paper.

In addition to the five modified shear box test methods, Snaith, Bell, and Dubois (1979) developed the octagonal shear box test to study the behavior of an

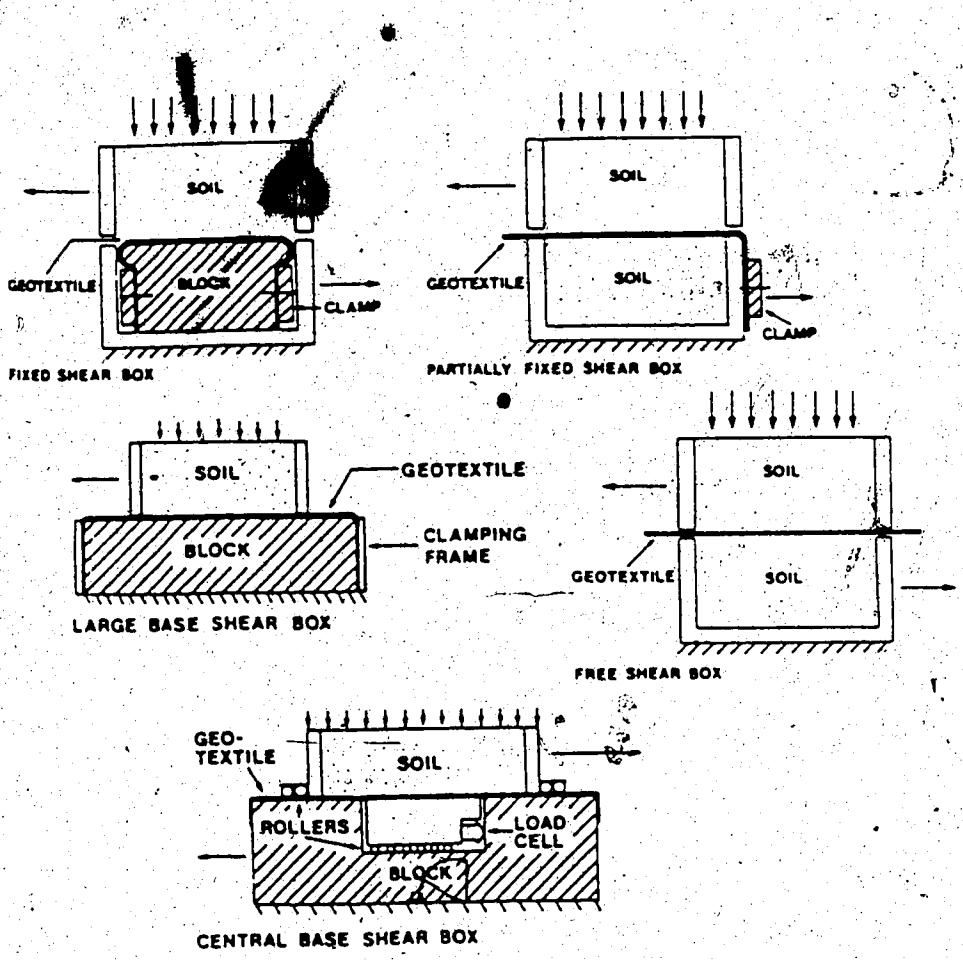

Figure 2.1 Direct Shear Box Test Methods
(Modified from Richards and Scott, 1985)

embedded geotextile in a cohesive soil (Figure 2.2). The plane of the geotextile can be inclined from $\theta = 0°$ to $\theta = 180°$. At $\theta = 0°$ and 180°, the plane of the geotextile coincides with the intended shear plane; the test simply becomes a free direct shear test. Ingold (1980, 1981, 1983) and Jewell (1980, 1980) also performed a series of free shear box tests on reinforcements that were inclined at various angles from the intended shear plane.

Wernick (1977) developed a "True Direct Shear Apparatus" to measure the shear resistance between soil and an anchor. This apparatus consisted of a conventional shear box and a modified loading platen. The loading cap, supported by the roller bearings (Figure 2.3), is not permitted to tilt during the test, but can move in the vertical direction. Hausmann and Ring (1980) commented on the possible use of the "True Direct Shear Apparatus" to measure the dilatancy characteristics of granular soil. Thus, it is possible to further modify this apparatus to determine the influence of geotextiles on the dilation behaviour of sand.

The various sizes of direct shear boxes which have been used range from 6 x 6 cm² to 60 x 60 cm². Ingold (1982, 1984) conducted a series of direct shear tests to study the effect of shear box sizes and two test methodologies. He used 6 x 6 cm^2 and 30 x 30 cm^2 boxes, and tested reinforced sand in the fixed and partially fixed shear modes. He found the shear box results were in good agreement with one

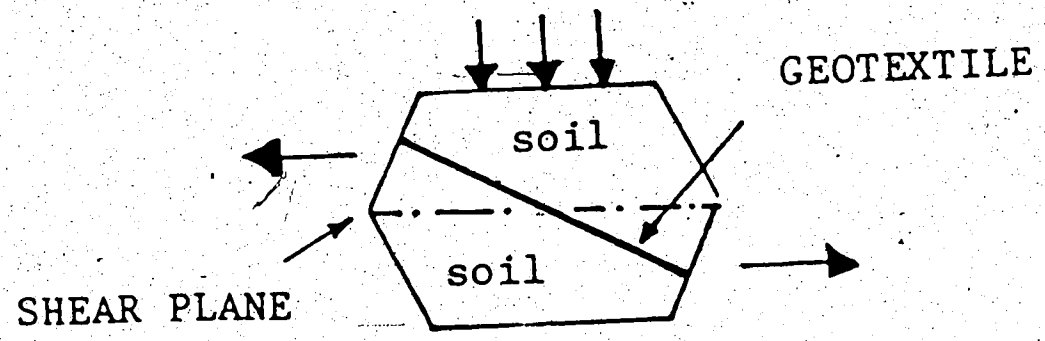

Figure 2.2 An Octagonal Shear Box Test
(Modified from Snaith, Bell, and DuBois, 1977)

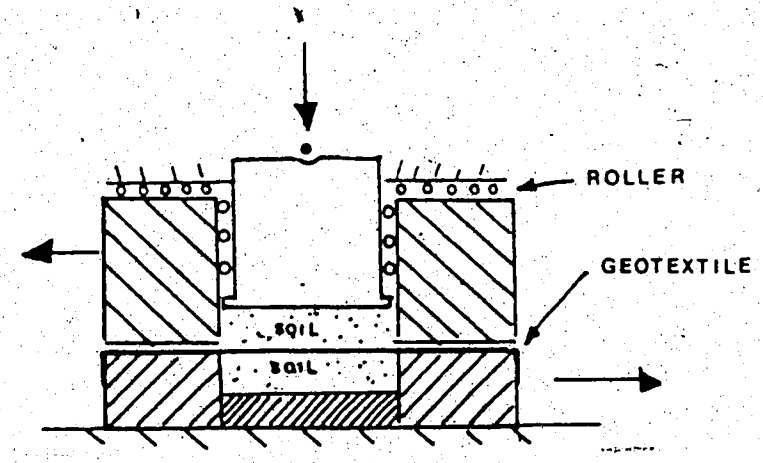

Figure 2.3 A True Direct Shear Test Apparatus
(Modified from Wernick, 1977)

another for normal pressures greater than 100 kPa. Guilloux, Notte, and Gonin (1984) also found that the shear box size did not have any significant effect on a moraine soil. On the other hand, DeGoutte and Mathieu (1986) found the large and small shear box test results were very different. They attributed the difference in strength to the greater wall effect of the smaller shear box. As a result, they used the large shear box for most of their tests.

The use of the conventional 6 x 6 cm^2 shear box has been limited because of the sample size effect. Ingold (1982) stated that the sample size effect may not be significant for geotextiles, but would be important for geogrids where a unit cell of the grid may be larger than the shear area of the box. Also, the conventional box only allows 10 to 12 mm of soil-geotextile relative displacement which may not be adequate to reach the peak or residual strength of the reinforced soil. Researchers such as Christie (1982) Haliburton, Anglin, and Lawmaster (1978), Ingold (1980, 1981, 1982, 1983), and McGown and Andrawes (1982) employed small boxes for their fixed geotextile shear box tests.

2.2.1 Advantages and Disadvantages of the Direct Shear Box Test

There are several advantages and disadvantages of using the direct shear box test. The test itsef is inexpensive, fast, and simple to carry out. It is a very quick test to

measure the short-term shear strength parameters of reinforced soils in terms of the total stresses. The apparatus is also available in various sizes, and it can be easily modified to accommodate any type of reinforcement. Another advantage of the direct shear test is that the specimen is constrained to fail along a predetermined shear plane, thus the interface behaviour of the soil-reinforcement can be assessed directly. Various comparisons have been made between the plane strain and the direct shear test results of granular soils (Bolton 1986; Jewell and Wroth 1987; Hanna and Youssef 1987). These results show that for typical sands the tangent of the plane strain angle of friction is about 20 to 25% greater than that of the direct shear. Thus, the frictional angle of sand obtained from the conventional direct shear test is conservative and will have a hidden factor of safety of approximately 1.2.

Jewell (1980) stated one of the limitations of the direct shear test is that the detailed stress-strain behavior of the reinforced soil cannot be directly determined from the boundary measurements of force and displacement. This is because the directions of the planes of principal stresses rotate as the shear strain is increased. The other disadvantages of the direct shear test, discussed by Ingold (1982) and Richards and Scott (1985), are:

* The problem of stress concentrations at the tested

specimen boundaries, which leads to non-uniform stress distributions within the specimen.

* The development of passive and active pressure zones inside the specimen may cause the loading platen to tilt, which results in non-uniform vertical stress distribution at the shear surface.
* The shear displacement is limited to the travelled length of the shear box.

2.3 Test Assumptions

In order to interpret direct shear test results, researchers generally assume that the reinforced specimen experiences uniform stress and strain in the interface shearing zone. The boundary measurements of force and displacement may be used as an overall measure of the stress state and deformation.

In an attempt to verify the assumption of uniform stress and strain, Jewell (1980) used a radiography technique to determine the strain field of an unreinforced Leighton Buzzard sand in a direct shear box test. He found that the external boundary measurement of shear displacement was in good agreement with the internal measurement made by the radiograph. Moreover, the internal and external vertical displacement measurements were identical. He concluded that a uniform band of strain was developed at failure in the unreinforced sand, and the assumption was appropriate.

Hausmann and Ring (1980) also conducted direct shear tests to investigate the thickness and uniformity of the shear zone at the interface of a reinforced and unreinforced sand. Cylindrical columns of dyed sand were placed in the shear box. After the test, a gelatine solution was used to set the sand in-place, and the dyed sand was dissected. The dissection revealed that at the interface the thickness of the shear zone is density dependent (Figure 2.4), and he confirmed the uniformity of shear band found by Jewell.

2.4 Compaction Method

For a cohesive soil, an optimum water content and a maximum dry density are commonly chosen to specify a standard degree of compaction to be achieved during the construction of a reinforcing structure. For a granular soil, the index density tests are performed to determine a dry density for the field compaction specification. In order to model the field soil and reinforcement interface interaction, the laboratory compaction method that is used must be representative of the field construction procedure.

The method used to compact a soil specimen in the direct shear box tests varies with the size of the boxes, the types of soil, and the field compaction density requirement. For loosely compacted granular soil, Jewell (1980), McGown and Andrawes (1982), and Myles (1982), and Richards and Scott (1985) chose the pouring method to achieve the required densities. To achieve the dense

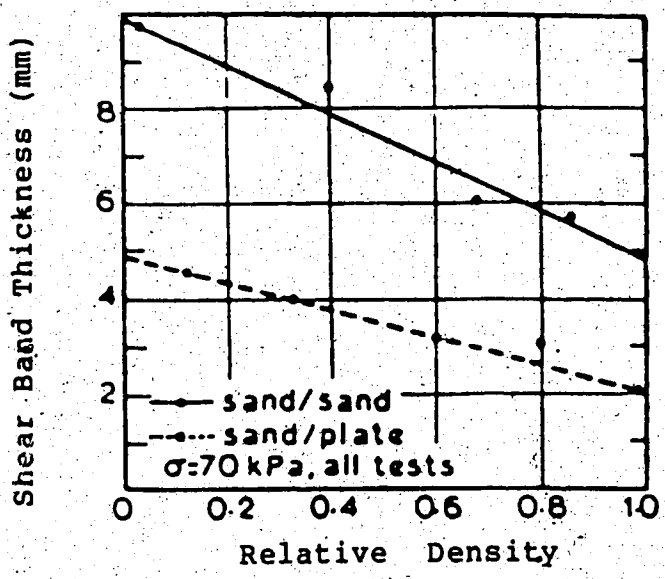

Figure 2.4 Thickness of Shear Zone and Density
(Modified from Hausmann and Ring, 1980)

condition, Richards and Scott (1985) employed the tamping methods. Martin, Koerner, and Whitty (1982) and Miyamori, Iwai, and Makiuchi (1986) used the 2.5 kg manual hammers for compaction, while Sarsby and Marshall (1983) employed the vibrating electric hammer approach to obtain the desired densities.

For cohesive soils, the 2.5 kg manual hammer compaction method was used by Snaith et al. (1979) and Saxena and Wong (1984). The static compaction method was employed by Ingold (1980), Jewell (1980), and Jewell and Jones (1981). In general, the pouring method is used with the small shear box for low density requirements while the 2.5 and 4.5 kg hammers and vibrating hammers are employed to compact soils in the larger size shear boxes for high density requirements.

2.5 Mechanisms of Soil and Reinforcement Interaction

There are two main mechanisms that govern the soil-reinforcement interface shear behavior. These have been determined experimentally using the modified direct shear box tests, by Jewell et al. (1984), Rowe, Ho, and Fisher (1985), Sarsby (1985), and Williams and Houlihan (1987), and disscussed by Giroud (1984), Giroud et al. (1985), and Milligan and Palmeira (1987). The two mechanisms are:

1. Shearing between soil and solid surfaces of the reinforcement which are in the direction of relative soil movement.

2. Interlocking and shearing of soil over soil through the openings in a reinforcing material.

The shearing resistance between the soil and the solid surface areas of a reinforcement is defined by the skin friction angle δ_G. It can be measured directly from a modified direct shear box test. The frictional resistance of the second mechanism should equal the internal friction angle of the unreinforced soil ϕ, which can be determined in the conventional direct shear test.

Jewell et al. (1984) developed a theoretical equation to describe the interaction of the two mechanisms between non-cohesive soil and grid reinforcement. The expression can be written as:

$$\tan \delta_T = a \tan \delta_G + (1-a) \tan \phi \qquad [2.1]$$

where

δ_T = total angle of the interface friction.

a = ratio of solid area of the reinforcement to the total area of the reinforcement.

δ_G = angle of interfacial friction of the solid reinforcement.

ϕ = angle of internal friction.

The theoretical expression shows that the soil properties such as the grain size distribution, shape, and density together with the confining pressure can influence interface shear resistance significantly. The reinforcement

parameters such as the structure of the reinforcement, contact surface texture, aperture size, and deformability can highly affect the the interface interaction. Jewell et al. (1984) and Sarsby (1985) conducted a series of direct shear box tests to investigate the effect of particle size and geogrid aperture size on the interface friction resistance. Their results showed that the highest coefficient of friction resistance, tan δ_T, was reached when the ratio of the minimum aperture dimension to D_{50} of soil was 3.5.

The importance of contact texture was evaluated by Williams and Houlihan (1987). They performed a series of shear tests on granular and cohesive soils reinforced with various geotextiles and geomembranes. Their results showed that the primary mode of interface resistance of the smooth surfaced geomembranes and geotextiles is the direct sliding of grains against the surface of the reinforcement. The frictional resistances of the rough textured geotextiles are governed by the adhesion, dilation, interlocking and sliding of the soil grains on the sliding surfaces. When the, interface shear resistance was greater than the shear strength of the soil, the shear surface was found to shift into the adjacent soil at a distance of about 0.04 to 0.32 cm from the interface.

The effects of soil particle angularity and geotextile deformability were evaluated by Collios et al. (1980), Akber and Hammanji (1985), and Williams and Houlihan (1987). They

ascertained that the interface contact efficiency increased with increasing particle angularity and reinforcement flexibilty. The role of density on the interface shear resistance was examined by Hausmann and Ring (1980), and was found that for granular soil, the shear band thickness increased with decreasing relative density. Collois et al. (1980), Ingold (1982, 1983), and Akber and Hammamji (1985) concluded from their test results that the frictional resistance was directly dependent on the confining stress when the stress was greater than 100 kPa.

2.6 Results for Modified Direct Shear Box Tests

2.6.1 Soils Reinforced with Geotextiles or Geogrids

Table A.1 presents the results of granular soil-geotextile or soil-geogrid interface friction data that have been published by other researchers; results for cohesive soil are given in Table A.2.

The interface efficiency, E, is defined as $\tan \delta_{soil\text{-}reinforcement} / \tan \phi_{soil\text{-}soil}$ (Collis et al. 1980; Degoutte and Mathieu 1986; Myles 1982; Richards and Scott 1985). The efficiency values for the geotextiles in Table A.1 have been calculated. These range from 0.60 to 1.16 which means that between 60% to 100% of soil strength was mobilized at the interfaces. The interface friction angle between the granular soil and geogrid is close to the soil's effective internal friction angle with increasing geogrid opening

size.

The efficiencies for cohesive soil reinforced with geotextiles vary from 0.48 to 1.14 (Table A.2). Small values of interface adhesion were also found by Williams and Houlihan (1987). Very few geogrids have been tested in the direct shear apparatus. The few that were tested found that the interface friction angle was approximately 68% to 85% to that of the soil.

The following observations can be made from the results of Table A.1 and A.2.

1. In soil reinforced with a geotextile or a geogrid, the interfacial friction between loosely compacted granular soil and reinforcement is similar to the unreinforced soil. Its efficiency is therefore very close to one.
2. The interfacial friction between dense granular soil and reinforcement is less than that of the unreinforced soil. The reduction in efficiency may be related to the construction and geometry of the reinforcement.
3. The interfacial friction increases with increasing surface roughness independent of the type of soil and the type of reinforcement. The textured surface may provide better interlocking with the soil grains than the smooth surface, thus the efficiency increases.
4. In granular or cohesive soil reinforced with

geogrids with the same planarity, the one with the bigger opening dimensions has higher interfacial friction. It appears that a greater amount of soil to soil interaction occurs in the larger openings than in the smaller openings which results in a higher efficiency value.

5. For granular soil reinforced with woven geotextiles having a similar percent of open area, a stiff and thin geotextile mobilizes slightly higher frictional resistance than a flexible and thin geotextile. However, a thick and flexible non-woven geotextile yields a higher friction angle than both a thin and flexible and a thin and stiff woven geotextile. It appears that thickness and stiffness of geotextiles have some influence on the interfacial friction.

2.6.2 Soils Reinforced with Geomembranes

Since one of the interface interaction mechanisms is the sliding of soil along the solid surface of the reinforcement, a summary of published direct shear test results with geomembranes is examined. Table A.3 presents the results for granular-geomembrane interface friction data; results for cohesive soil-geomembrane are given in Table A.4.

An average efficiency of 0.75 has been calculated for the data in Table A.3. The cohesive soils-geomembranes (Table A.4) show efficiencies varying from 0.34 to 1.00.

Small interface adhesions were also found by Williams and Houlihan (1987).

Regardless of the type of soil and the type of polymer, the interfacial friction of geomembranes increases with increasing surface roughness. For materials with the same roughness, the thin and less stiff geomembrane mobilizes greater strength than the thick and stiff one.

3. PROPERTIES OF THE SOILS AND THE REINFORCEMENTS

3.1 Introduction

This chapter describes the index properties of the cohesive and granular soils used in the modified direct shear tests. The other properties of the soils such as grain size distribution, compaction dry density and water content relation, and consolidation behaviour are also given. The total and effective shear strength of these soils are reported. The construction method and the geometry of the five types of reinforcements are given.

3.2 Properties of the Cohesive Soil

3.2.1 Index, Particle Size Analysis, and Specific Gravity Tests

A well graded silty clay soil supplied by the Alberta Transportation laboratory was used for all the consolidated undrained direct shear box tests. This silty clay soil was taken from a borrow pit near the Devon testfill. The clay had been air-dried and clumps had been broken and bagged in ninety 20 kg batches. The consistency of the silty clay was determined by taking a specimen from each of four different 20 kg batches. Each specimen was tested to determine the Atterberg limits and particle size distribution (ASTM D421, D422, and D4318). The liquid and plastic limits averaged from the four tests were 40.8% ± 1.3% and 20.6% ± 0.2%. The

typical grading curve (Figure 3.1) shows 23.5% of the grain size is finer than 2 μm. This gives an activity of 0.9. A few specks of coal were found among the soil grains from the grain size analysis. Five specific gravity tests (ASTM D854) gave an average G of 2.70 ± 0.01.

3.2.2 Compaction

The compaction dry density and water content relation was determined by the: dynamic and kneading compaction methods. Figure 3.2 shows that the compaction curve achieved by impacting the 2.50 kg hammer 25 times on each of the three lifts of soil is similar to that by kneading compaction. The higher compaction effort achieved by applying 25 blows of 700 kPa contact pressure of the mechanic foot on each of the three layers of soil had no significant effect on the silty clay soil dry density. The average optimum water content from the two compaction curves was 20.1% and the corresponding maximum dry densitywas 1.68 g/cm^3. The estimated degree of saturation was 87%.

During the preliminary testing, it was found that the same maximum dry density could be achieved in the 300 mm^2 box. A 4.54 kg hammer attached with a 10.2 cm square steel foot was used to apply 64 blows per layer for three layers of soil. The compactive effort was 447.6 kJ/m^3 which represented 75.5% of the standard compactive effort. Using this method the silty clay was compacted to a dry density of 1.68 g/cm^3 ± 0.02 g/cm^3. At the compacted water content of

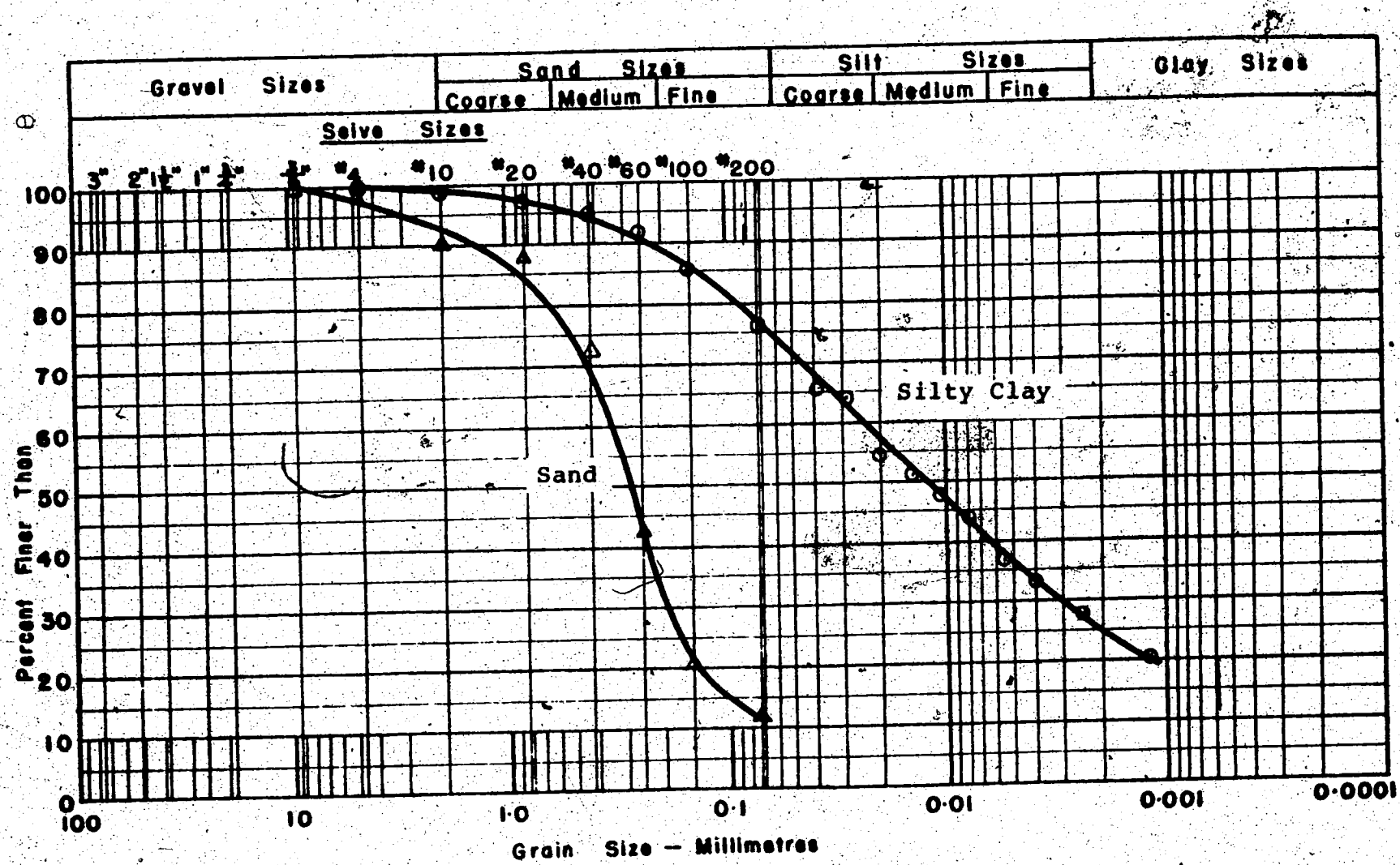

Figure 3.1 Grain Size Distribution for Silty Clay and Sand

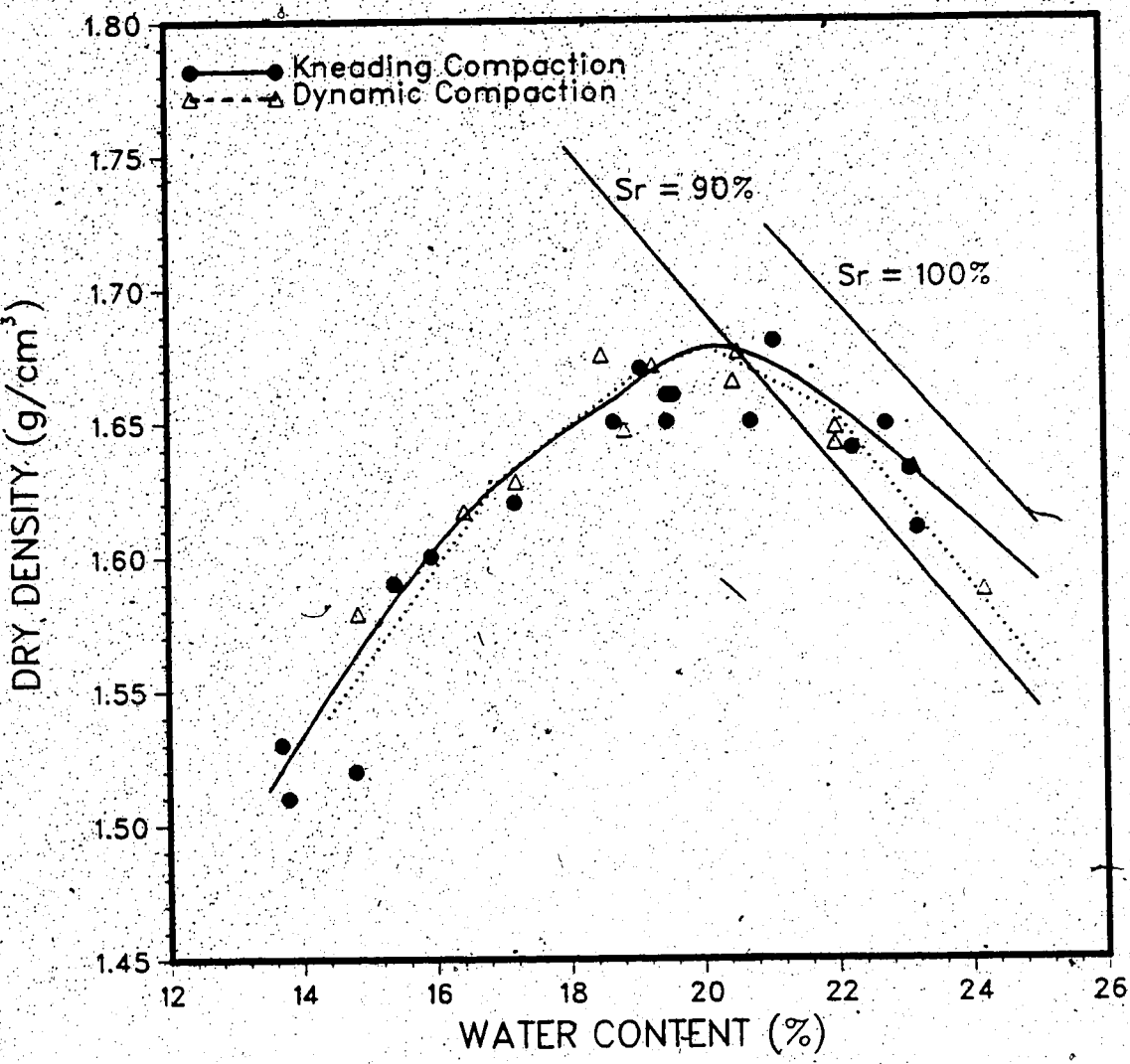

Figure 3.2 Compaction Curves for Silty Clay

23.3% ± 0.6%, this rendered a degree of saturation of approximately 98% to 100%. Thus, the dry density of 1.68 g/cm^3 and a water content of 23.0% was specified for all silty clay specimens.

3.2.3 Oedometer Test

The consolidation characteristics of the silty clay was determined from the results of three oedometer tests. Each oedometer specimen was carefully trimmed from the sample which had previously been compacted in the large shear box. The dry density of the whole sample was 1.68 g/cm^3 at the water content of 23.1%. However, the measurement of the specimens indicated that the average as-compacted dry density was only 1.61 g/cm^3. At the water content of 23.0%, the degree of saturation was 90.0%.

Consolidation was completed within 24 hours under each applied vertical load. The percent strain versus normal stress plot (Figure 3.3) shows that the preconsolidation pressure of this silty clay was between 140 to 175 kPa. The coefficient of consolidation was determined for each specimen at each normal stress, and was found to have a mean value of 2.5 x 10^{-8} m^2/s ± 1.1 x 10^{-8} m^2/s. This magnitude of C_v means that for a 12 m high silty clay fill under a double drainage condition, it will take approximately nine years to complete 50% consolidation.

The possible sources of errors that might lead to the difference in density between the 300 mm^2 sample and the

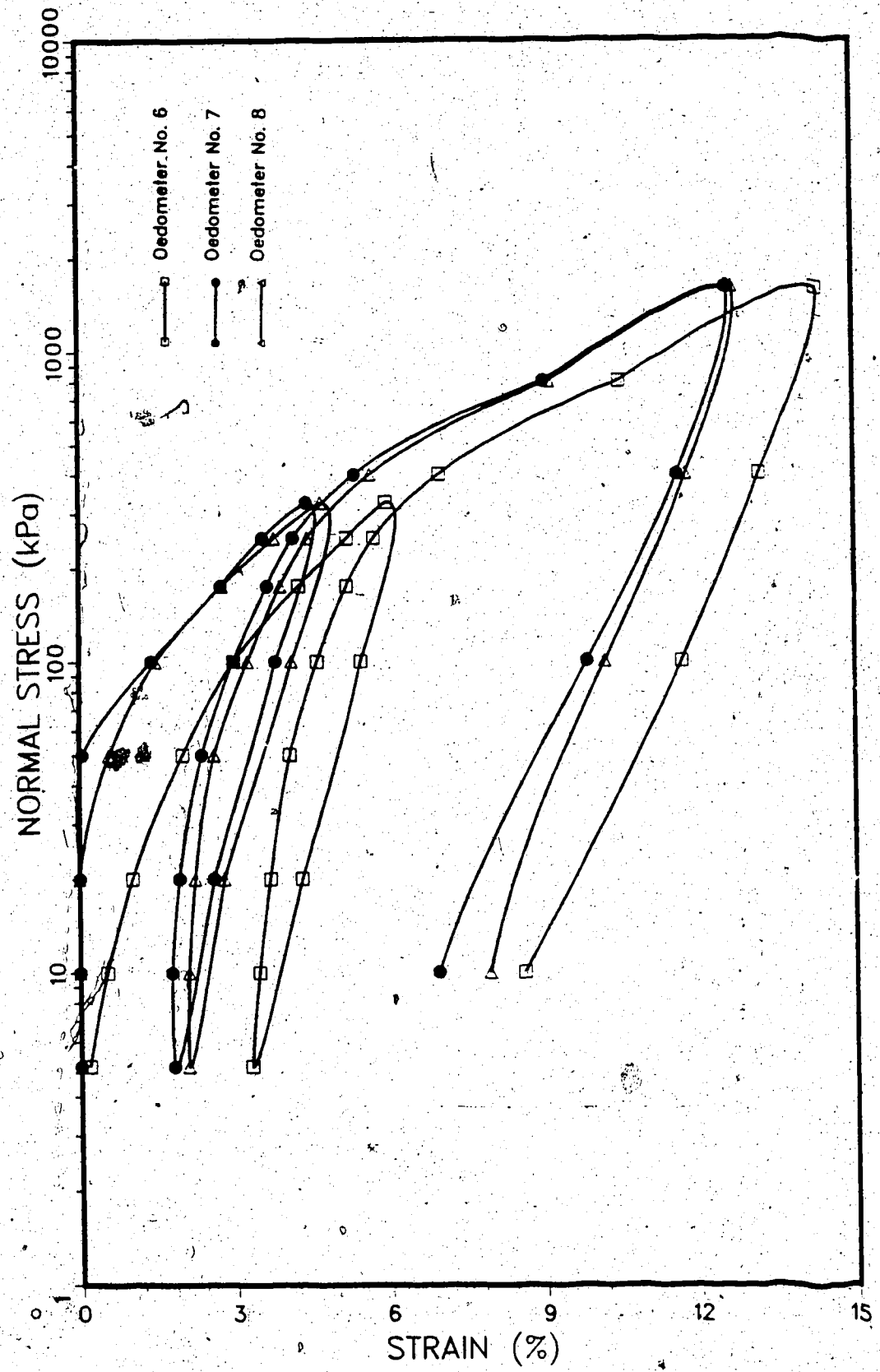

Figure 3.3 Percent Strain versus Normal Stress Plot for Oedometer Test Results

oedometer specimens were examined. The scale on which the soil was weighed was calibrated, and the internal dimension of the box was measured. The method of measuring the heights of the sample was checked. No error was identified. However, the compaction curves indicated that at the water content of 23.0%, the dry density was 1.63 g/cm^3, and the degree of saturation was 95.0%. Hence, it is possible that the overall sample dry density was 1.63 g/cm^3 instead of 1.68 g/cm^3.

3.2.4 Total Shear Strength

The consolidated undrained shear strength of the silty clay was determined with both 300 and 60 mm^2 shear box tests. In the large shear box, the sample was compacted inside the box, and it was consolidated under the confining pressure for 24 hours. It was then sheared at the rate of 3.05 mm/min. Using the average value of the coefficient of consolidation, the rate of shear deformation required to dissipate 95% of the pore pressure is about 3.8 X 10^{-8}mm/min (equation from Bishop and Henkel 1978). Thus, the shearing rate of 3.05 mm/min is fast enough to ensure the undrained condition during shear. The consolidation curves and the failure envelope are shown in Figures 3.4 and 3.5.

Comparative tests were carried out using the 60mm^2 box. The sample was compacted in a mold by the kneading method to give a dry density of 1.58 g/cm^3 and a water content of 23.5%. Several specimens were cut from the sample. The consolidated undrained test results are also

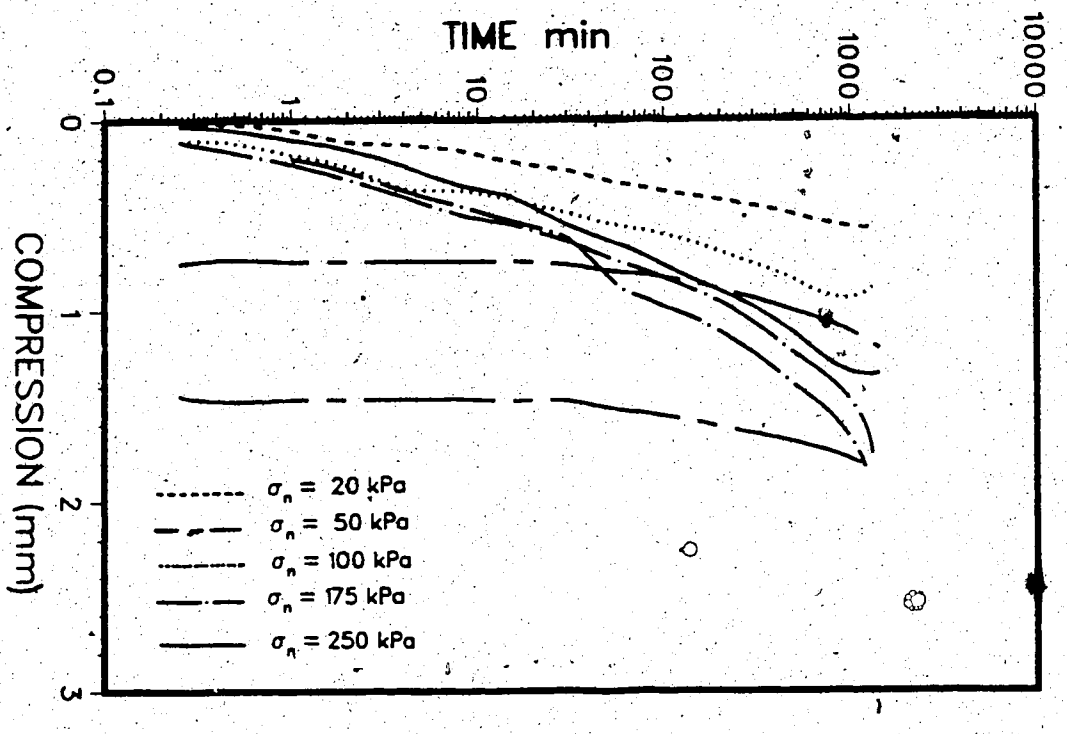

Figure 3.4 Consolidation Results of the Large Shear Box Tests on Silty Clay

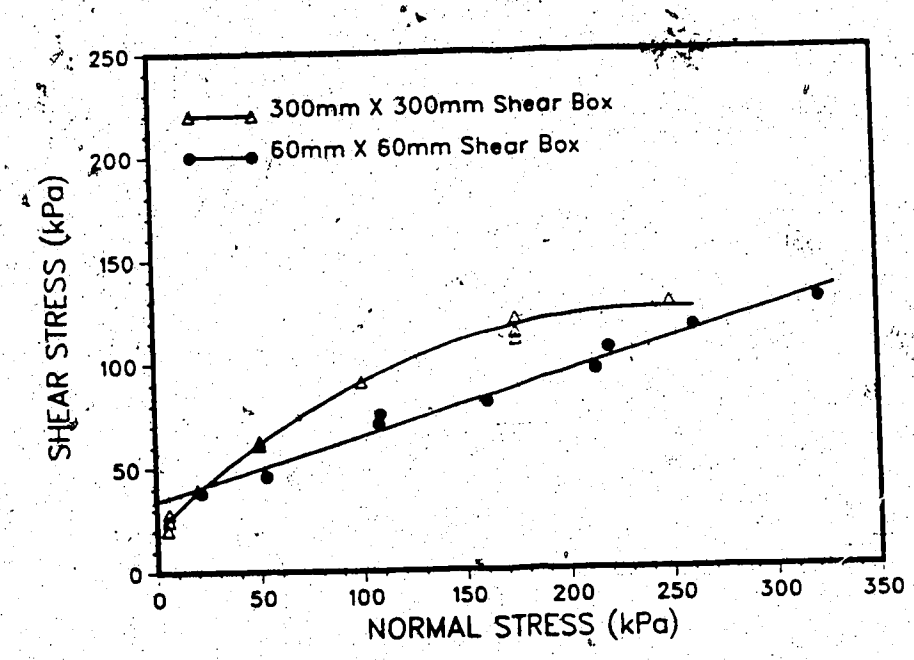

Figure 3.5 Mohr-Coulomb Failure Envelopes of Direct Shear Tests on Silty Clay

shown in Figure 3.5. The apparent angle of internal friction is 17.0°, and the apparent cohesion intercept is 34.2 kPa.

A comparison between the results of the two shear boxes indicates that higher shear strength and non-linear Mohr-Coulomb envelope were obtained with the large shear box (Figure 3.5). The variation in shear strength could be due to the 5% difference in initial density. Under the same consolidation pressure, the smaller specimens which had the lower initial density would have achieved a smaller density. Thus, a smaller amount of shear force was required to overcome the interfacial shear resistance which resulted in lower shear strength.

The discrepancy in shear strength may also be caused by the different compaction methods that were used to prepare the 300 and 60 mm^2 specimens. As discussed by Seed, Mitchell, and Chan (1961), silty clay material is particularly susceptible to structural changes resulting from different compaction methods. Even for specimens that were compacted to the same water content and dry density, kneading compaction induces larger shear strains during compaction compared to dynamic compaction and results in a higher degree of dispersion, higher pore pressure, and lower strength at low strains. In addition, the influence of wall friction between the side of the box and the specimen was greater in the smaller box because of the scale effect. The ratio of the thickness to length of the specimen was 0.42 for the small box and 0.32 for the large box.

One factor that may have influence the shape of the Mohr-Coulomb envelope is the difference in test conditions. In the small shear box test, water was added to the shear box after the specimen was placed inside the box. Although the permeability of the silty clay is low, it is possible that the specimen had become fully saturated under the consolidation pressure and the test conditions. In contrast, the specimen in the large shear box was not immersed in water. It remained partially saturated until the applied pressure was high enough to cause the full saturation. In addition, the preconsolidation pressure of the remolded clay is about 175 kPa. Any applied normal pressure less than this value will yield a slightly overconsolidated soil; this may contribute to the curvature in the large shear box results (Figure 3.5). As will be seen in the next section, such a curvature of the failure envelope is not found among the non-cohesive soil results. Thus, this particular feature may be due to the test conditions of the cohesive soil.

Mitchell (1976) also pointed out that curved failure envelopes are observed for some clays. He suggested two possible causes for the stress dependency behavior. Under a low normal stress, less energy is required to shear the soil without rearranging the orientation of the particles. Under a high normal stress less work is spent to rearrange the soil particles because particle reorientations may have been developed during the application of the high confining pressure.

3.2.5 Effective Shear Strength

The effective shear strength of the silty clay was determined with consolidated undrained triaxial tests with pore pressure measurements. Nine specimens were prepared from five samples which had previously been prepared by kneading compaction. The average of the nine dry densities was 1.59 g/cm^3, and the water content was 24.0%. The Mohr-Coulomb and p-q diagrams for undrained and effective stresses are plotted in Figures 3.6 and 3.7. The undrained angle of internal friction was 14.9° which is lower than the direct shear test undrained value (ϕ_T=17.0°). As explained earlier, due to the dynamic method of compaction the triaxial specimens had yielded a lower shear strength. The undrained cohesion intercept was 41.5 kPa. The effective angle of internal friction and the effecitve cohesion intercept are 30.1° and 6.7 kPa.

3.3 Properties of the Granular Soil

A uniformly graded medium sand supplied by the Alberta Transportation laboratory was used for all the consolidated drained direct shear box tests. The sand had been air-dried and bagged. The grain size distribution curve is shown in Figure 3.1. The coefficient of uniformity is 12.7. The relation between dry density and water content, was established by a 2.50 kg hammer dynamic compaction method (Figure 3.8) since the dynamic compaction method would be used to compact the sand in the large shear box. The maximum

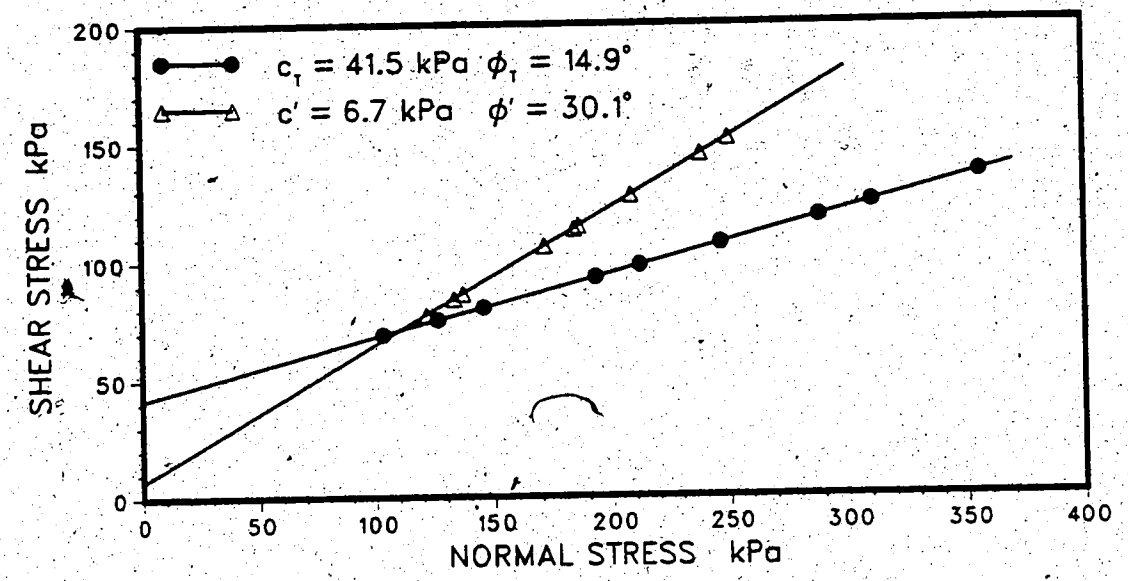

Figure 3.6 Total and Effective Mohr-Coulomb Envelopes of Silty Clay

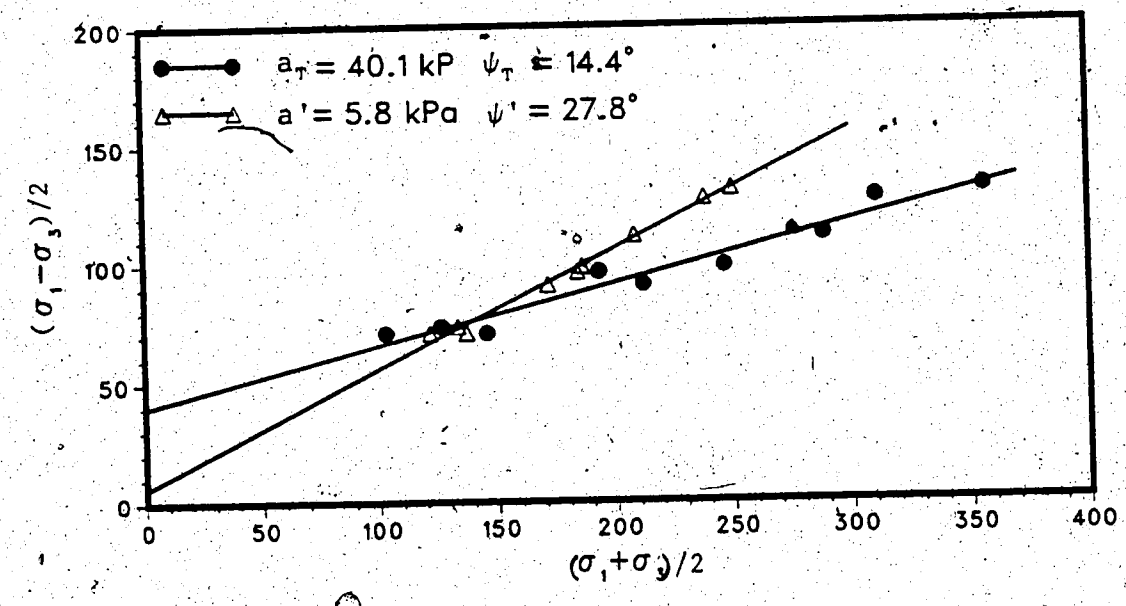

Figure 3.7 Total and Effective Stress p - q Diagrams of Silty Clay

dry density of the sand was determined in accordance with the ASTM D4253 vibratory compaction test. Three tests were performed giving a mean maximum dry density of 1.91 g/cm^3 ± 0.01 g/cm^3. The minimum dry density was determined by the pouring method as described in ASTM D4254. The test was repeated three times giving a mean of 1.42 g/cm^3 ± 0.01 g/cm^3. The three specific gravity test results gave an average G of 2.64.

The preliminary compaction trials in the modified direct shear box indicated that consistant compaction could be achieved using a 2.50 kg hammer fitted with a 10.2 x 10.2 cm^2 steel compaction foot. 64 blows per layer were applied over the three layers of air-dried soil. The compactive effort was 164.1 kJ/m^3 which represented 27.7% of the standard compaction energy. Using this method it was possible to obtain a dry density of 1.77 g/cm^3 ± 0.02 g/cm^3. This represents 95.5% of the maximum dry density achieved in the standard compaction test and gives a relative density in the range of 0.74 to 0.82 with a mean value of 0.78.

The consolidated drained shear strength of sand was determined with the 300 mm^2 shear box tests. The applied normal stress was 20, 50, 100, 175, and 250 kPa. The peak and residual effective internal angles of shearing resistance of 42.5° and 39.1° were obtained from the results (Figure 3.9).

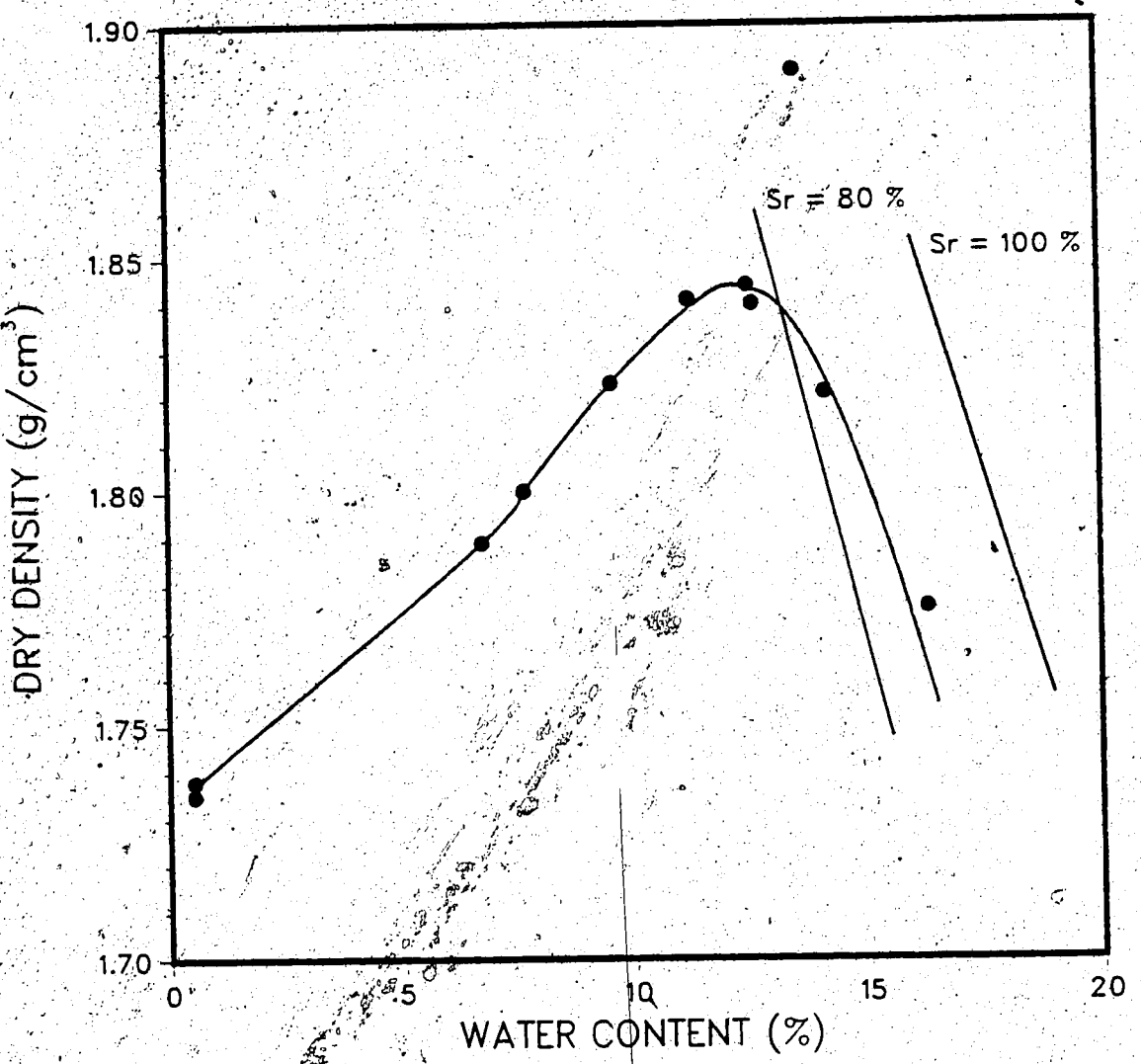

Figure 3.8 Standard Proctor Compaction Curve for Sand

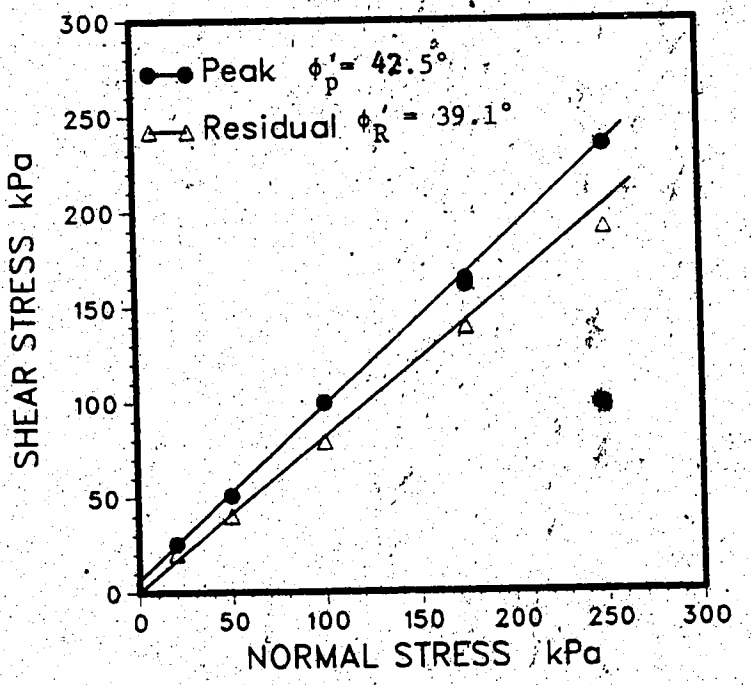

Figure 3.9 Peak and Residual Shear Strength for Sand

3.4 Properties of the Reinforcements

The interfacial shear resistance of four types of geogrids and one type of geotextile were investigated in the testing program. These materials have high tensile strength and have been widely used for soil-reinforcement. The geogrids are SR2, SS2, TNX-5001, and ParaGrid 50S. The geotextile is P600. Three of the geogrids, SR2, TNX-5001, and ParaGrid 50S, were used as part of the Devon project. The construction method and the geometry of these reinforcements are summarized in Table 3.1. Photographs of these reinforcements are shown in Plates 3.1 to 3.5.

Table 3.1 Properties of Geogrids and Geotextile

Geogrid/ Geotextile Tradename	Type of Polymer	Structure	Junction Method	Geometry					Tensile Properties
				Weight (g/m^2)	Open Area (%)	Aperture Size (mm)	Thickness (mm)	Color	Peak Tensile Strength (kN/m)
ParaGrid 508	Polyester Polypropylene	Square Grid	Welded	530	78	* MD 66.2 CMD 66.2	* T 2.50 A 3.75	White/ Yellow	50
P600	Polypropylene	Woven Split Film	Woven	220	0	1.5×10^{-3} 5.0×10^{-3}	0.75	Black	1400N Grab Test
TNX-5001	Polyester (Polyethylene and Terephthalate)	Rectangular Grid	Welded	544	58	MD 89.7 CMD 26.2	T 0.75 Junction 1.50	Black	87.5
SR2	High Density Polyethylene	Uniaxial Grid	Planar	930	55	MD 99.1 CMD 15.2	T 1.27 A 4.57	Black	78.8
SS2	Polypropylene	Biaxial Grid	Planar	345	77	MD 25.4 CMD 33.0	T 1.02 Junction 3.81	Black	17.1

* MD = Machine direction
CMD = Cross machine direction
* T = Tension member
A = Anchor member

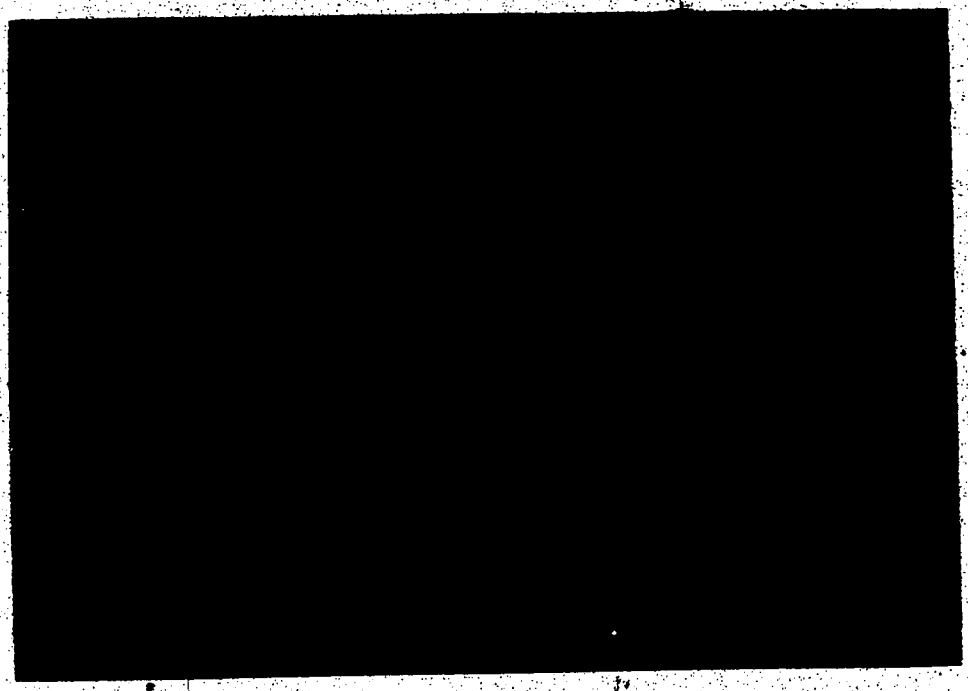

Plate 3.1 Uniaxial Geogrid SR2

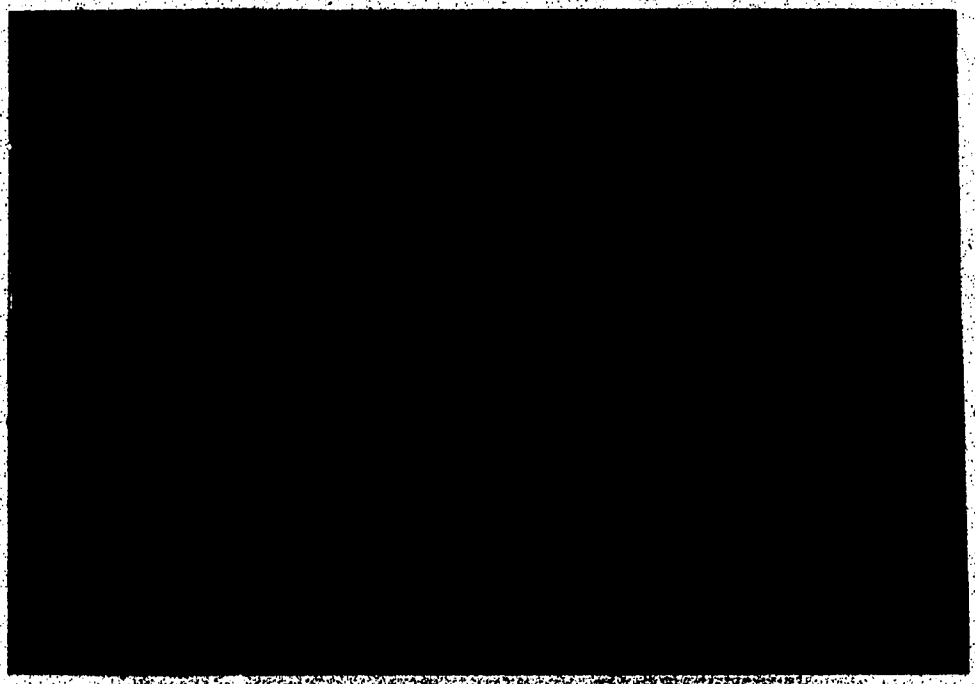

Plate 3.2 Geogrid TNX-5001

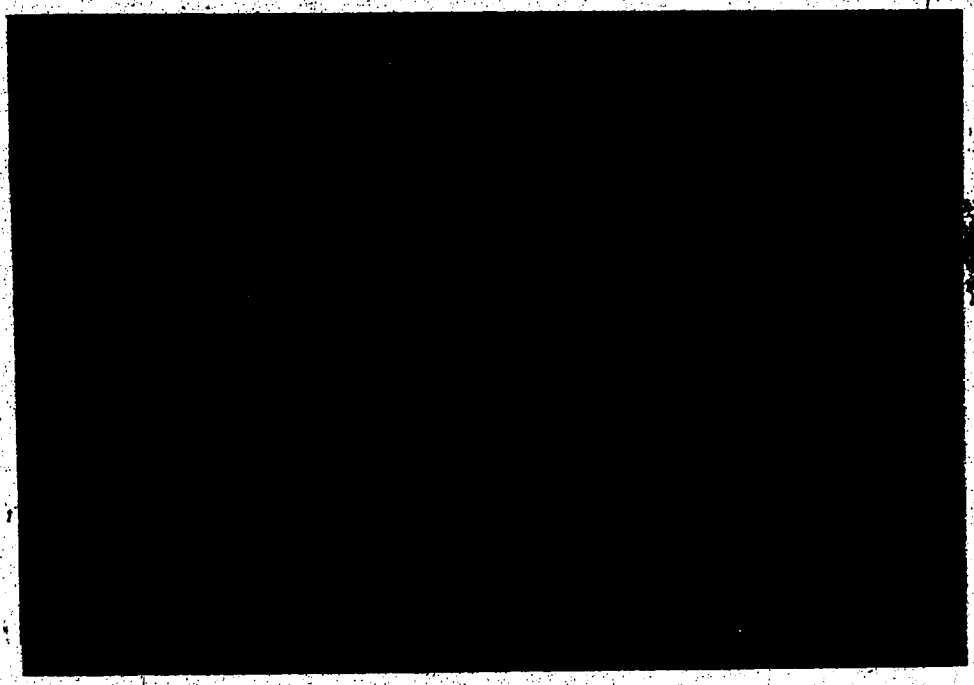

Plate 3.3 Biaxial Geogrid SS2

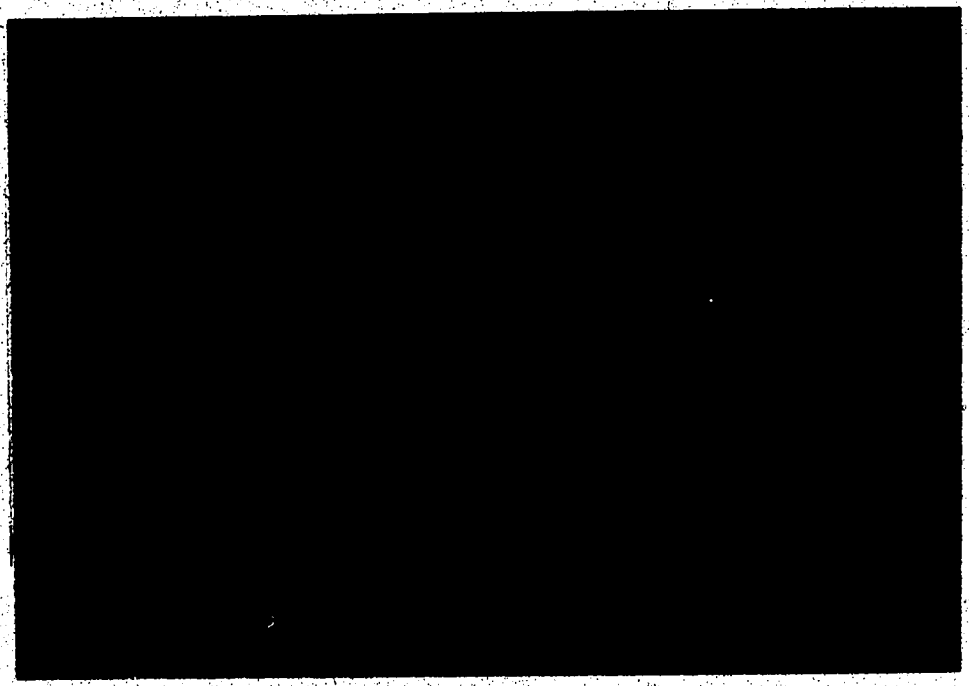

Plate 3.4 Geogrid ParaGrid 50S

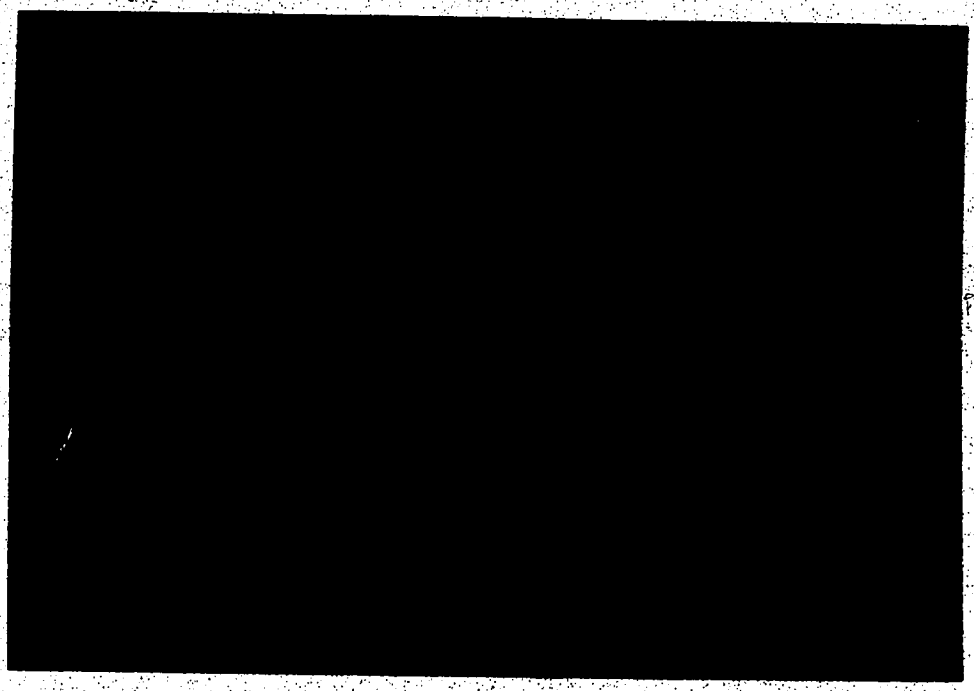

Plate 3.5 Woven Geotextile P600
Fabric Count: Warp direction = 6 yarns per centimetre
Weft direction = 6 yarns per centimetre
(CGSB 6-M77)

4. DESCRIPTION OF APPARATUS AND TESTING PROCEDURES

4.1 Introduction

In this chapter the mechanical details for the direct shear apparatus, the normal stress loading system, and the devices for boundary measurements are described. The test procedure, the selection of normal stresses, and the rate of shear are discussed.

4.2 Direct Shear Apparatus

Most aspects of soil-reinforcement interface behaviour can be studied through the use of a direct shear apparatus. Modifications and mechanical details of an apparatus to measure the strength and deformation behaviour at the soil-reinforcement interface are described.

4.2.1 Description of the Direct Shear Apparatus

The Wykeham Farrance large capacity direct shear machine was modified to measure interface behaviour. The mechanical details of the shear apparatus are illustrated in Figure 4.1.

The upper and lower shear boxes are similiar to those commonly used in the conventional direct shear tests (Figure 4.2). The reinforced sample dimensions of 30 x 30 cm^2 were chosen to minimize the size effect and to accommodate the geogrids with large unit cells. The leading edge of the bottom shear box is modified to permit the

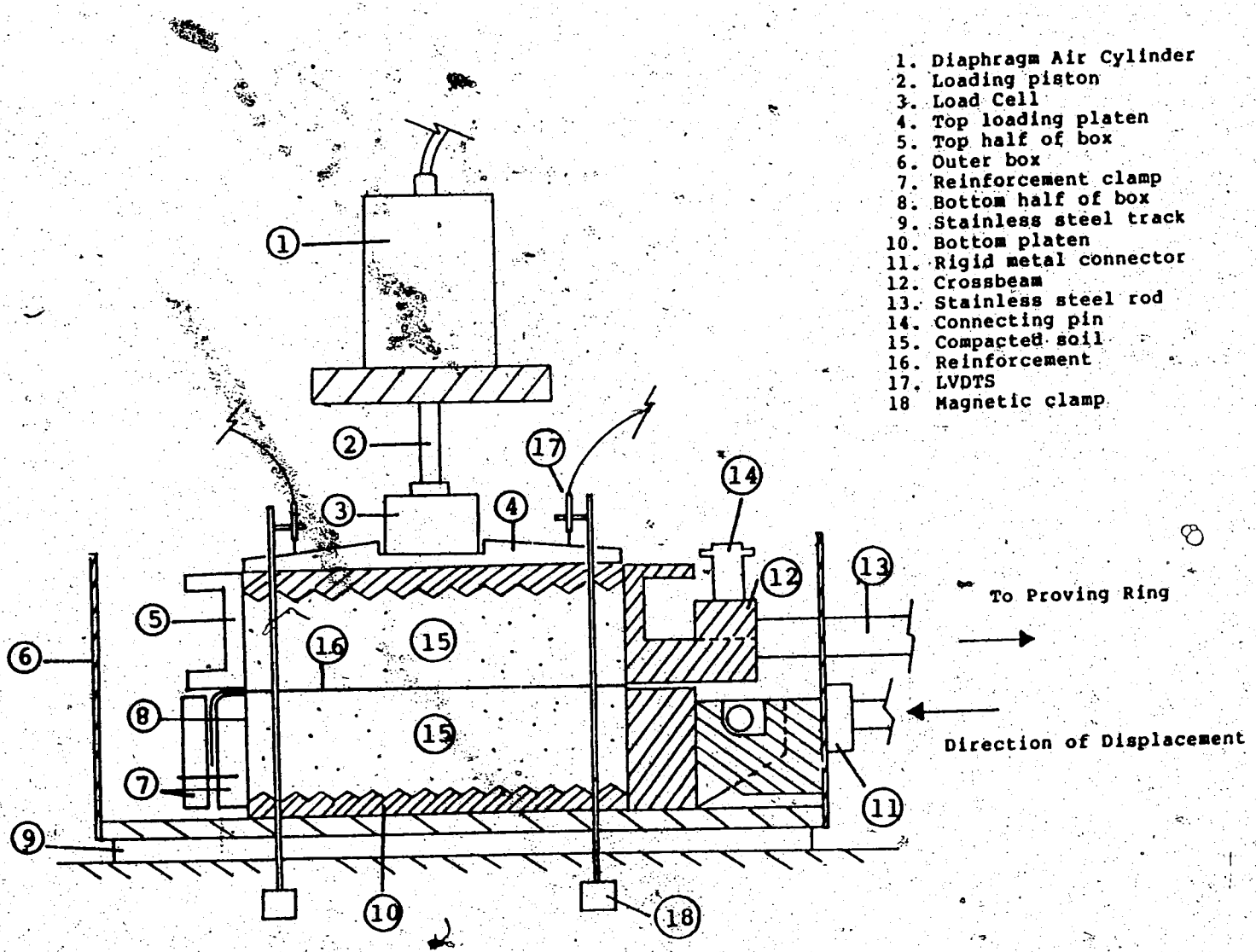

Figure 4.1 Wide Width Direct Shear Box Apparatus

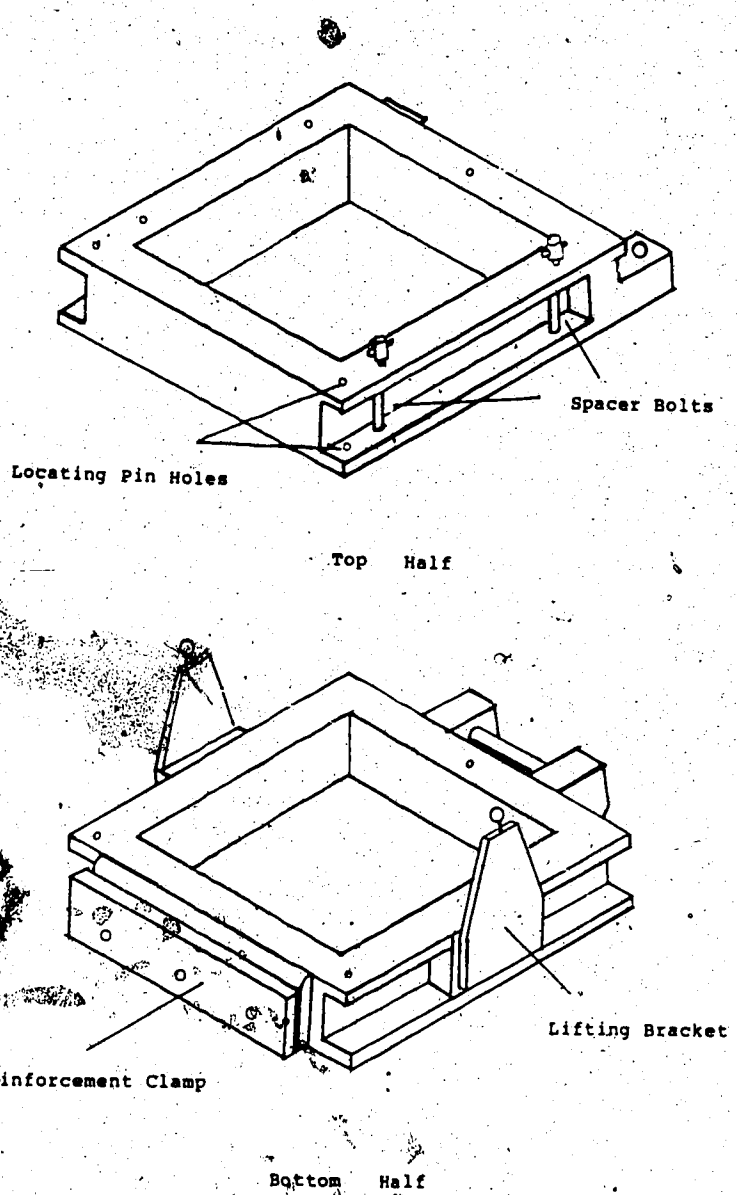

Figure 4.2 Upper and Lower Shear Boxes

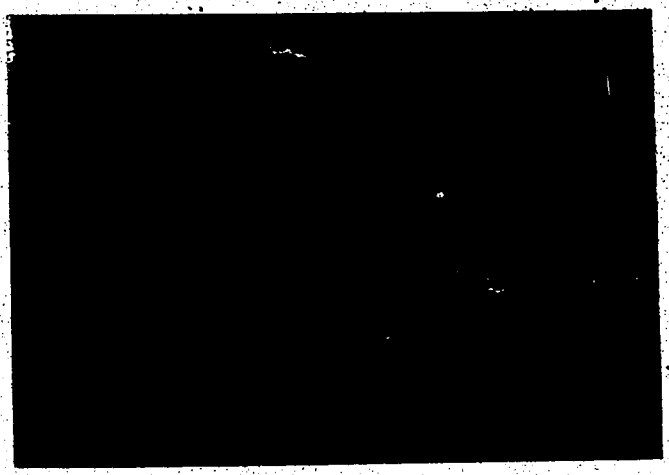

Plate 4.6 Modified Leading Edge and Clamps

clamping of the reinforcing material (Plate 4.1).

The shear boxes are contained within a larger outer box which runs on a polished stainless steel track. Free movement is allowed in the direction of shear, and any lateral movement is prevented.

The vertical load was exerted by a Diaphragm Air Cylinder, a Bellofram, which is connected to a air regulator to monitor the air pressure. The cylinder has an extremely sensitive response to small pressure variations. Thus, the air pressure can easily be adjusted to keep the normal load constant during the test.

The shear load is applied to the apparatus by an electrical motor driving a mechanical screw jack via a 42 speed gearbox. The shearing force is then transmitted to the shear box by a rigid solid metal connector which applies the shear load at the mid-plane level of the sample. The shear displacement rates can be varied from 0.00012 to 6.1 mm per minute.

4.2.2 Boundary Measurements of Forces and Displacements

The normal load was applied directly from a Diaphragm Air Cylinder to a load cell which was placed on the center of a loading plate. The applied load was accurately measured and maintained by the load cell. This measuring device is able to monitor the vertical stress to an accuracy of ± 0.1 kPa.

The shear load was applied through a displacement control device. The upper half of the shear box is held stationary, and is rigidly connected to a crossbeam and two steel rods, which pass through the wall of the outer box to the proving ring. Thus, the generated shearing resistance to the horizontal displacement was measured by the proving ring. The proving ring has a capacity of 100 kN, and the shear force can be measured to an accuracy of ±10 N.

The shear displacement of the two halves of the box was measured by a Linear Variable Differential Transformer (LVDT) which has 50 mm of travel. It can measure the horizontal displacement to the nearest 0.005 mm. The vertical displacement was measured by four LVDTs. One LVDT was placed on each quarter of the loading plate to better measure the compression and dilatant behaviour of the reinforced soil. The LVDT gives readings to an accuracy of ± 0.005 mm.

4.2.3 Calibration of Measuring Devices

The purpose of calibration is to define the accuracy of each instrument. The LVDT was calibrated by an electronic micrometer. The load cell was calibrated by a 44.5 kN proving ring in a compression machine. Similarly, the proving ring was calibrated by a 4.5 kN and a 133.5 kN proving ring. Each calibration result was plotted and analysed by the Linear Regression method. The calibration curves are shown in Appendix B.

A 30 x 30 x 8.28 cm³ aluminium metal block was placed inside the direct shear box to measure the amount of machine compression caused by the application of each normal load. The shear box was assembled and placed inside the shear apparatus. The load cell and LVDTs were positioned on the loading plate. The initial readings were taken, and the normal load was applied. The vertical compression data were recorded (Figure B.8). When the compression ceased, the load was removed, and the shear box and the metal block were taken apart. The whole procedure was repeated for each normal load.

4.2.4 Datalogger Acquistion Control Unit

Data logging was performed by a Fluke 2240B Data Acquisition Control Unit. It was used to monitor and record the applied normal load, shear force, and all LVDT measurements during the testing program. The datalogger allows a variable recording period to be specified.

4.3 Test Procedures

The selection of consolidation stresses, the rate of shear, the thickness of compacted soil samples, and the method of placing the reinforcement inside the shear box will be discussed. The sample preparation procedures and compaction are described for both the silty clay and sand. The test procedure for each stage of the direct shear test is also described.

4.3.1 Selection of Normal stress and Rate of Shear

In this test program, the normal stress range of 50, 100, 175, and 250 kPa were chosen to consolidate the samples. These pressures were selected to represent the vertical stresses experienced by a 2.5 m, 5.0 m, 8.75 m, and 12.5 m high embankment, at the foundation interface.

A critical design situation may occur when an additional stress is rapidly applied to the soil in an embankment which has become consolidated and is at equilibrium with the existing stress system. This rapid rate of loading may induce an undrained shear failure of the whole structure. The consolidated undrained direct shear test is appropriate for modeling this type of field behavior. The shear displacement rate of 3.05 mm/min was chosen to represent the undrained rate of loading.

4.3.2 Determination of Soil Sample Thickness

During the early stage of the test program, four trial tests were performed on the silty sand. The objective was to study the influence of soil thickness on shear strength. Each of the first three samples was compacted in two layers, and had a dry density of 1.73 g/cm^3. The thicknesses were 7.0 cm, 9.7 cm, and 11.9 cm. These were consolidated under a normal pressure of 250 kPa, and were sheared at a rate of 3.05 mm/min.

The results are shown in the shear stress and displacement plot (Figure 4.3). The difference in maximum

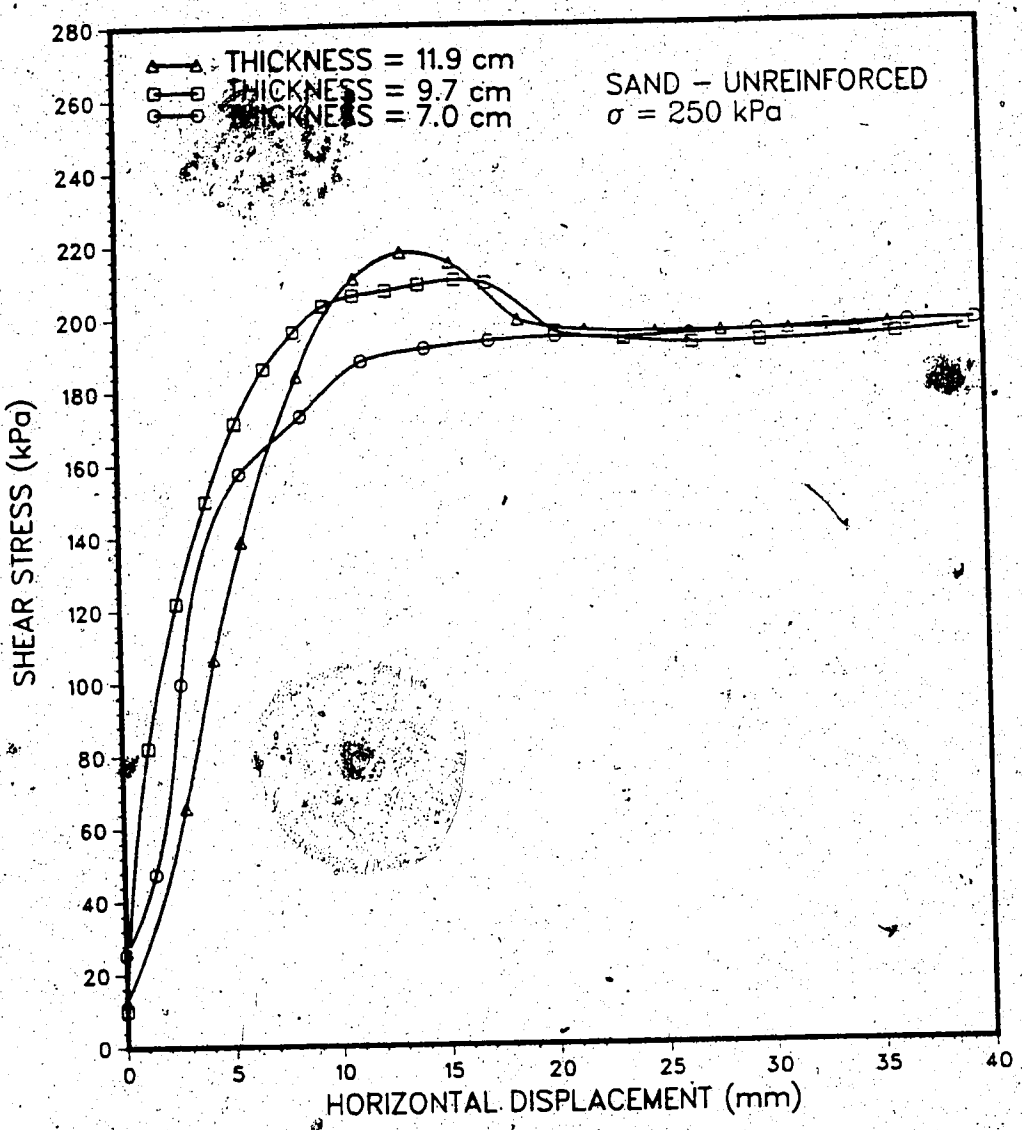

Figure 4.3 Effect of Soil Thickness on Shear Stress Behaviour

shear strength between the 7.0 and 11.9 cm samples was 9% while there was little difference in strength between the 9.7 cm and 11.9 cm samples. The difference in the amount of shear displacement required to mobilize the maximum shear strength and the shape of the curves strongly indicate that the sample thickness influences the results.

The fourth sample was used to study the influence of the numbers of compacted layers on density and shear strength. The sample was compacted in three layers. The compacted height was 9.6 cm, but the density was increased to 1.79 g/cm^3. The peak shear strength was 7% greater than that of the 11.9 cm sample; however, the shear stress and displacement behaviour was similar. The peak shear strength of the 9.6 cm sample was 10% higher than that of the 9.7 cm, and the displacement to the peak was smaller (Figure 4.4). Bishop (1950) recommended the minimum ratio of sample thickness to its length of 0.25 for direct shear tests. For the 9.7 cm high sample the ratio is 0.32. Thus, the thickness of approximately 10 cm and three layers compaction were specified for each sample.

4.3.3 Reinforcement Placing

All the geogrids were clamped in the same manner: the tension members were placed in the direction parallel to the shearing while the anchor members were placed transverly to the shear direction (Plate 4.1). For the woven geotextile P600, the warp direction was parallel to the shearing.

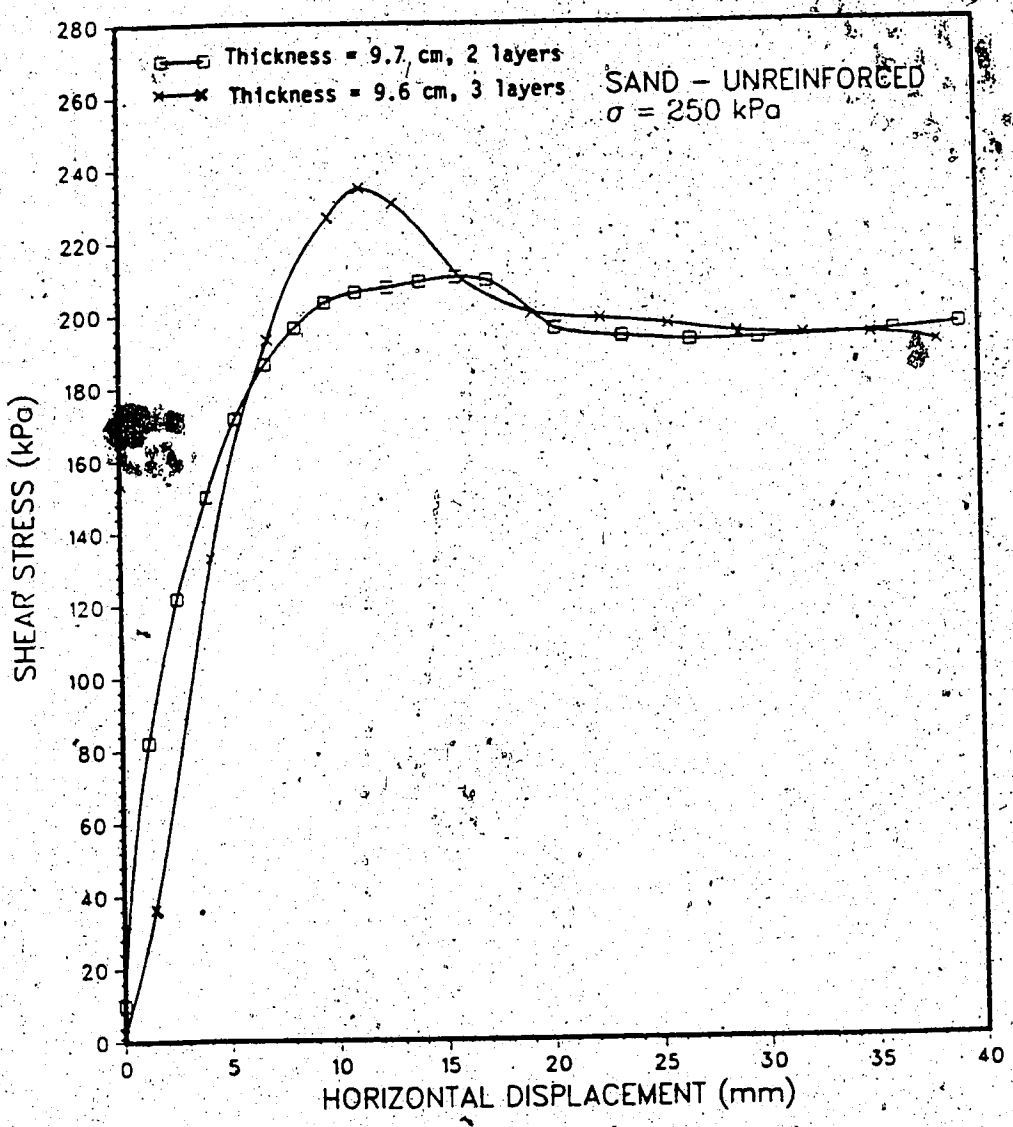

Figure 4.4 Effect of the Number of Compacted Soil Layers on Shear Stress

4.3.4 Devon Silty Clay

4.3.4.1 Sample Preparation

The hygroscopic water content of each 20 kg batch of air-dried silty clay was determined. A fresh bag of soil was prepared for each test at a water content of 23.0%. After mixing the soil with tap water, it was stored in two plastic bags and cured in a moisture room for at least 18 hours to allow moisture content equilization. At the end of the curing period it was sifted through a 0.5 inch sieve to break up any clumps, and the soil was ready for compaction.

It was found during the initial property index tests that the duration of curing time had an effect on the relationship between the dry density and the water content. Increasing the length of the curing period resulted in a decrease in dry density. This finding was also noted by Casagrande and Hirschfeld (1960). They found that a different length of curing period yielded different dry density and water content relation curves.

4.3.4.2 Compaction Procedure

Each sample was composed of three compacted layers. A series of preliminary tests demonstrated that to obtain a dry dentsity of 1.68 g/cm^3, 64 blows per layer had to be applied to the clay soil using a 4.5 kg manual compaction hammer attached with a 10.2 cm^2 steel plate.

To reduce the boundary and interface friction, the internal walls and flanges of the two halves of the shear boxes were thoroughly cleaned, and coated with several layers of Teflon or Silicone lubricant. The boxes were then placed on the flat surface of a concrete compaction block. Four raiser plates, a saturated porous stone, and a filter paper filled the the bottom of the box to render the required height. Three strips of 2.54 cm wide and 25.4 cm long Bidim U64 geotextile were cut and sprayed with the lubricant. These strips were used to fill in the gap over the flanges which was created by the reinforcement when it was inserted between the boxes. These strips prevented loose soil from escaping. A reinforcement clamp was mounted on the leading edge of the bottom half of the shear box.

The two halves of the shear boxes were secured together, and the internal dimensions of the box were measured by a pair of vernier calipers at the mid-point of the four sides of the box. The vernier calipers can measure to the accuracy of 0.02 mm. The box was separated; the reinforcement was inserted and held in place. The three strips of U64 geotextile were taped on the flanges of the lower box. The two halves were clamped together, and the internal dimensions were measured again. The reinforcement and the U64 were then removed, and the boxes were placed together for compaction.

Approximately 5.5 kg of loose clay soil was weighed and placed in the box. The soil was compacted by applying the blows in four series of 16 blows. To determine the thickness of the compacted layer, an average depth was measured from the top of the upper box to the surface of the compacted layer along the four sides of the box. The thickness of the sample was calculated by substracting the four measured depths from the heights of the box. Subsequently, the wet density of the first layer was determined.

Next the upper box was removed, and approximately 3.5 kg of loose soil was placed on top of the compacted layer. The loose soil was slightly packed and levelled by a hand trowel. The graded soil projected about 10 mm above the top of the bottom box, so that after compaction the surface of the reinforcement would lie within the fixed shear plane of the apparatus.

One end of the reinforcement was clamped on the leading edge, and the free end was laid flat inside the box on top of the levelled soil. The three strips of U64 geotextile were taped on the flanges of the bottom box. The two boxes were tightened together by three threaded locating pins. Another 2.5 kg of loose soil was placed on top of the reinforcement and compaction was resumed. The internal measurements were taken again, and the corresponding thickness and wet density of the two compacted layers were calculated and corrected with the

density of the reinforcement.

The final 5.50 kg of loose soil was placed and compacted to achieve the total thickness of approximately 9.7 cm. The total wet density of the reinforced sample was calculated. The compacted water content of each layer was determined from the loose soil used for each individual layer.

The surface of the final compacted layer was graded to provide a relatively flat surface. The filter paper and porous stone and loading plate were placed inside the box. A hydraulic crane was used to lift the shear box from the concrete block and position it inside the shear apparatus.

4.3.4.3 Consolidation Stage

The load transducer was placed on the center of the loading plate, and an LVDT was positioned on every quarter of the plate. Initial readings were recorded by the datalogger, and the time interval for automatic readings was set. The required normal pressure was gradually applied by the diaphragm air cylinder which was monitored and transmitted by the load transducer to the sample. The vertical compression was measured by the LVDTs and recorded by the datalogger. To prevent evaporation of moisture from the soil during consolidation, layers of Saran Wrap were used to cover the shear box and the outer box. The consolidation stage was discontinued when the primary consolidation had been

completed.

4.3.4.4 Shearing Stage

All the slack was removed from the system by reseting the proving ring without appling shear load to the sample. Four spacer screws were inserted in their holes. The locating pins were loosened so that a 2.5 mm spacing between the two halves of the boxes could be achieved by winding all the screws the same number of turns. After the required gap was obtained, the spacer screws and the locating pins were removed, and the gap was checked to ensure that the two halves of the boxes were still separated. A guide bearing was clamped on each side of the flanges of the upper shear box to prevent the box from tilting.

The normal pressure was checked, and the initial readings of the LVDTs and proving ring were recorded. The direct shear machine was set to shear the sample at a rate of 3.05 mm/min. Readings of the horizontal displacement, changes of sample height, and shear force were gathered and recorded by the datalogger at specified time intervals.

Shearing was ceased when the shear force became constant, or passed through its peak and decreased to a constant residual value. The normal pressure and the measuring devices were removed and the entire shear box was lifted out of the shear apparatus. The loading plate, porous stone, and filter paper were removed, and

the upper box was dislodged from the reinforced sample. The relative position of the soil-reinforcement interface and the intended shear plane was checked visually. Then the sample was taken out from the box and a soil specimen was removed from each layer to determine the water content after the test.

Bidim U64 geotextile was not required for the shear test of the reinforcement P600 geotextile because the thickness of the geotextile was too small to create any separation when inserted between the boxes. The same test procedure was used for the unreinforced soil with the omission of inserting the reinforcement and U64 strips.

4.3.5 Silty Sand

The hygroscopic water content of the sand sample was determined for each test. Since the silty sand was tested in the air-dried condition, there was no mixing or curing required.

A 2.5 kg hammar with a 10.2 cm^2 steel foot was used to compact the three layers of sand. To obtain the dry density of 1.76 g/cm^3, 64 blows per layer were applied to the soil.

The compaction and test procedures employed to compact the sand were similar to those described in section 4.2.2.2 for the silty clay except that 5.35 kg, 5.41 kg, and 5.35 kg of loose soil were placed respectively for the first, second, and third layers.

5. TEST RESULTS FOR REINFORCED SAND

5.1 Introduction

The modified direct shear apparatus described in the previous chapter was used to determine the interface properties for sand with four types of geogrids and one type of geotextile. The results of this test program are presented and analyzed in this chapter. The influence of the construction and geometry of the reinforcement on the interfacial shear strength is examined. Other factors that may cause reduction in strength are discussed.

A total of 35 consolidated drained tests were performed. Ten preliminary tests were conducted during the modification of the shear apparatus and the development of test procedures. The remaining 25 tests were performed using the modified apparatus. Data for each set of tests are presented in Appendix C (Tables C.1 to C.4).

5.2 Shear Stress and Displacement Behaviour

Two sets of curves showing the typical shear stress-displacement behaviour of the unreinforced sand and the sand reinforced with SR2 are provided in Figures 5.1 and 5.2. Other shear stress-displacement curves for sand reinforced with SS2, TNX-5001, ParaGrid 50S, and P600 are shown in Figures C.1 through C.5. All shear stress-displacement curves of the dynamically compacted sand exhibited strain-softening behaviour at all stress levels

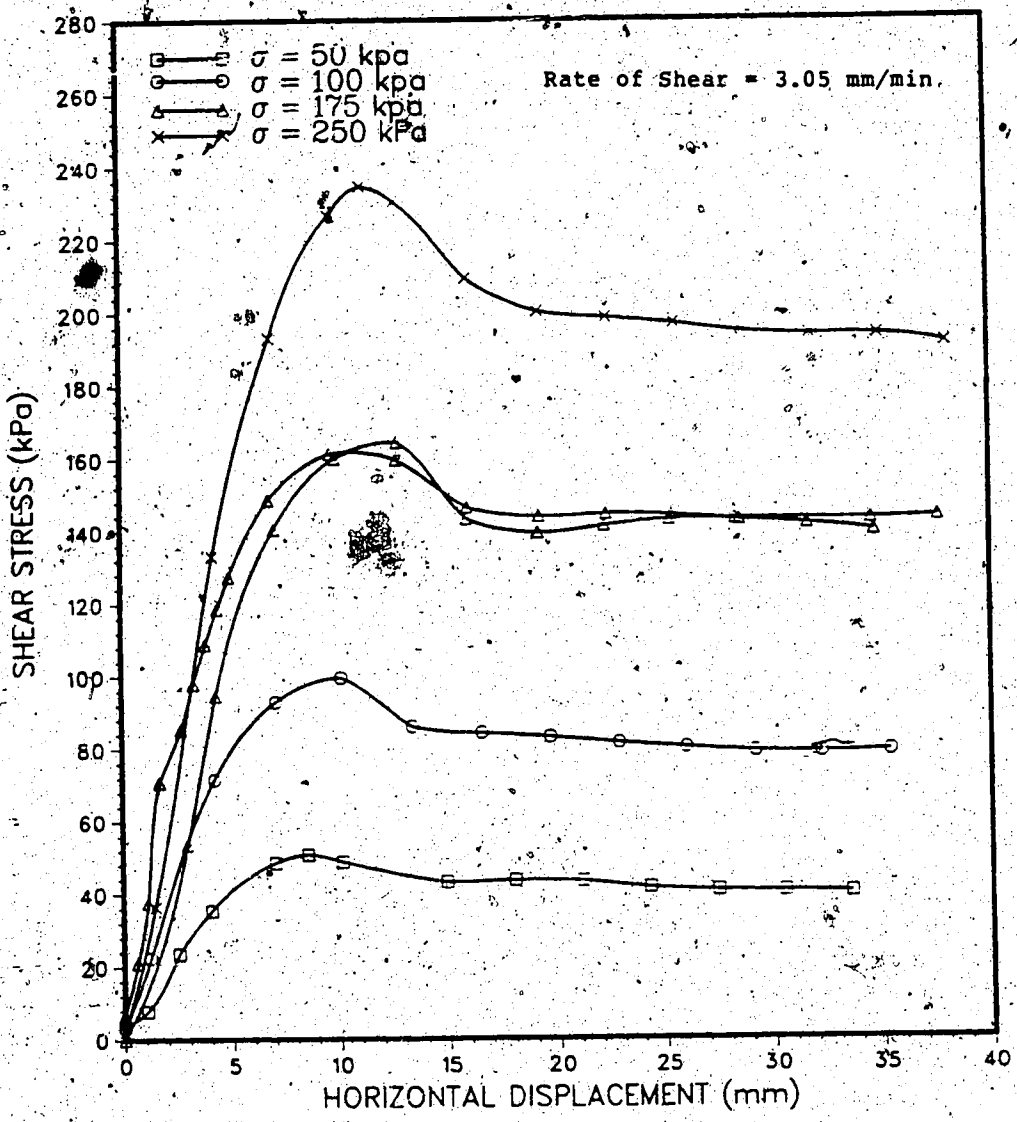

Figure 5.1 Shear Stress and Deformation Curves for Unreinforced Sand

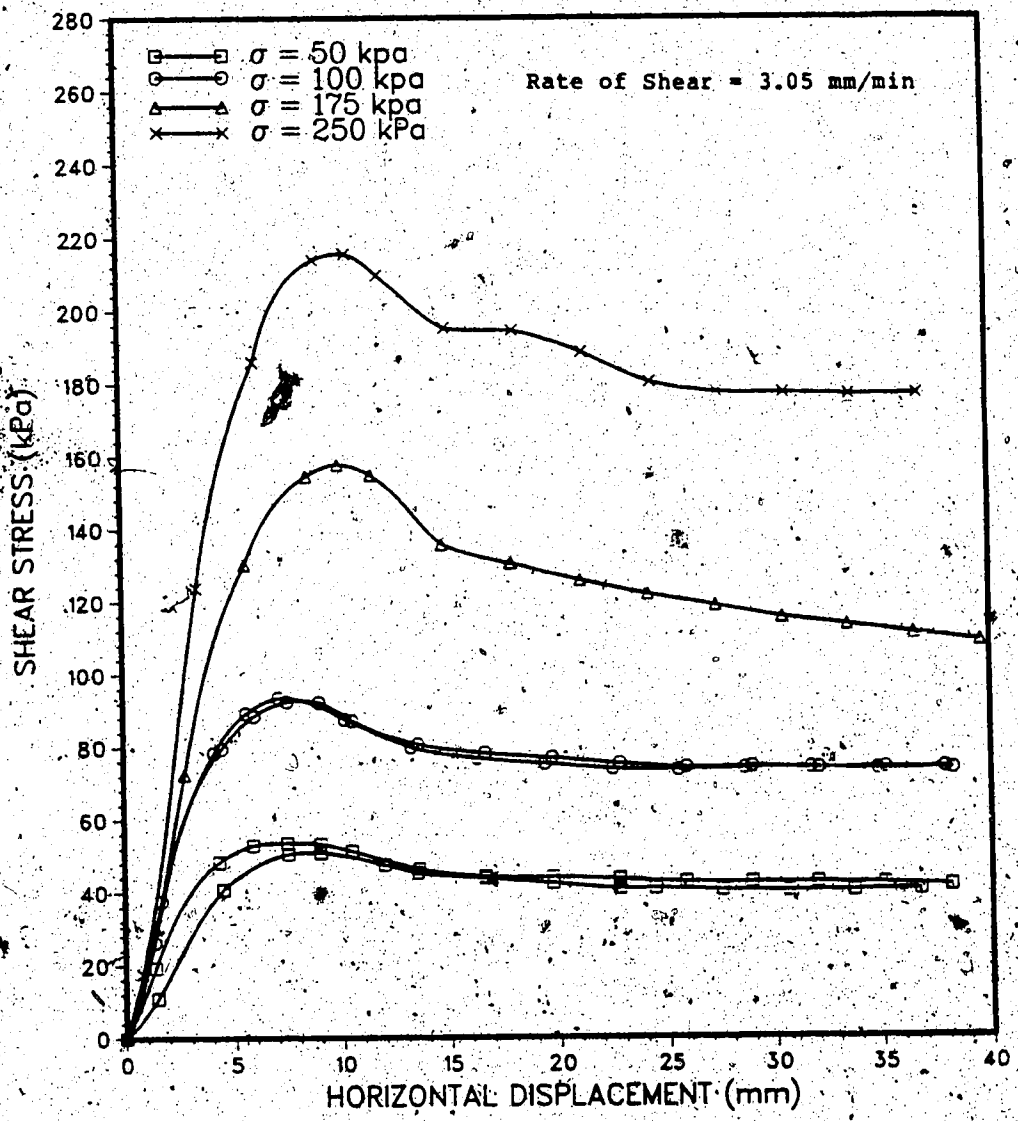

Figure 5.2 Shear Stress and Deformation Curves for Sand Reinforced with Geogrid SR2

independent of the type of reinforcement. The shear stress developed rapidly to a well-defined peak value before decreasing to a constant value for both unreinforced and reinforced samples.

The amount of horizontal displacement required to mobilize the peak shear stress ranges from 5.5 mm to 12.4 mm. The displacement at peak shear stress increases with increasing normal stress, but for a given stress level the displacement to peak is approximately the same for both unreinforced and reinforced samples. Sand reinforced geogrids mobilized peak strength at similar displacements; the woven geotextile, P600, reached peak strength at smaller horizontal deformations (5.5 to 8.1 mm) than did the geogrids. It is possible that the smaller deformation was attributed to the rough surface texture and the planarity of P600 which may require a smaller amount of particle reorientation to mobilize the peak strength.

The residual shear stress values are attained when the horizontal displacement reaches 15 to 20 mm. Again, smaller amounts of shear displacement (7.0 to 12.0 mm) are mobilized for the residual values of P600.

5.3 Volume Change Behaviour

The vertical versus horizontal displacement plots are presented in Figures 5.3 and 5.4; others are shown in Figures C.5 to C.8. The curves are typical for dense samples, that is, they show a small initial compression

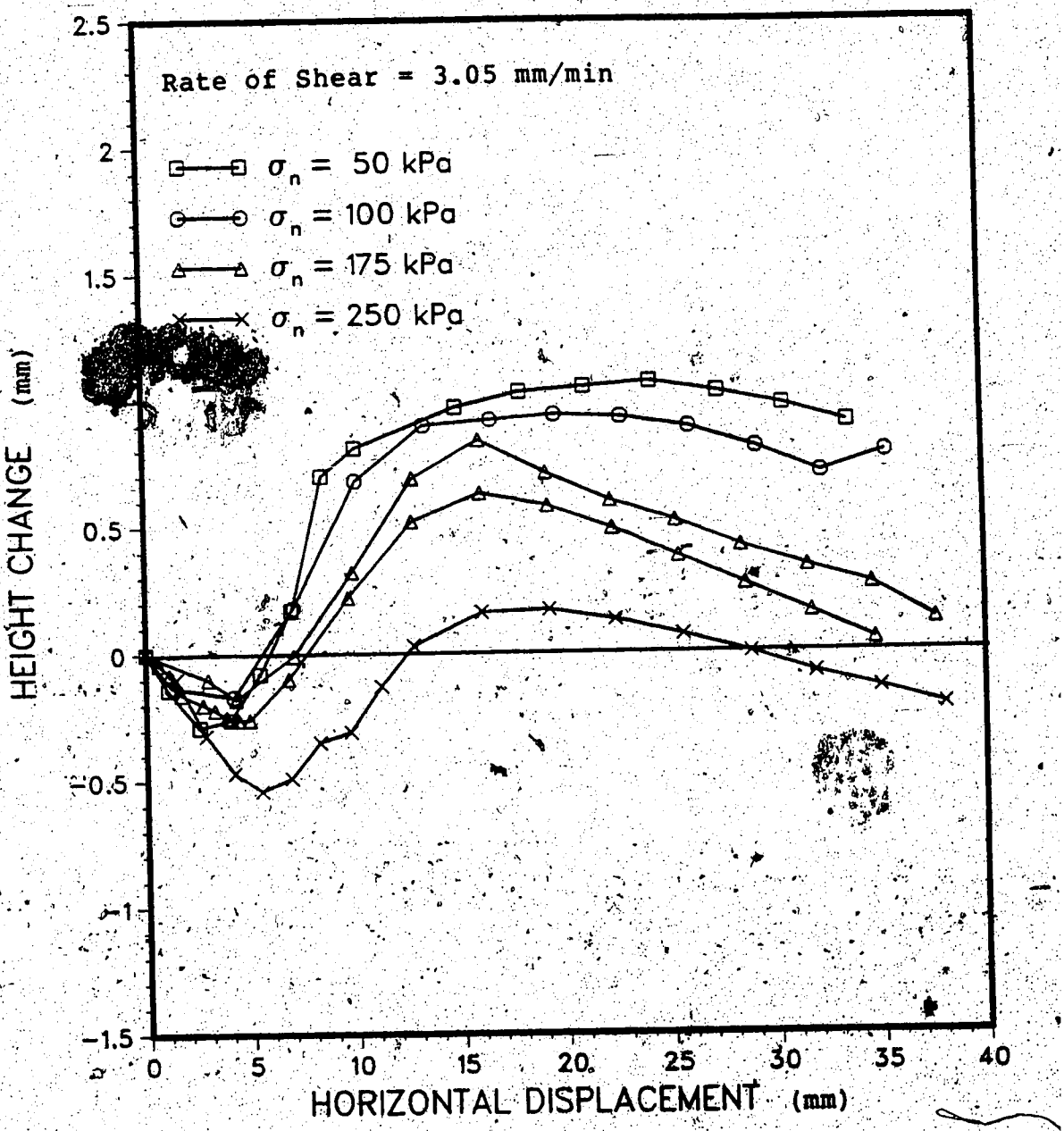

Figure 5.3 Vertical and Horizontal Displacement Curves for Unreinforced Sand

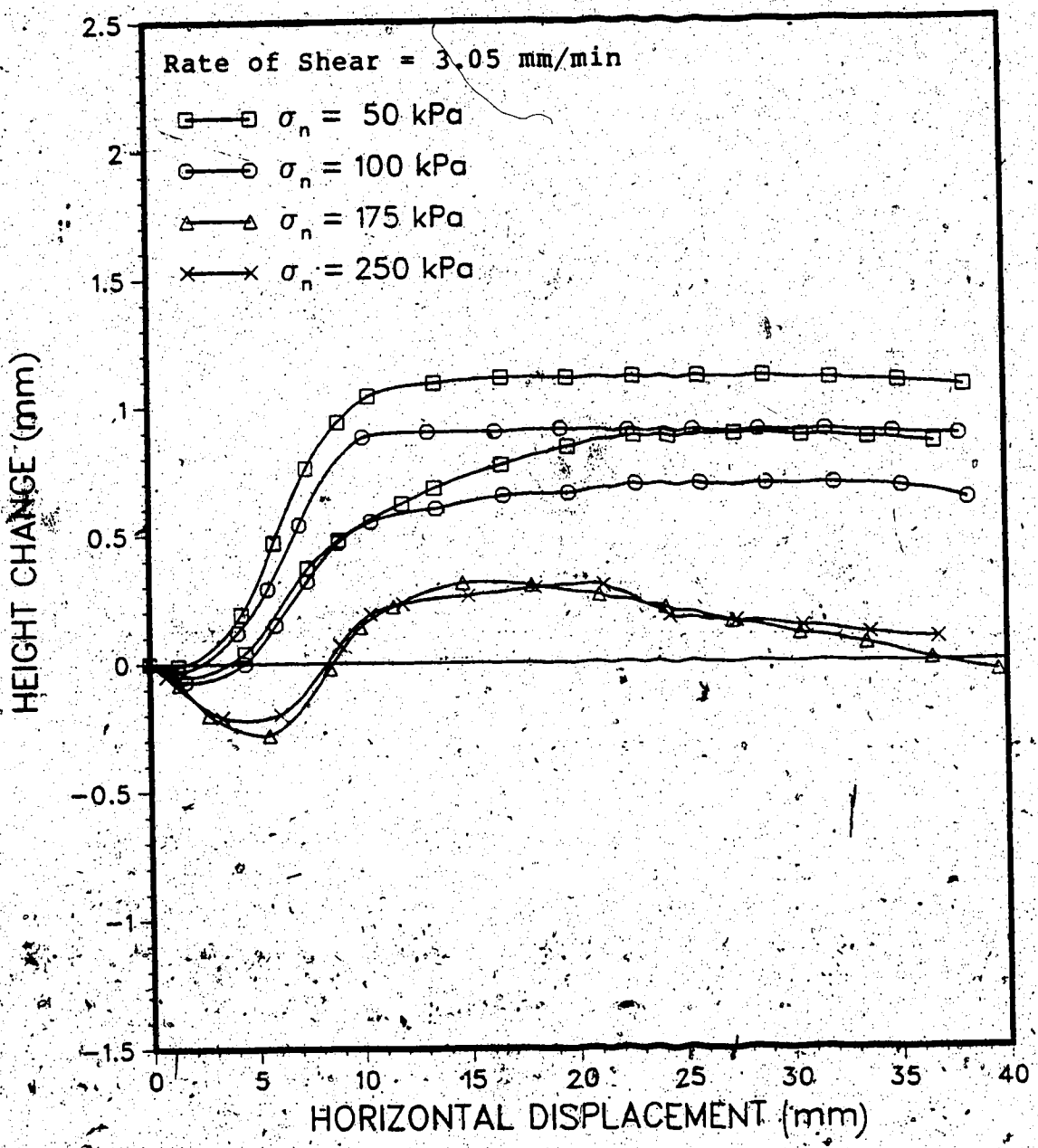

Figure 5.4 Vertical and Horizontal Displacement Curves for Sand Reinforced with Geogrid SR2

followed by rapid dilation. The following observations are evident from the volume change curves:

1. In general, a greater degree of dilation occurs with geogrid reinforced sand compared to that of the geotextile reinforced sand. This suggests that the large aperture of the geogrids allows a greater amount of soil to soil interlocking which results in the larger amount of dilation. P600, with its closely spaced yarns, allows a smaller degree of expansion.
2. Specimens attain peak shear stress when the dilatancy rate is at a maximum. Generally, as the normal stress increases, the dilatancy rate and the magnitude of the overall specimen expansion decreases.
3. For a given normal stress, the overall specimen expansion rates are smaller for reinforced sand than for unreinforced sand. This decrease is more pronounced with P600 because of the limited amount of soil to soil interaction.

5.4 Peak Shear Strength

The peak and residual shear stress envelopes for the reinforced sand are plotted in Figures C.9 to C.14. The plots of peak shear stress against normal stress indicate linear relationships for both reinforced sand and unreinforced sand. The peak total angle of interfacial

friction is slightly lower for reinforced sand. Among the reinforced sand samples, the peak angle of interfacial friction is higher for the geogrid reinforcing (40.0° to 41.5°) than for the geotextile (36.2°).

In some cases a small interfacial cohesion or adhesion intercept is attained when the shear strength envelope is projected back to zero effective normal stress. No physical meaning can be attached to the cohesion intercept suggested by this extrapolation. It has been found that this intercept is uncertain unless tests are performed at a very low effective stress and is thus commonly ignored (Lamb and Whitman 1976; Mitchell 1976). For the test results shown here, the intercepts are assumed to be experimental errors and are not discussed further.

5.5 Residual Shear Strength

The residual or constant volume value of shear strength is measured when the specimen has undergone a large horizontal deformation without further volume change or strength gain. The plots of the residual value of shear stress versus normal stress also indicate linear relationships (Figures C.9 to C.14). The residual angle of interfacial friction is lower for the reinforced sand than for the unreinforced sand.

5.6 Efficiency Values

The peak and residual values of efficiency for both unreinforced and reinforced sand are summarized in Figures 5.5 and 5.6. The efficiency is given by

$$E = \frac{\tan \delta'_T}{\tan \phi'} \qquad [5.1]$$

where,

δ'_T = the effective total angle of interfacial friction between the reinforcement and the sand.

ϕ' = the effective angle of internal friction of the unreinforced sand.

The peak efficiency values range from 0.75 to 1.04 with a geogrid efficiency of 0.95 ± 0.04. The highest E corresponds to the geogrid TNX-5001 while the lowest E corresponds to the geotextile P600. As shown in Figure 5.7 the high efficiency value of the geogrid can be attributed to the extensive soil to soil interaction through the apertures. This implies that geogrids do not represent significant planes of weakness within a compacted granular fill. The slightly lower efficiency values indicate that the roughness of P600 did not provide adequate soil and reinforcement interaction to force the shear plane into the adjacent soil layer. The geotextile may represent a more potential sliding plane within a granular fill than a geogrid.

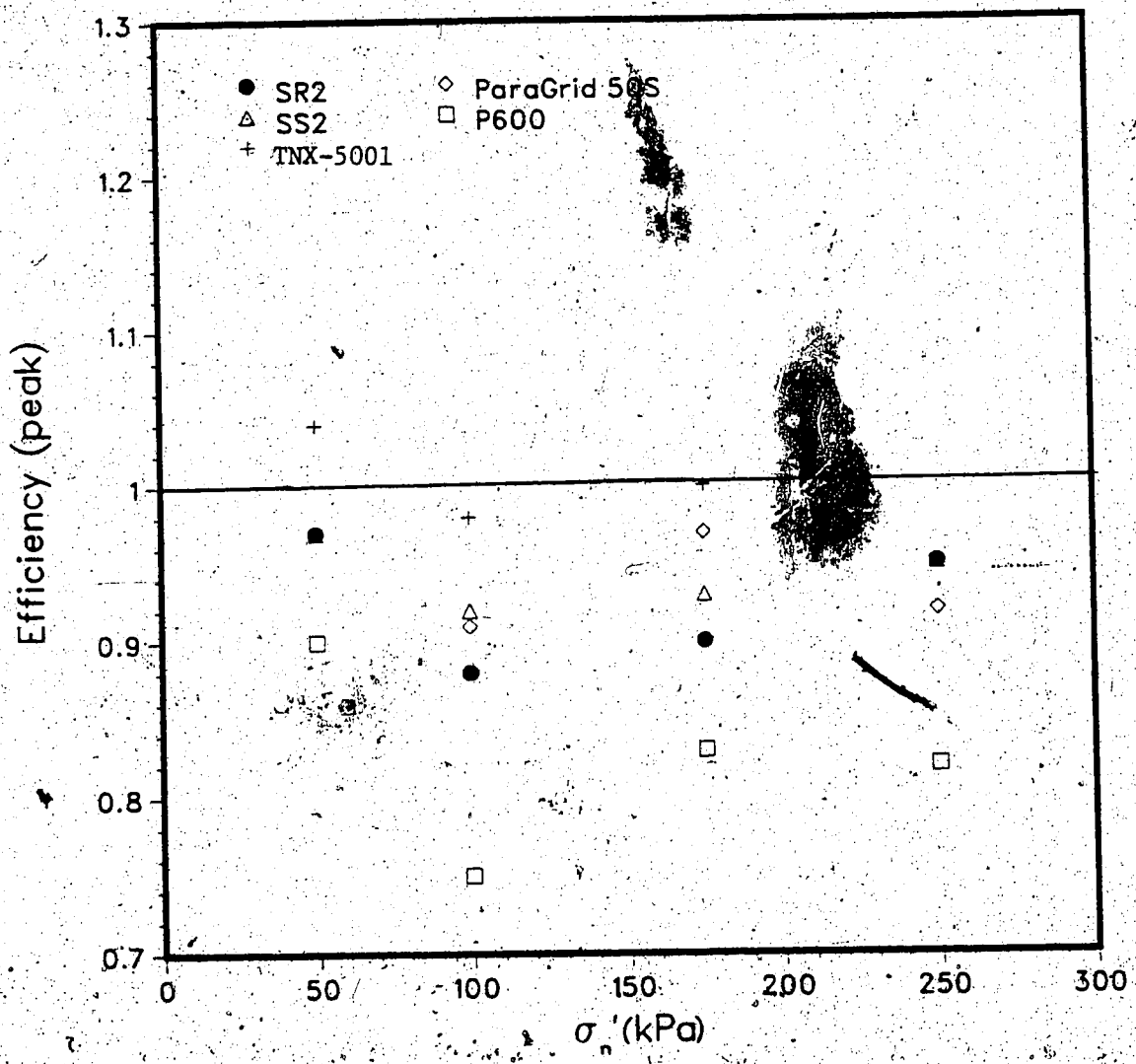

Figure 5.5 Peak Efficiencies of Sand Reinforced by Geogrids and a Geotextile

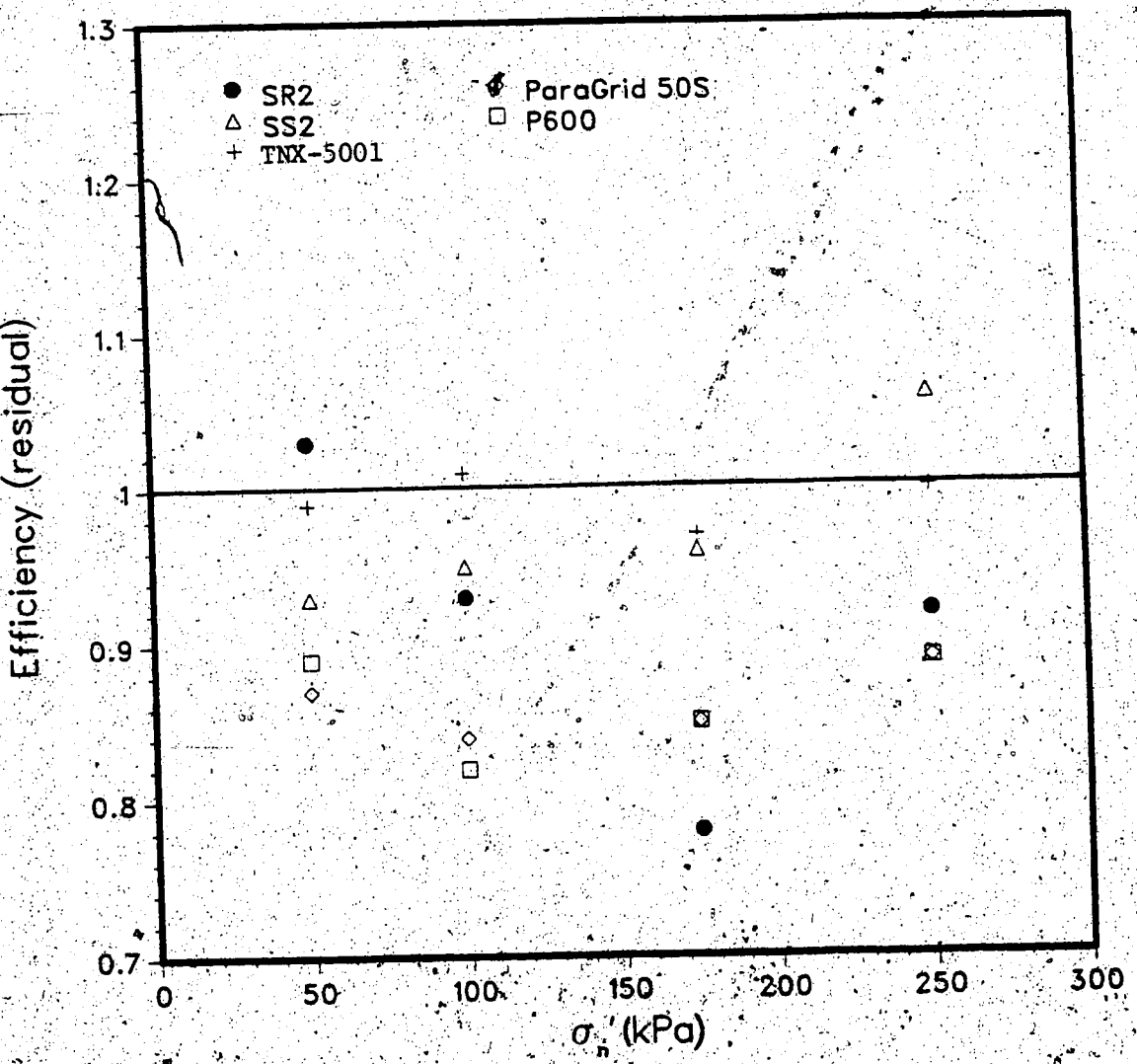

Figure 5.6 Residual Efficiencies of Sand Reinforced by Geogrids and a Geotextile

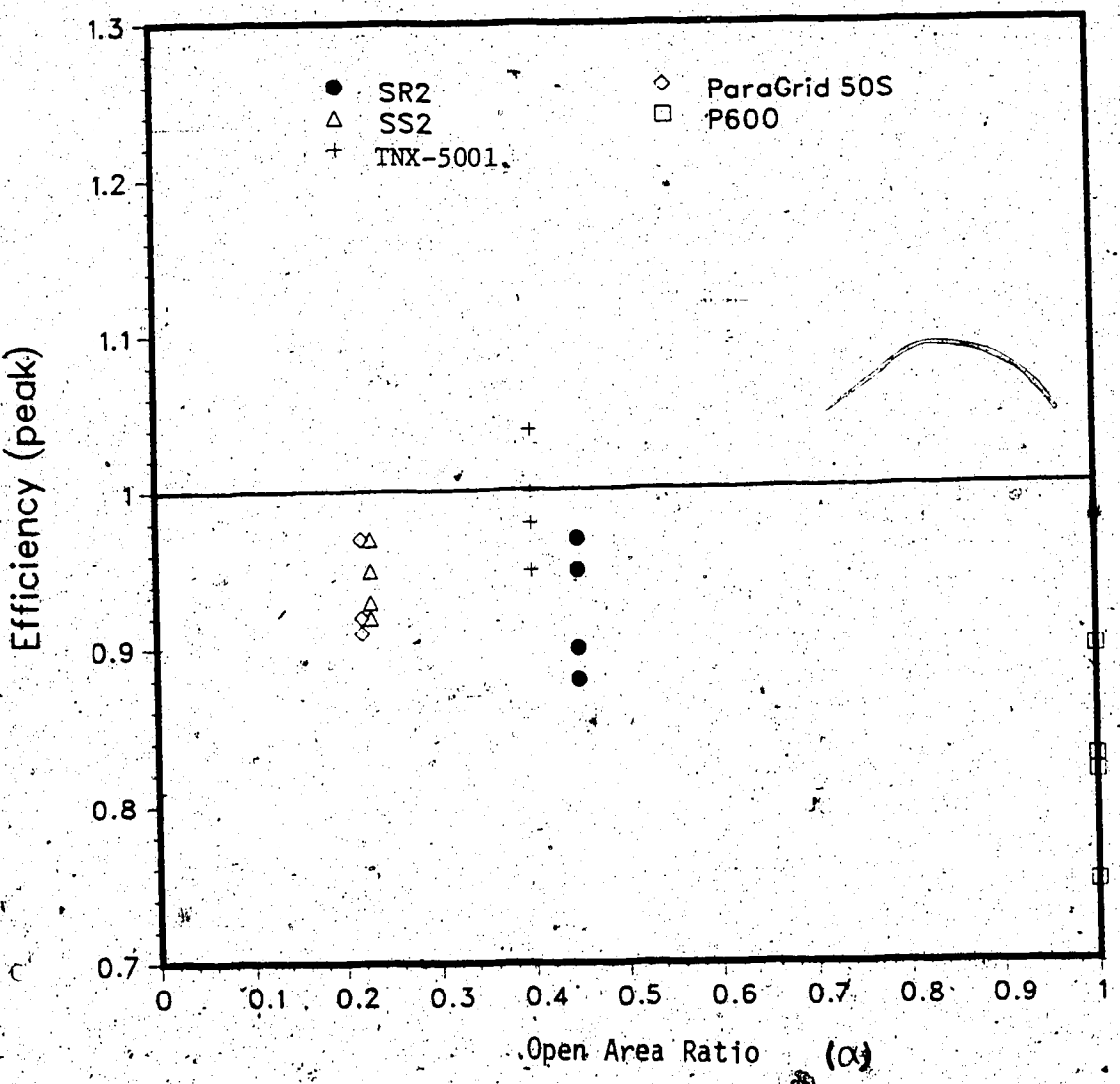

Figure 5.7 Influence of the Open Area Ratio in Geogrid and Geotextile on Peak Efficiencies

The residual efficiency values vary between 0.78 and 1.06. The largest reduction between the peak and residual efficiency is shown by ParaGrid 50S. Its residual efficiencies are very close to that of P600.

5.7 Effects of Reinforcement Properties

5.7.1 Peak Strength

Research reported in Chapter 2 shows that interfacial shear strength is primarily a function of soil and reinforcement properties. Since only one type of granular soil was tested and all experiments were conducted in the same manner, the effect of reinforcement properties such as the percent of open area, the aperture shape, the aperture dimensions, and the surface roughness can be studied by comparing the various interfacial shear strengths.

The symbol a denotes the ratio of the solid area of the reinforcement to the total area of the reinforcement. Since the geogrids SR2 and TNX-5001 have similar a values (0.45 and 0.42), their shear envelopes can be compared first to study the influence of the dimensions of the apertures, the surface texture, and the planarity on the interfacial shear strength. Second, a similar comparison of properties of the geogrids SS2 and ParaGrid 50S is made. Finally, the shear strength envelope of P600, a geotextile, is compared with the geogrids to give an overall assessment of the influence of these properties on the interfacial friction.

Figure 5.8 shows that the peak interfacial shear strength envelopes of reinforced sand are less than the effective internal friction angle of the sand itself. Comparing the two geogrids, the interfacial shear strength of TNX-5001 (41.5°) is very close to that of sand (42.5°). The total angle of interfacial friction of SR2 is 40.0°. The overall efficiency values for TNX-5001 and SR2 are 0.97 and 0.92. In contrast, P600 displays the lowest total angle of interfacial friction (36.2°) and has an average efficiency value of 0.80.

Although the geogrids TNX-5001 and SR2 have similar a values and similar aperture shapes, the aperture dimensions are different. The area of the aperture of TNX-5001 is 1.6 times larger than SR2. It seems from the results that the fewer, larger apertures of TNX-5001 may have provided a greater amount of soil to soil interaction compared to that of SR2. This may cause the slightly higher interfacial shear strength. Therefore, the interfacial friction is not only a function of the percent of open area but is also a function of the dimensions of the apertures. Similar conclusions have been drawn by other researchers (Collios et al. 1980; Jewell et al. 1984; Williams and Houlihan 1987).

Jewell et al. (1984) and Sarsby (1985) have found from their results that there was a relationship between efficiency and the ratio of aperture width to D_{50} of soil. Specifically, they found that the highest efficiency value was reached when the ratio was 3.5. To further investigate

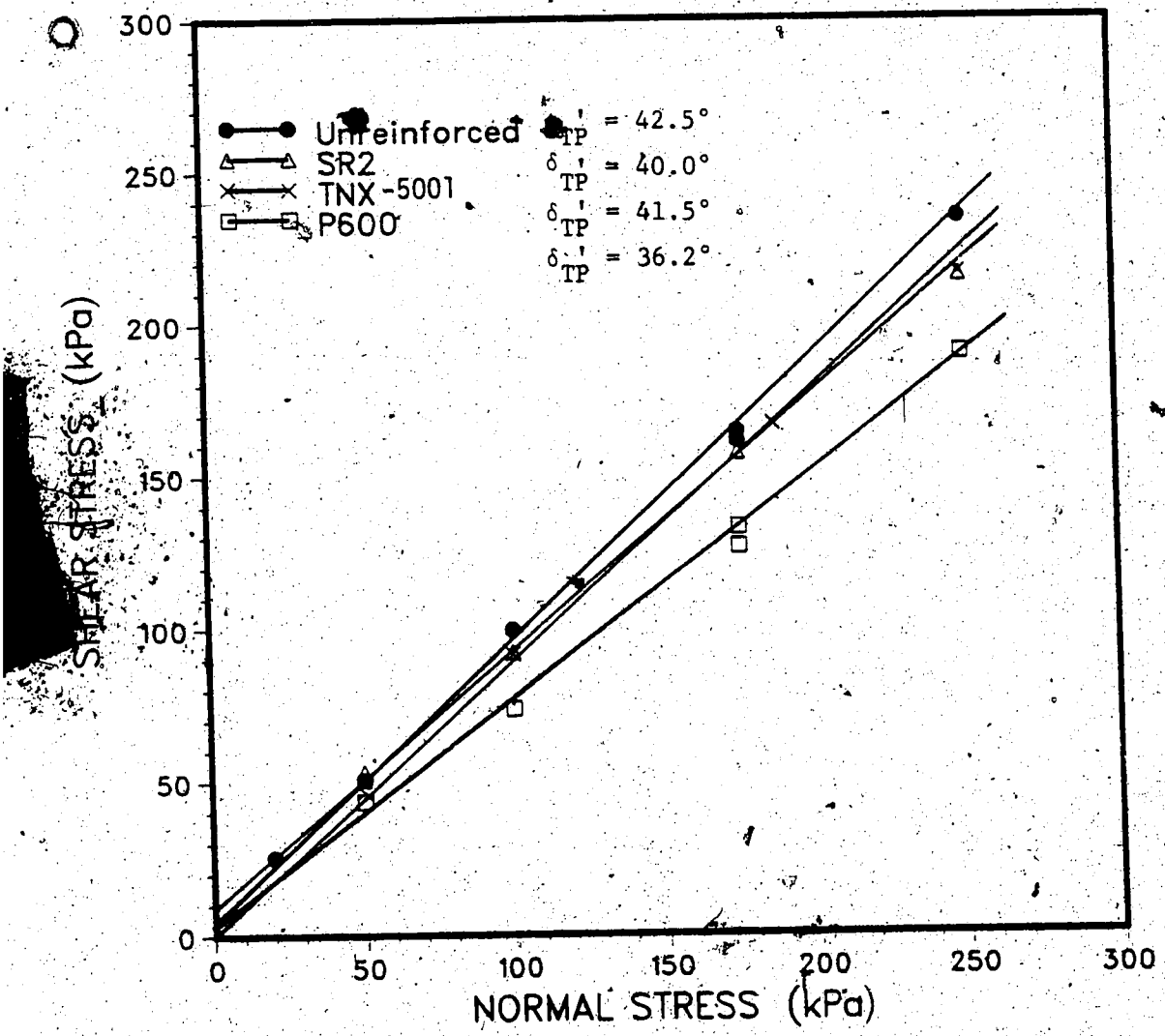

Figure 5.8 Peak Interfacial Shear Strength Envelopes of Reinforced Sand

the effect of aperture dimension on the interfacial strength, the peak efficiency is plotted against the ratio of the aperture width to D_{50} of the sand. Figure 5.9 demonstrates that some of the efficiency values of the geogrids tested in this program are slightly higher than those of Jewell and Sarsby. The efficiency values appear to be relatively constant over the range of tested aperture widths. Thus, it appears that when the soil particles are small compared to the aperture width of the reinforcement, the aperture width has little influence on the interfacial friction.

The surface texture of the two geogrids are alike except that the surface of TNX-5001 is smoother and harder than SR2. It appears from the results that the small difference in surface properties is not significant enough to cause any difference in strength. Thus, the sightly smoother surface has no apparent effect on the strength.

One difference between the properties of the two geogrids is their planarity. The ratio of the thickness of the anchor member to the tension member of SR2 is 3.74 and of TNX-5001 is 2.0. The difference in thickness of the geogrids indicate that TNX-5001 has a more plannar surface compared to SR2. One possible influence of the variation in thickness is that the shear surface may not coincide with the surface of the SR2. Due to the test conditions, it was not possible to examine the shear surface of the reinforced sand. However, the examination of the shear surface of the

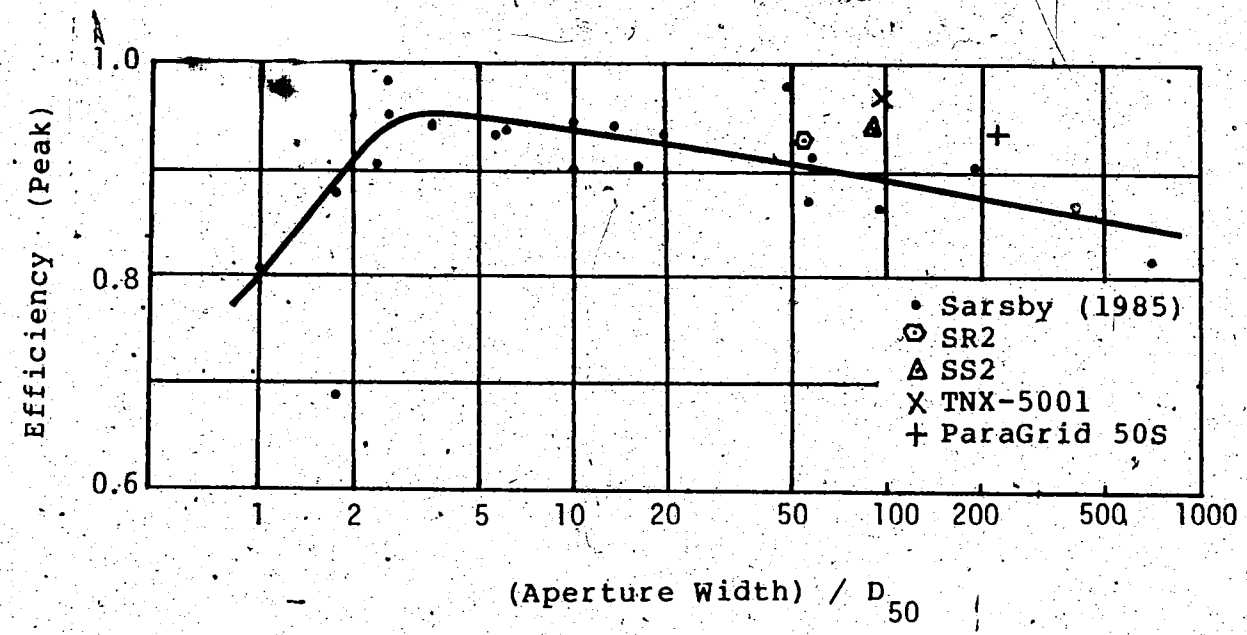

Figure 5.9 Influence of Aperture Dimension on the Peak Efficiency

reinforced clay tests showed that the shearing was taken place along the soil and reinforcement interface. The planarity of geogrids has little effect on the interfacial shear strength.

Figure 5.10 presents the peak interfacial shear strength envelopes for sand with ParaGrid 50S, SS2, and P600. Unlike TNX-5001 and SR2, there is no difference in the total angles of interfacial friction between ParaGrid 50S and SS2. The overall efficiencies are 0.93 and 0.94. The lowest interfacial friction is shown by P600.

In many ways the physical properties of the two geogrids are similar. Besides having similar α values (0.22 and 0.23) and similar aperture shapes, the planarity, and the stiffness of the two geogrids are also alike. Similar deformations to peak strength and efficiency values were found.

One difference between the two geogrids is the aperture dimensions. The ParaGrid 50S aperture size is larger than that for SS2; the area of the aperture of ParaGrid 50S is 5.2 times larger than SS2. Since the ratio of the solid area of the reinforcement to the total area of the reinforcement is small, the majority of the total area of the reinforcement consists of openings. For this reason, the aperture dimensions do not seem to have a significant effect on the interfacial friction (Figure 5.9).

Another difference between the two geogrids is that SS2 has a smooth surface while ParaGrid 50S has an embossed

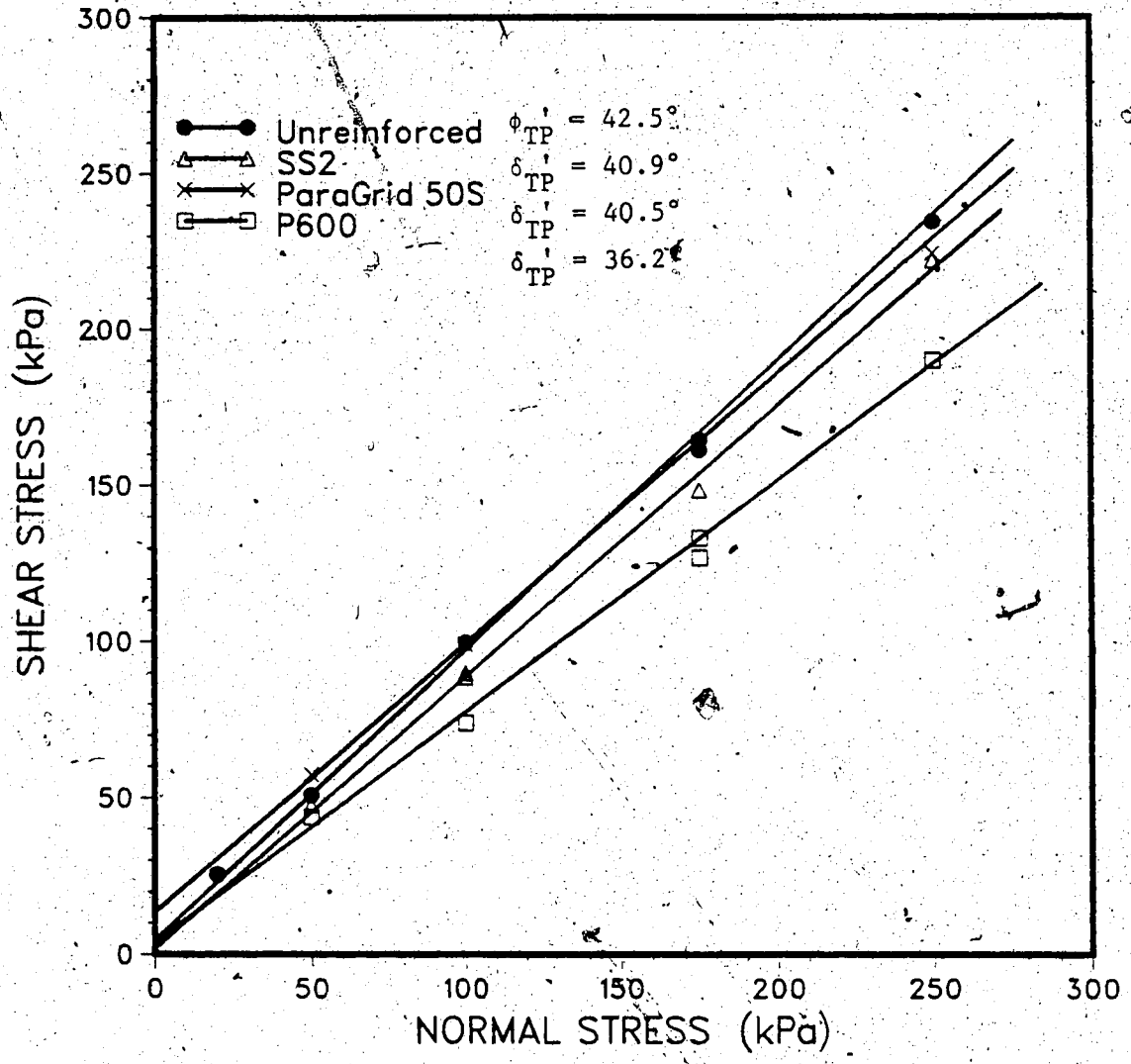

Figure 5.10 Peak Interfacial Shear Strength Envelopes of Reinforced Sand

surface. Thus, the effect of surface texture may be examined.

A close examination of the surface of ParaGrid 50S after testing revealed that sand fills the voids of the embossed surface. Thus, in addition to the soil to soil interaction in the apertures, additional soil to geogrid interlocking is generated through the filling of the voids. However, this additional interlocking has not made a significant contribution to the interfacial friction since the interfacial shear strength of ParaGrid 50S was not higher than SS2.

From the comparison of the strength envelopes of the geogrids it appears that when more than 50% of the total area consists of openings, the aperture dimensions and the embossed surface do not have a significant influence on the interfacial friction.

P600 with an a value of 1.00 exhibits relatively high values of efficiency (an average value of 0.80) in comparison to the geogrids. In theory the a value of 1.00 represents a case of a solid sheet of reinforcement. However, when the surface was examined after the tests, sand grains were found embedded in the tiny openings between the yarns. Although the openings (150 to 500 μm) are extremely small compared to the aperture size of the geogrids, it appears that their presence are important in providing soil to soil interaction.

In addition, P600 has a rough surface which contributes to the mobilization of the frictional strength during shear. Hence, the moderately high interfacial friction is due to the rough surface texture of the geotextile and the small amount of soil to soil interaction in the tiny openings.

The comparison of the strength envelopes of the geogrids and the geotextile shows that the construction method of the reinforcement and the geometry significantly influence the soil and reinforcement interaction. Consequently, geogrids which permit a greater degree of soil to soil interaction exhibit higher interfacial strength than the woven geotextile.

5.7.2 Residual Strength

For the direct shear condition, the residual effective angle of internal friction is the same as the friction angle measured at the constant volume condition, $\phi'_R = \phi'_{cv}$ (Hanna and Youssef 1987; Jewell and Wroth 1987). Bishop (1971) also expressed ϕ'_R as the difference between the measured peak angle and the corresponding dilation rate (ϕ'_p - arctan $(dv/dh)_p$).

First, the accuracy of the measurements of the friction angle at constant volume conditions will be shown. Second, the frictional strength of both the reinforced and ureinforced sand will be compared to study the cause of a decrease in friction.

Figure 5.11 shows that the directly measured ϕ'_R and δ'_{TR} are in good agreement with the residual friction angles calculated by Bishop's expression. Despite the stress concentrations at the boundaries and consequently the tilting of the loading platen in the direct shear box test, it seems that the boundary measurements accurately recorded the internal state of stress within the specimen.

Figure 5.12 and 5.13 present the residual interfacial shear strength envelopes. Similar to the peak strength behaviour, the residual total angle of interfacial friction δ'_{TR} for reinforced sand (34.1° to 37.9°) is slightly lower than for unreinforced sand (39.1°). The δ'_{TR} value of TNX-5001 (37.9°) is the highest among the geogrids while the δ'_{TR} value of ParaGrid 50S (34.1°) is the lowest and is the same as the geotextile P500. It appears that aperture size and surface roughness have little effect on the residual strength of geogrids. Thus, the residual interfacial strength must be affected by the presence of the solid reinforcement.

5.8 Dilation Strength

Figure 5.14 shows that the boundary measurement of sample expansion during shear decreases with increasing effective normal stress. For the same value of normal stress the dilation of a reinforced sample is less than that of an unreinforced sample. It appears that the dilation rate is reduced by the presence of the reinforcement. To investigate this effect, the influence of the ratio of the solid area of

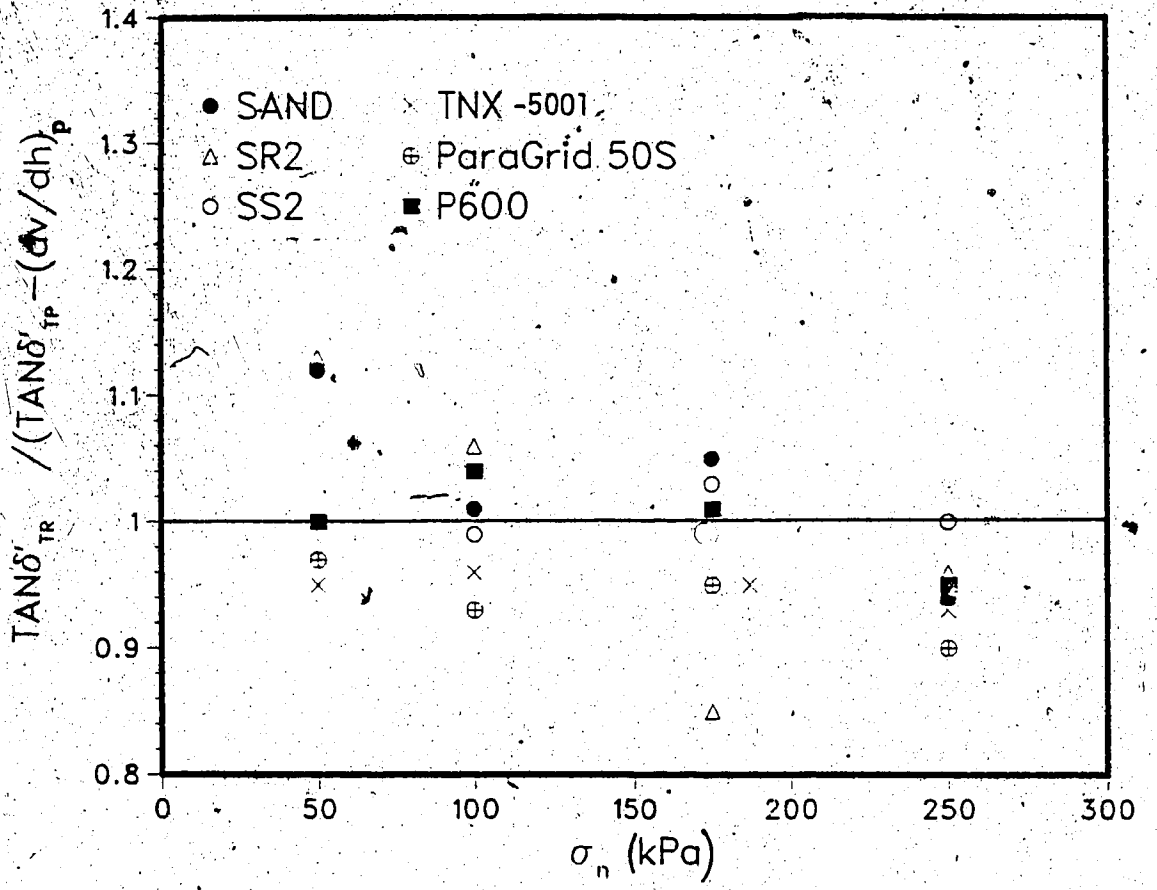

Figure 5.11 Accuracy of the Boundary Measurements of the Direct Shear Box Test

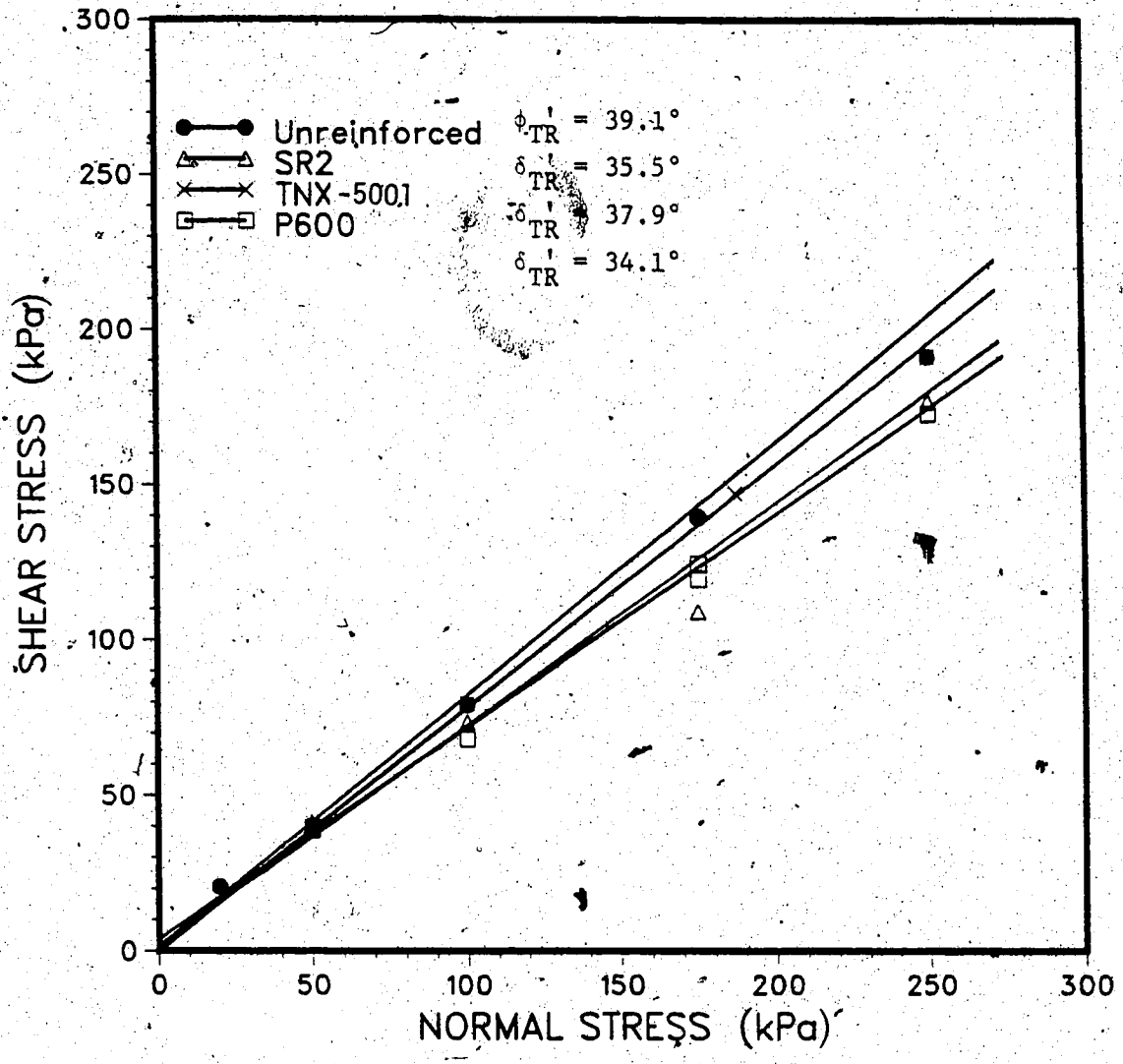

Figure 5.12 Residual Interfacial Shear Strength Envelopes of Reinforced Sand

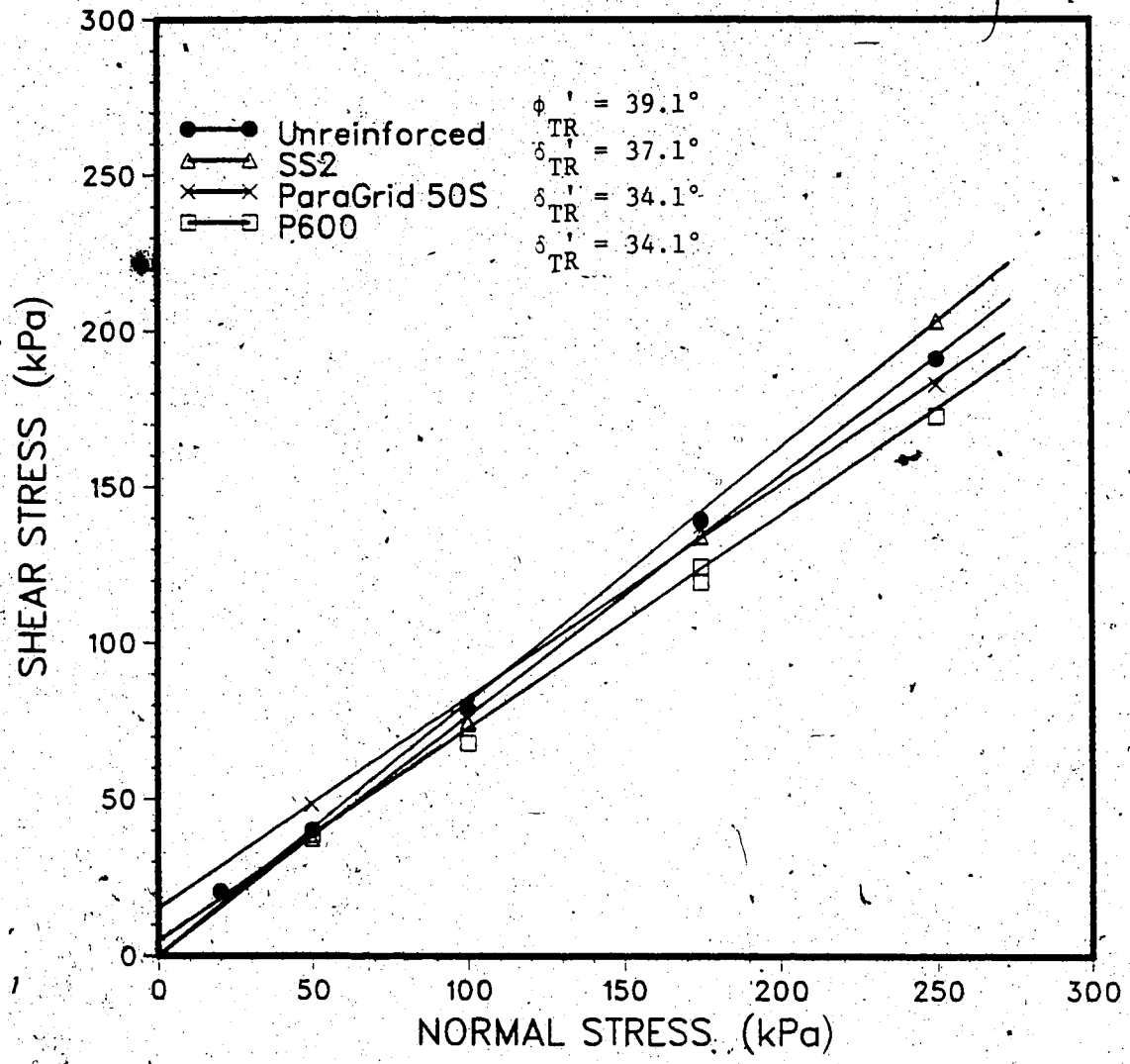

Figure 5.13 Residual Interfacial Shear Strength Envelopes of Reinforced Sand

the reinforcement to the total area of the reinforcement, a, on the dilation rate at peak strength $(dv/dh)_p$ is examined.

Figure 5.15 illustrates that the maximum dilation rate decreases with increasing a. This implies soil expansion occurs predominantly in the apertures of geogrid and little soil expansion takes place on the solid reinforcement. It is possible that less energy is spent to rearrange the soil particles on the solid part of the reinforcement because of its relatively smooth surface compared to the surface of the soil particles. The dilation rate of the reinforced sand is decreased, unless there is a large amount of open area. The greatest reduction in dilation rate occurs when a is equal to 1.00 (P600) which allows very little soil to soil interaction. The dilation rate $(dv/dh)_p$ approaches that of the solid sheet of reinforcement but is not zero.

To examine the effect of the geometry of the reinforcement on the dilation rate, the expansion behaviour of the reinforced samples are compared. ParaGrid 50S has the greatest sample expansion while TNX-5001 exhibits the smallest expansion. In contrast, P600 has the overall lowest dilation rate even though the weave has created a rough contact surface. Thus, the physical characteristics of the reinforcement such as the aperture dimensions and the embossed surface may have some influence in sample dilation.

To investigate the effect of reinforcement planarity on dilation rate, $(dv/dh)_p$ is plotted against the ratio of anchor member or junction thickness to D_{50}. Figure 5.16

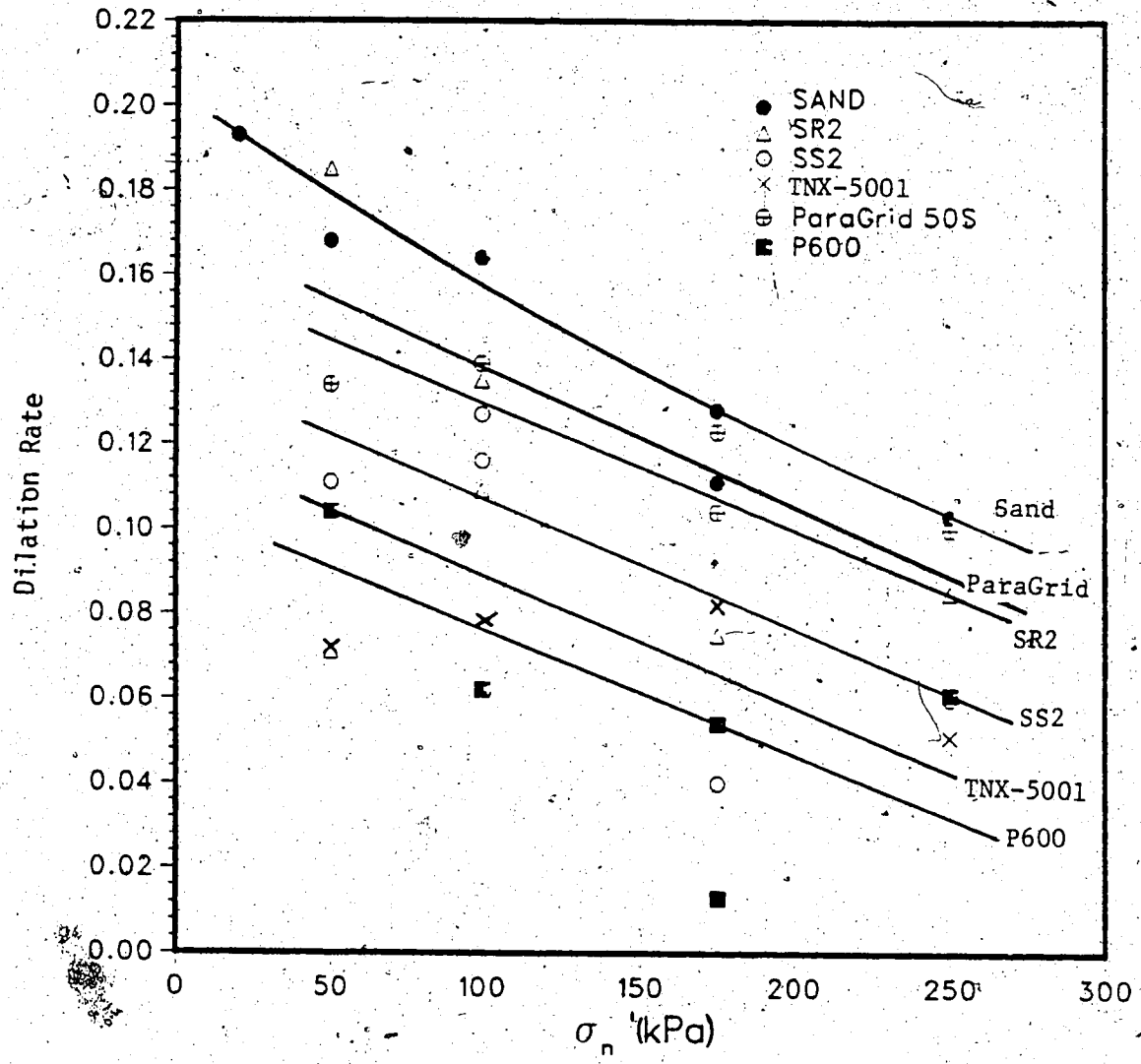

Figure 5.14 Influence of Reinforcement on Dilation Rate

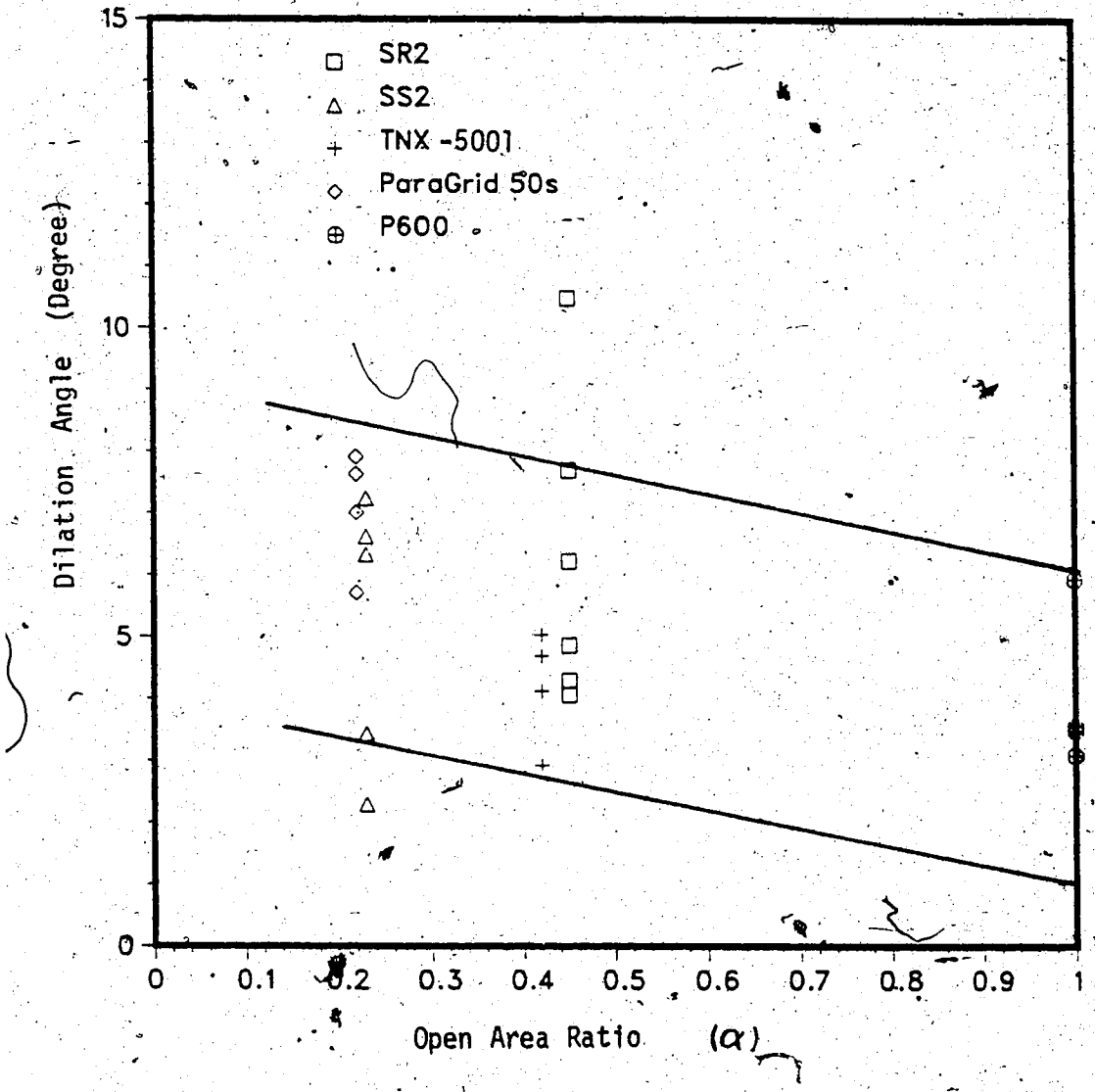

Figure 5.15 Influence of the Open Area Ratio on Dilation Rate

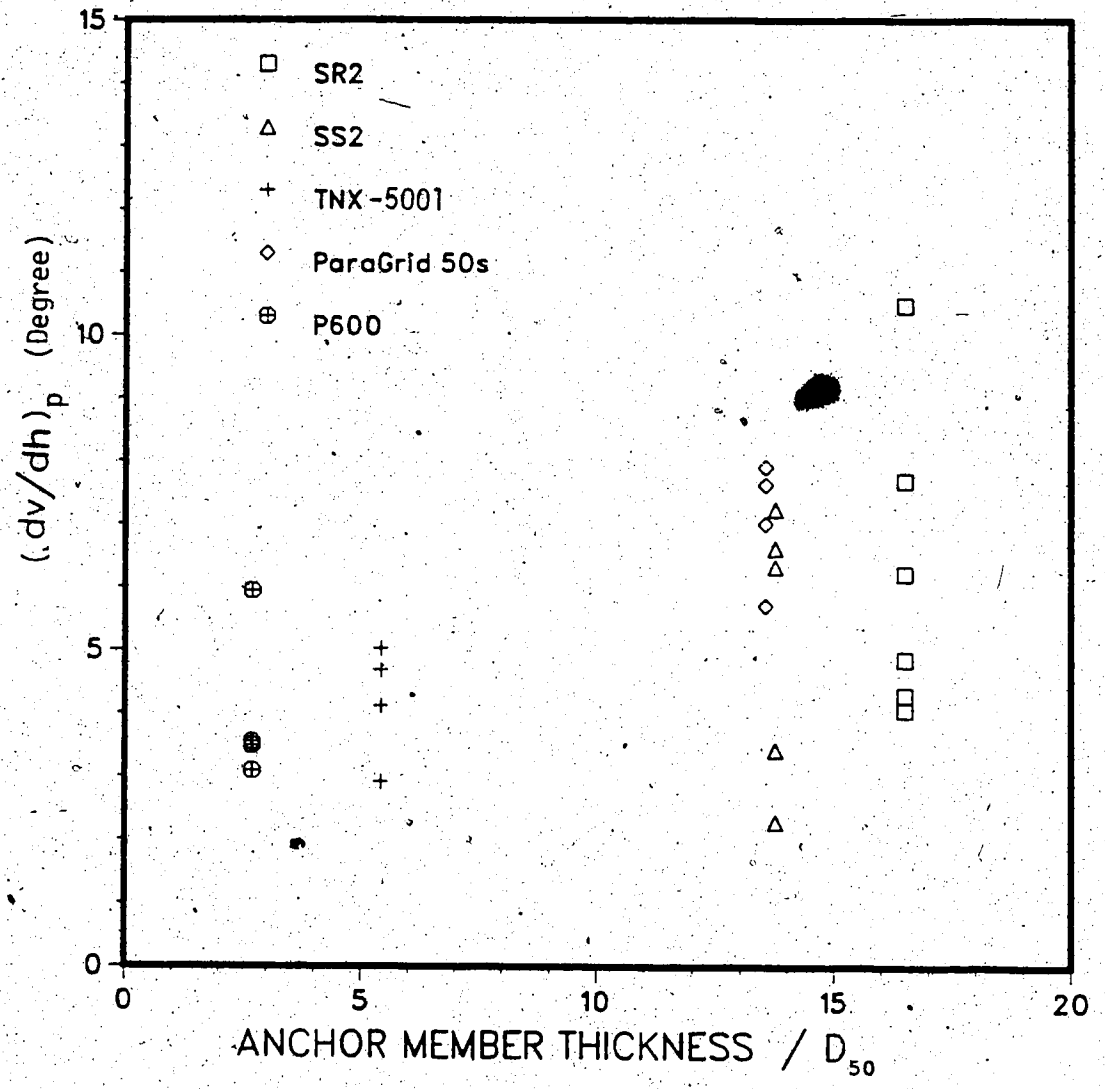

Figure 5.16 Effect of Planarity on Dilation Rate

indicates that the dilation rate increases with increasing junction thickness to D_{50} ratio. It appears that the presence of the junctions becomes significant compared to the small particles; a large amount of volume expansion is required to slide the soil particles over the junctions. The combination of embossed contact surface and planarity gives ParaGrid 50S the high dilation rate.

5.9 Interfacial Friction of Solid Reinforcements

5.9.1 Peak Angles

To date, the two main mechanisms that govern the soil-reinforcement interface shear behaviour have been identified and theoretical equations such as 5.2 have been developed to describe the interaction (Jewell et al. 1984).

$$\tan \delta'_{Tp} = a \tan \delta'_{Gp} + (1-a) \tan \phi'_p \qquad [5.2]$$

where,

δ'_{Tp} = peak total angle of interfacial friction.

a = ratio of solid area of the reinforcement to the total area of the reinforcement.

δ'_{Gp} = peak total angle of interfacial friction of the solid reinforcement.

ϕ'_p = peak effective angle of internal friction.

Equation 5.2 divides the measured total angle of interfacial friction into two parts. It assumes that the interlocking resistance of soil particles occurs only through the apertures ($(1-a)\tan\phi'_p$) and that the shear resistance of soil to the solid surface of the reinforcement takes place only along the tension and anchors members ($a \tan\delta'_{Gp}$). With these assumptions, equation 5.2 may be used to estimate the value of either δ'_{Gp} or δ'_{Tp} for a given type of reinforcement. The calculated δ'_{Gp} may be used to predict the efficiency for a sheet of reinforcement where direct sliding failure is a concern. Alternatively, δ'_{Tp} may be approximated from the known δ'_{Gp} and ϕ'_p for any reinforcement configuration.

Rowe, Ho, and Fisher (1985) conducted pull out tests and direct shear tests to show that equation 5.2 is valid. The reinforcement used was SR2 and the soil was a loosely compacted sand. The results showed that the directly measured δ'_{Tp} was the same as that predicted by equation 5.2.

Figure 5.17 presents the calculated δ'_{Gp} for each type of reinforcement at each normal stress level. Although the calculated δ'_{Gp} is slightly scattered, a general trend of decreasing δ'_{Gp} with increasing effective normal stress is evident. The geogrid TNX-5001 has the highest peak total angle of interfacial friction of the solid reinforcement while the embossed biaxial ParaGrid 50S yields a lower δ'_{Gp}. It appears that even though ParaGrid 50S has an embossed surface, this does not seem to have a significant influence

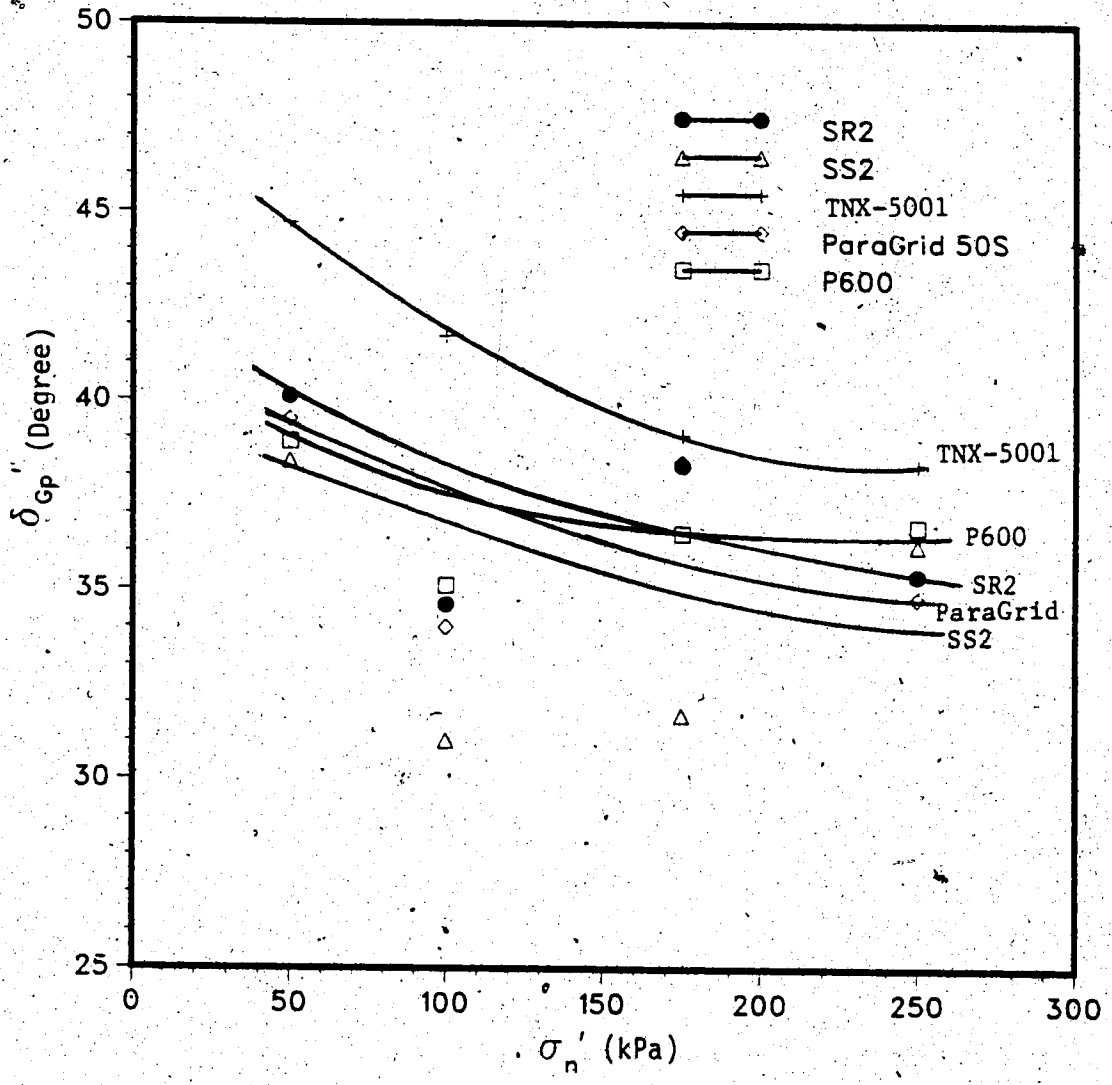

Figure 5.17 Summary Plot of Peak Total Angle of Interfacial Fricton of the Solid Reinforcement

on δ'_{Gp}.

Note that the δ'_{Gp} calculated here will overestimate the actual effective interfacial friction angle between a polymeric sheet and sand. The reason is that the approximated δ'_{Gp} includes the additional peak strength gained through the dilation of sand over the anchor members. This must be considered when using the estimated δ'_{Gp} value. The calculated δ'_{Gp} will best represent the interfacial friction for a ribbed sheet of reinforcement.

Since the calculated δ'_{Gp} includes the shear resistance between the soil and anchor members (or junctions), the thickness of the anchor members relative to the size of the soil particles will affect the amount of particle expansion and hence the value of δ'_{Gp}. In Figure 5.48 the values of $1/D_{50}$ is normalized by the thickness of the junctions. It appears that δ'_{Gp} reaches an optimum value when the ratio of the maximum thickness to D_{50} is 5.4. Below this value δ'_{Gp} rapidly decreases. The anchor members become thinner or the grains become larger. The presence of the members will be insignificant compared to the larger particles, thus little volume expansion is required to overcome the interaction between soil grains and members. δ'_{GP} becomes the angle of direct sliding of grains on a polymeric sheet.

For a maximum thickness to D_{50} ratio larger than the optimum value, δ'_{Gp} decreases slowly with increasing member thickness and decreasing particle size. This implies that the reinforcement surface is no longer a planar surface. In

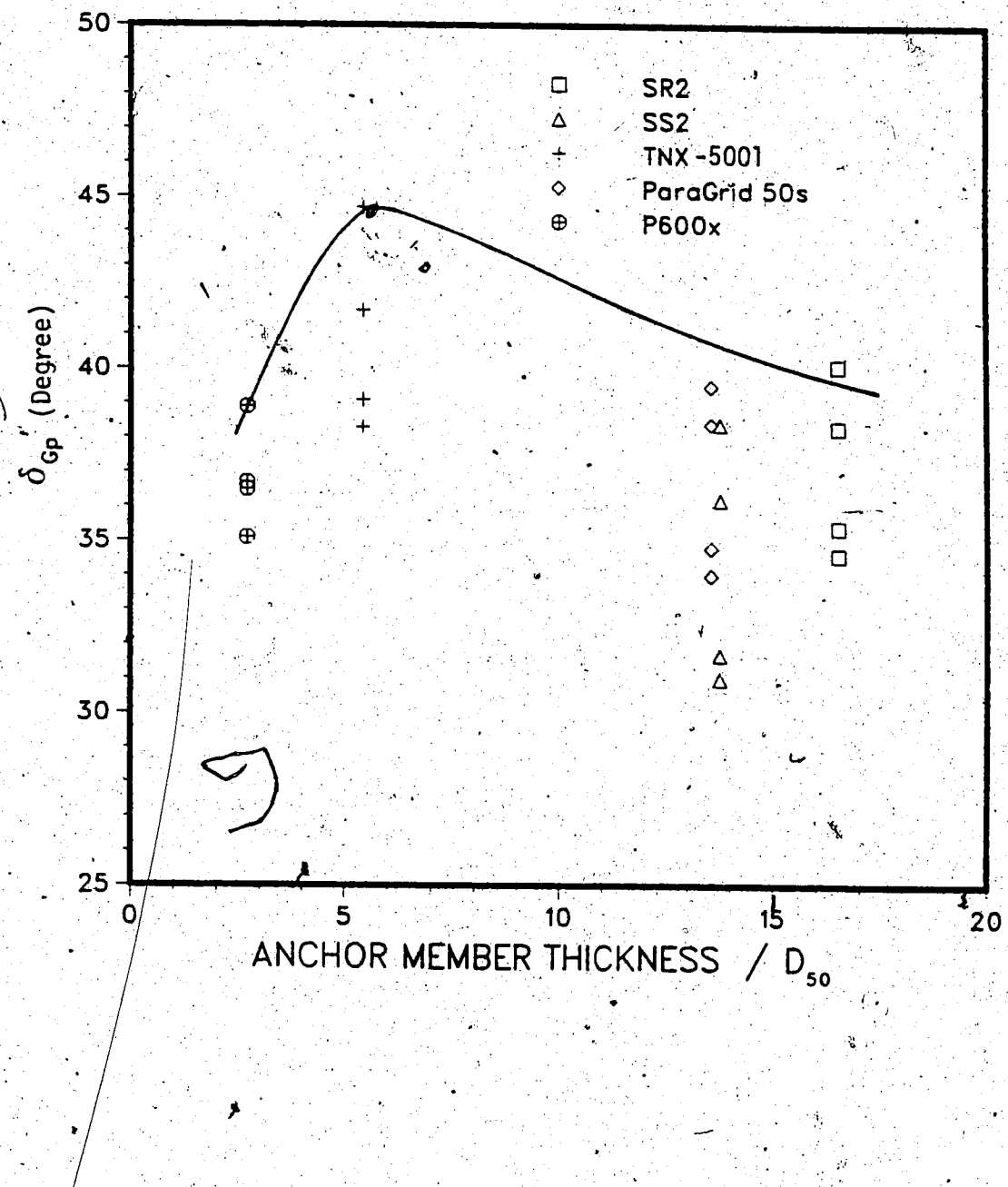

Figure 5.18 Effect of Planarity on Sheet type of Reinforcement

this case, large volume expansion is expected to take place around the anchor members which should result in a large δ'_{Gp}. It is possible that due to the greater degree of kinematic freedom of small soil grains in the shear zone, less energy may be required to rearrange the soil particles, thus δ'_{Gp} is slightly decreased.

5.9.2 Residual Angles

Using the same assumptions as in equation 5.2 the expression of the total angle of residual interfacial friction can be written as:

$$\tan \delta'_{TR} = a \tan \delta'_{GR} + (1-a) \tan \phi'_R \qquad [5.3]$$

where,

δ'_{TR} = residual total angle of interfacial friction.

δ'_{GR} = residual total angle of interfacial friction of the solid reinforcement.

ϕ'_R = residual effective angle of internal friciton.

The δ'_{GR} versus effective normal stress is plotted in Figure 5.19. The same trend of decreasing can be observed. The decrease of δ'_{GR} is not as large as δ'_{Gp} because the volume expansion effect is removed. TNX-5001 has the highest δ'_{GR}, followed by P600. The planarity and the surface roughness of a sheet type of reinforcement may have some influence on the residual interfacial friction.

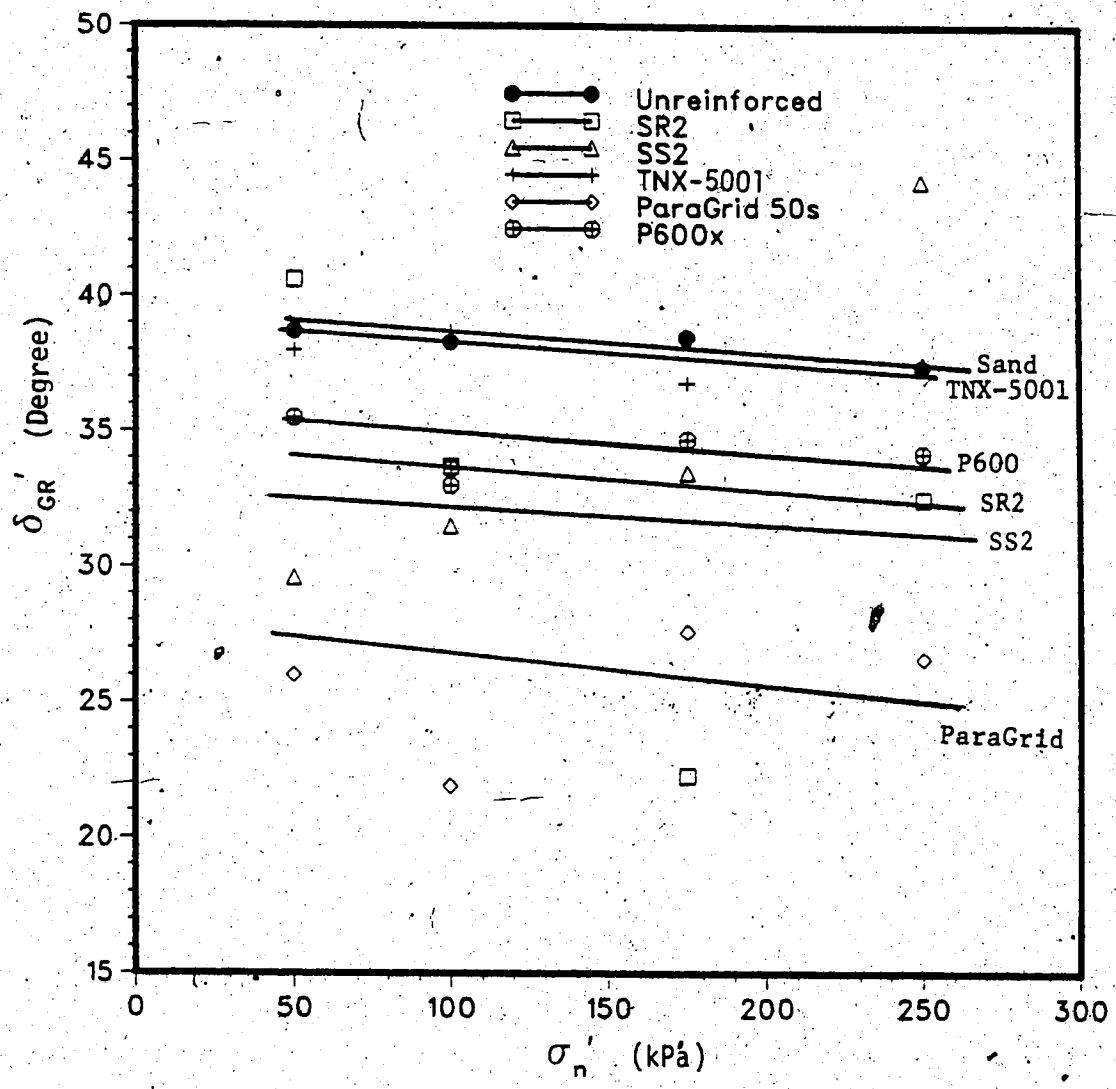

Figure 5.19 Summary of Residual Total Angles of Interfacial Friction of the Solid Reinforcement

5.10 Effect of Normal Stress

The maximum shear stress envelopes of the tested materials (Figure 5.12 and 5.13) indicate that the interfacial shear strength is normal stress dependent. As seen in Figure 5.14 and 5.17 the overall dilation rate and the peak angle of interfacial friction of the solid component of the reinforcement decrease with increasing confining pressure. Thus, the influence of normal stress on the interfacial friction should be examined.

It is known in the direct shear test that the stress concentrations at the boundaries have contributed to non-uniform stress distributions within the tested specimen (Ingold 1982; Richards and Scott 1985). Hence, the presence of reinforcement may further alter the normal stress distribution along the interface.

The frictional resistance to direct sliding of granular soil is proportional to the normal stress distribution at the points where soil grains come into contact with each other. Thus, an increase in confining pressure causes increased contact which increases the frictional resistance.

At the interface, only the soil particles which protrude through the apertures of the geogrids are in contact with other soil particles. Because of the incompressible nature of the sand grains, a greater portion of the normal stress will be carried by these particles. Since there is no reduction in the externally applied confining pressure, the vertical stress carried by the soil

particles on the solid surface of the reinforcement must be lessened. Figure 5.20 illustrates the hypothetical normal stress distribution in the interface.

If this hypothetical normal stress distribution is correct, the frictional resistance to direct sliding is increased over the apertures and decreased over the solid surface of the reinforcement. The increase of normal stress in the apertures leads to a decrease in particle interlocking. Consequently, the dilation rate is decreased.

5.11 Summary

1. The peak interfacial shear strength of reinforced sand is less than unreinforced sand.
2. The peak angle of interfacial friction is higher for geogrid reinforcement (40.0° to 41.5°) than for the geotextile (36.2°).
3. The percent of open area and the dimensions of the aperture have some influence on the interfacial shear strength; the aperture shape, planarity, and embossed surface of geogrids have no significant effect.
4. The surface roughness and tiny openings of a geotextile are important to the mobilization of the frictional strength.
5. The residual interfacial shear strength of reinforced sand is lower than unreinforced sand.
6. The residual total angle of interfacial friction for the geogrid reinforcement is similar to the geotextile. The

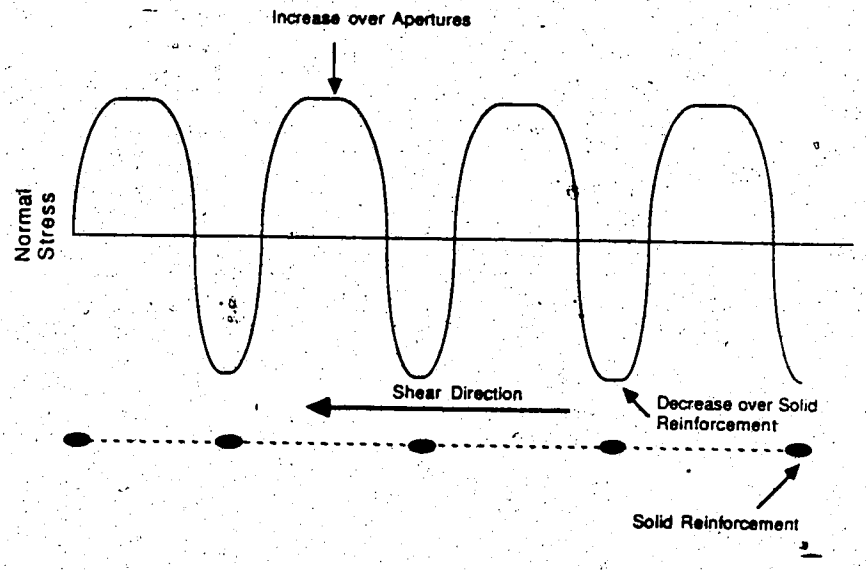

Figure 5.20 Hypothetical Normal Stress Distribution at the

aperture size, aperture shape, and surface roughness appear not to have an effect.

7. The percent of open area, aperture dimension, embossed surface, and planarity influence the dilation rate. The reduction of the shear dilation of the reinforced sand may also be caused by the non-uniform normal stress distribution at the interface.
8. For the tested materials, the embossed surface appears not to have any effect on the peak total angle of interfacial friction of the solid reinforcement. The planarity and the rough surface texture of a sheet type of reinforcement appear to have some influence the residual interfacial strength.

6. TEST RESULTS FOR REINFORCED CLAY

6.1 Introduction

The consolidated undrained direct shear test results of a cohesive soil with four geogrids and a geotextile are presented. These results are discussed in terms of total stresses. The influence of the reinforcement properties on the interfacial shear strength of the reinforced clay are studied.

A total of 46 consolidated undrained tests were performed. Six preliminary tests were conducted during the development of the test procedures. The remaining 40 tests were conducted in accordance with the test procedures outlined in chapter 4. The data from each test is summarized in Appendix D (Tables D.1 to D.6).

6.2 Shear Stress and Deformation

A series of twelve consolidated undrained direct shear tests were carried out on the unreinforced silty clay. The shear stress and displacement curves are summarized in Figure 6.1. The stress-deformation behavior of the dynamically compacted clay is like that of a strain-hardening soil. It exhibits a rapid rise in shear strength with increasing displacement before it levels off to achieve a peak value. The strain-softening behavior was displayed for normal stresses less than 50 kPa. This behavior was thought to be the result of the applied normal

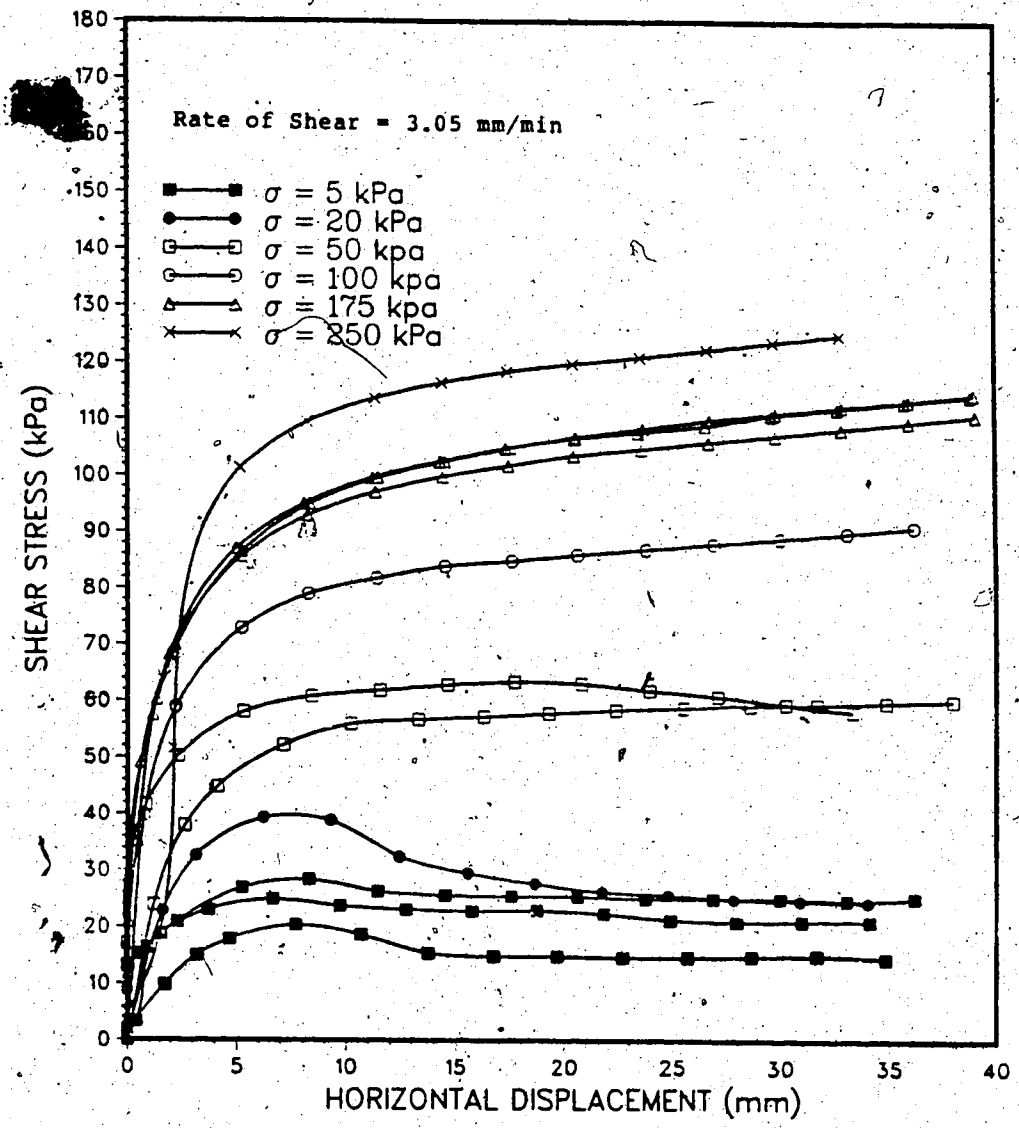
Rate of Shear = 3.05 mm/min
σ = 5 kPa
σ = 20 kPa
σ = 50 kpa
σ = 100 kpa
σ = 175 kpa
σ = 250 kPa
SHEAR STRESS (kPa)
HORIZONTAL DISPLACEMENT (mm)
0
10
20
30
40
50
60
70
80
90
100
110
120
130
140
150
170
180
0
5
10
15
20
25
30
35
40

pressure being significantly smaller than the preconsolidation stress (140 to 175 kPa).

The typical shear stress-deformation plot of a reinforced silty clay is shown in Figure 6.2. Strain-hardening behavior is found in all the test results for reinforced silty clay (Figures 6.2 and D.1 to D.4). The shear displacements required to mobilize the peak undrained strength (8 to 17 mm) are similar to those of the unreinforced clay (8 to 15 mm). The deformation to peak increases with increasing normal stress. The presence of the reinforcement appears not to have a significant effect on the shear displacement to peak.

Despite the displacement rate used in the tests, the vertical displacement measurements indicated that a small overall height change occurred in both the unreinforced and reinforced undrained shear tests (Figures 6.3 and 6.4). This implies that the stress concentrations at the specimen boundaries may cause the development of passive and active pressure zones inside the specimen. This may induce the loading platen to tilt, affecting the vertical displacement measurement. Similar results were also found by Jewell (1980) who performed undrained tests on kaolin clay reinforced with a metal grid. Southern (1982) also reported similar behavior for the undrained tests of sandy clay reinforced with SR2.

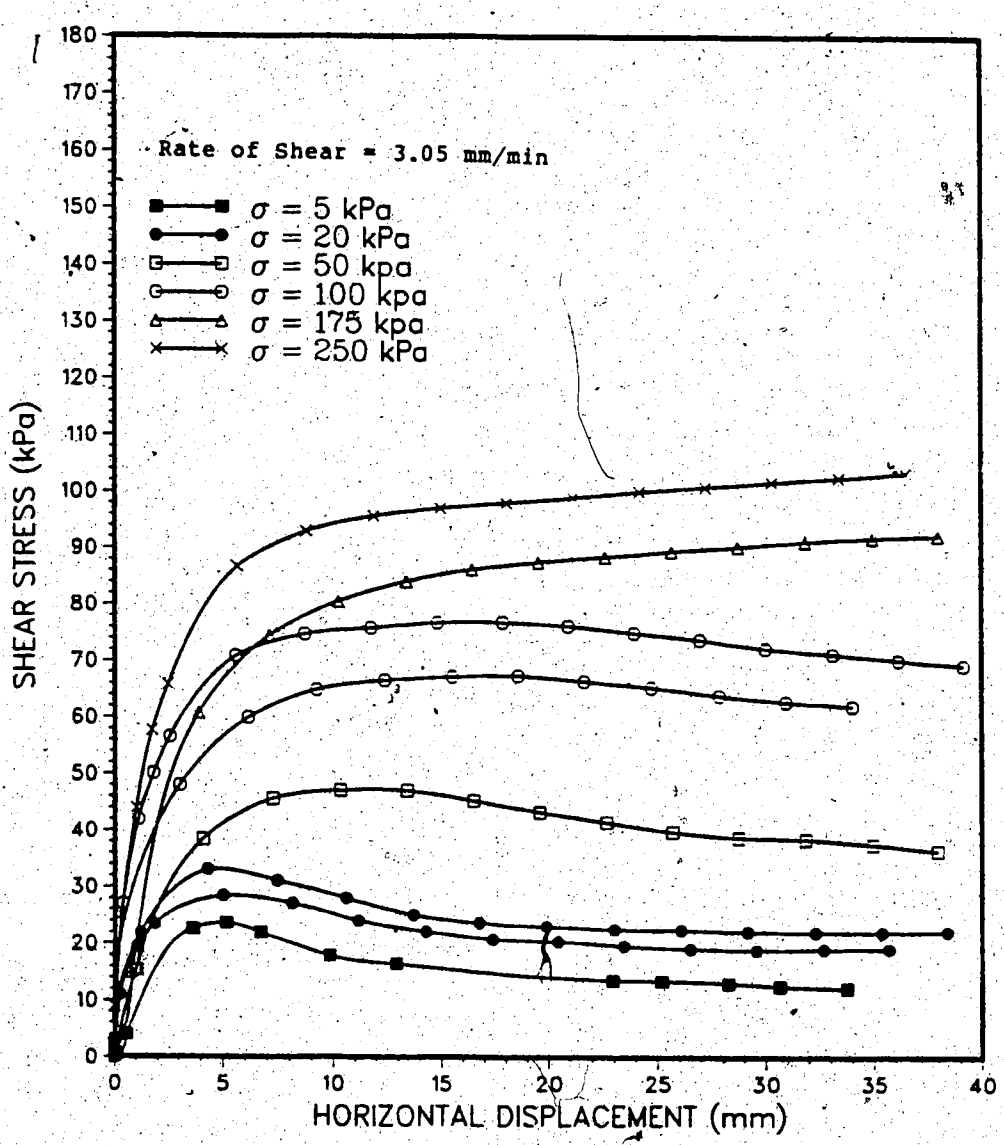

Figure 6.2 Shear Stress and Deformation Curves for Silty Clay Reinforced with Geogrid SR2

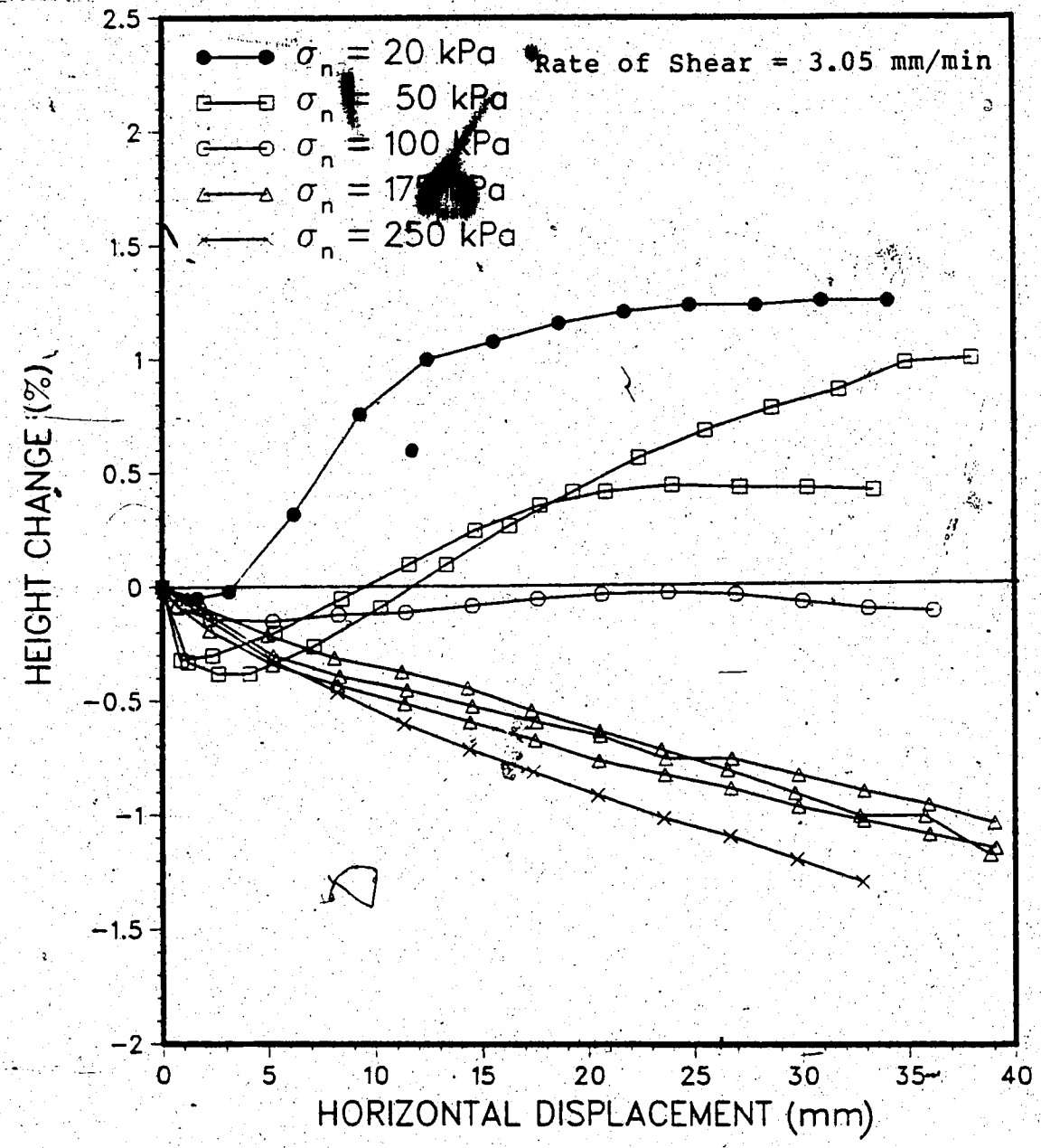

Figure 6.3 Vertical and Horizontal Displacement Curves for Unreinforced Silty Clay

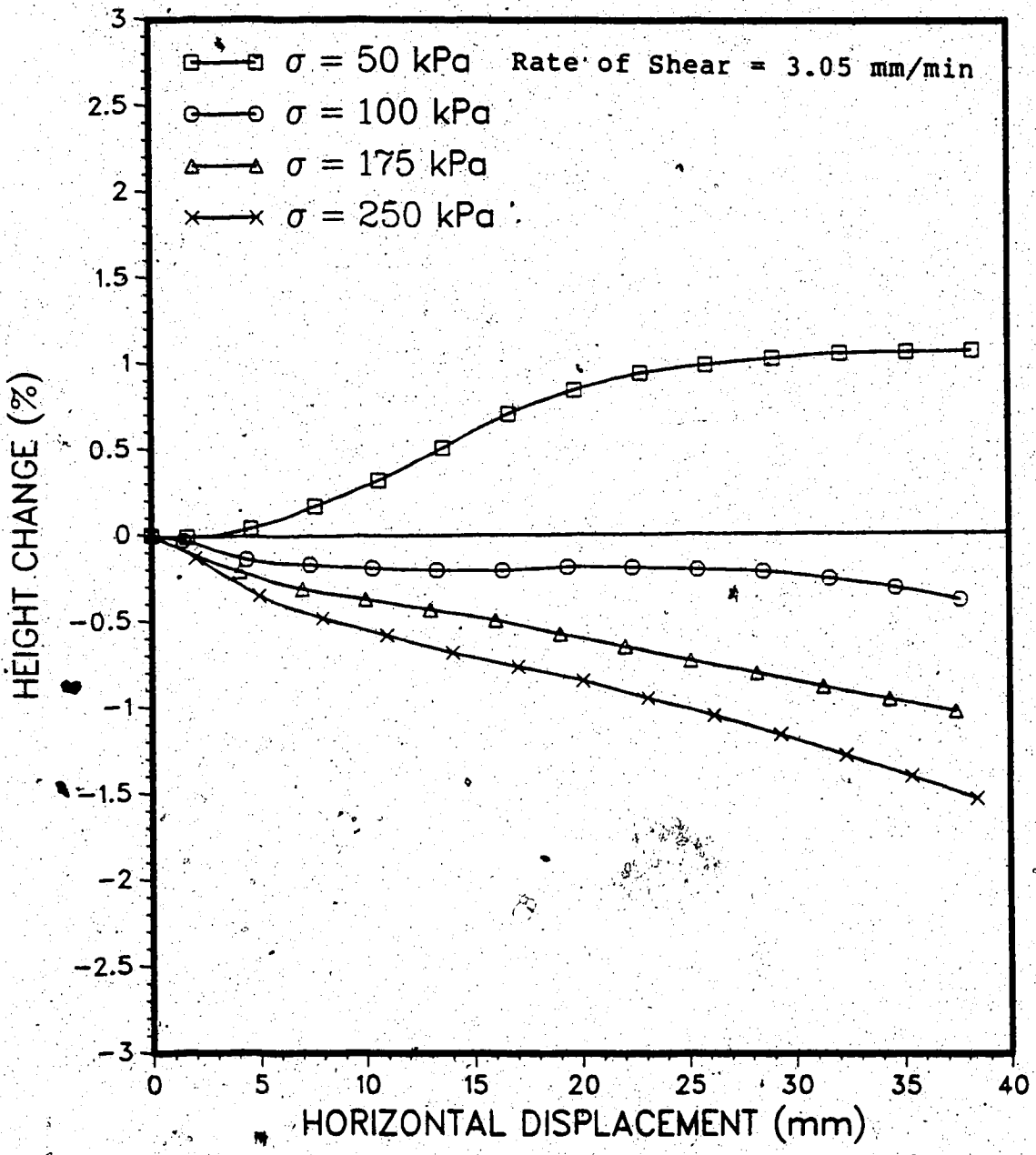

Figure 6.4 Vertical and Horizontal Displacement Curves for Silty Clay Reinforced with Geogrid ParaGrid 50s

6.3 Consolidation Results

Two sets of consolidation curves of the unreinforced and reinforced silty clay from the undrained tests are shown in Figures 3.4 and 6.5. The consolidation stage was completed within 24 hours prior to the undrained shear test. Other consolidation curves are shown in Figures D.5 to D.8. The consolidation results are also shown in the percent strain versus normal stress plot, Figure 6.6. It appears that a greater degree of consolidation was achieved by the specimens in the 300 mm^2 shear box compared to those in the oedometers.

6.4 Shear Strength

The undrained strength of a cohesive soil was originally divided by Coulomb into two parts: frictional strength and cohesive strength. Similarly the total interfacial shear strength of the reinforced clay τ_{Tp} can be divided into two parts:

$$\tau_{Tp} = c_{Tp} + \sigma_n \tan \delta_{Tp} \qquad [6.1]$$

where,

c_{Tp} = total interfacial cohesion intercept.

σ_n = normal stress.

δ_{Tp} = total angle of interfacial friction.

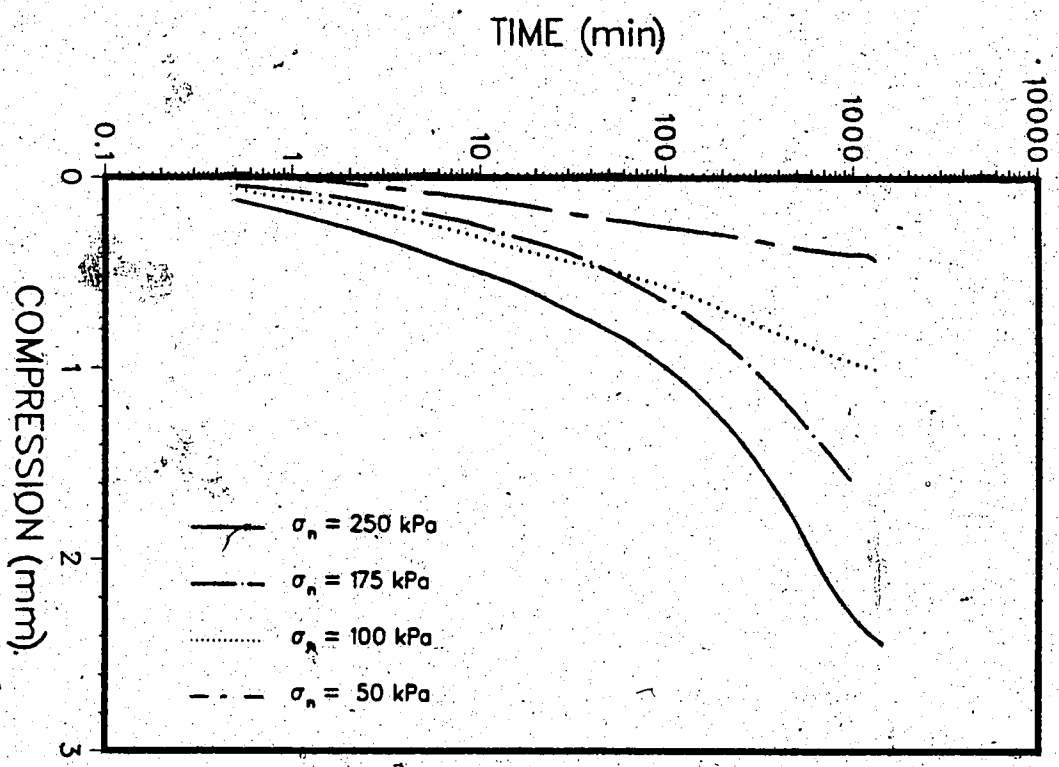

Figure 6.5 Consolidation Curves for Silty Clay Reinforced with ParaGrid 50S

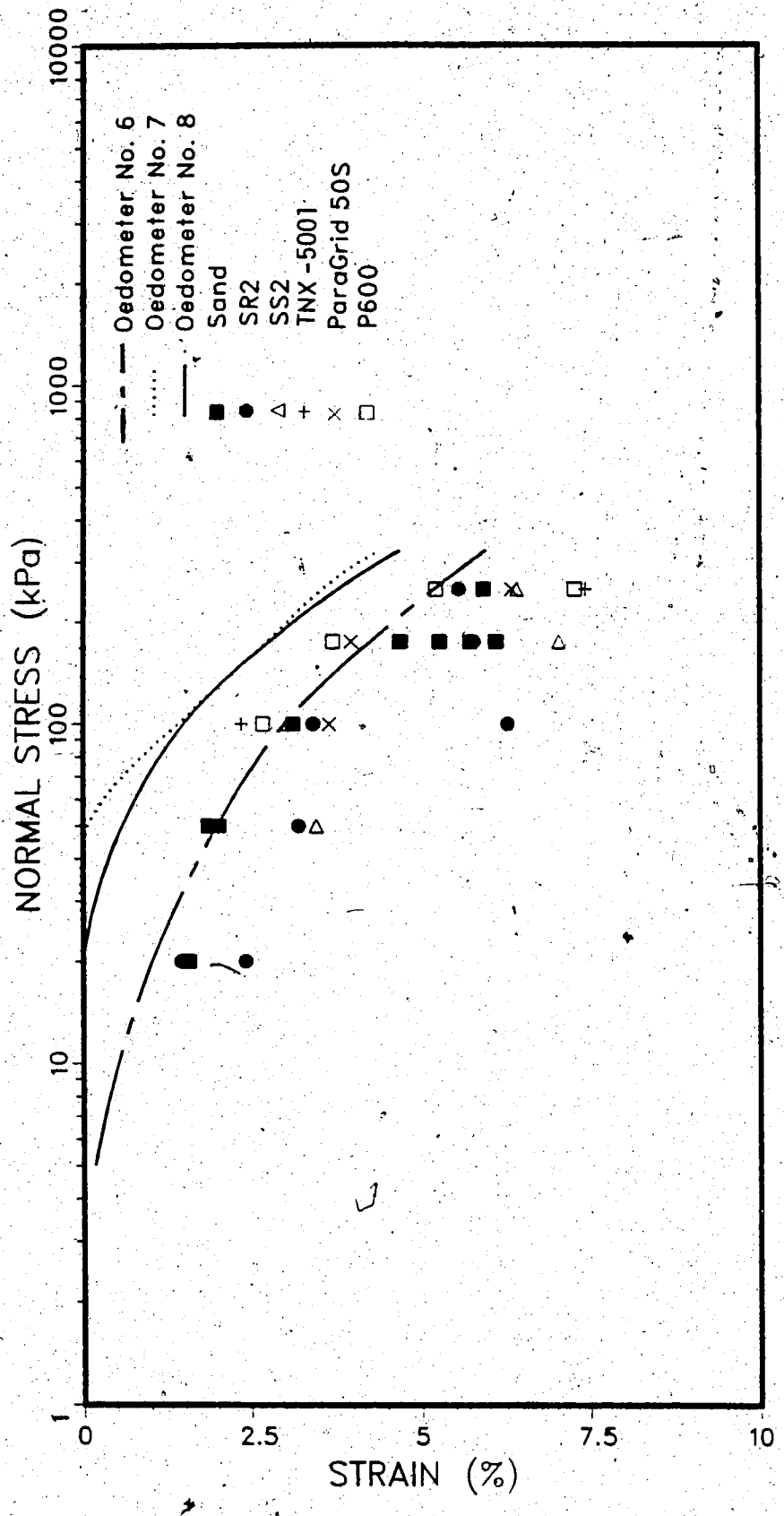

Figure 6.6 Summary of Consolidation Results for Direct Shear Tests

As discussed in the previous chapter the soil and reinforcement interaction that governs the interfacial shear strength of granular soil consists of two components. For a cohesive soil, the two components can be further divided into the cohesive and adhesive strength. Hence, the total interfacial shear strength can be written as the sum of the contributions. Equation 6.1 becomes

$$\tau_{Tp} = a(c_G + \sigma_n \tan\delta_G) + (1-a)(c_u + \sigma_n \tan\phi_u) \qquad [6.2]$$

where,

c_G = interfacial adhesion intercept of the solid reinforcement.

δ_G = angle of interfacial friction of the solid reinforcement.

c_u = undrained cohesion intercept.

ϕ_u = undrained angle of internal friction.

c_u and ϕ_u can be measured in a conventional direct shear test while c_G and δ_G of a single member can be determined from the modified shear box test. Assuming the contribution made by each component is correct, τ_{Tp} of any type of reinforcement may be estimated from equation 6.2. Alternatively, the influence of each component may be studied.

It is beyond the scope of this study to determine the exact contribution of each component and to compare the influence of each component. The lack of published results for large shear box tests on reinforced clay and the limited information obtained from this testing program make it impossible to demonstrate the validity of equation 6.2 without making numerous assumptions. Thus, the results of the reinforced clay obtained from this program are compared in terms of total interfacial shear strength or the Mohr-Coulomb failure envelope.

As discussed in the previous chapter, the shear strength on the shear surface is primarily a function of the properties of the reinforcement and of the soil. In this study, the properties of the silty clay were held relatively constant. Therefore, the interfacial shear strength of five types of reinforcement can be compared to give a qualitative assessment of the influence of the geometry of the reinforcement on the interfacial strength.

6.4.1 Effects of Reinforcement Properties on Shear Strength

The Mohr-Coulomb failure envelopes of two geogrids and a geotextile are compared in Figure 6.7. The interfacial shear strength of the reinforced clay is less than the unreinforced clay. All failure envelopes are gently curved indicating the interfacial strength is non-linearly normal stress dependent.

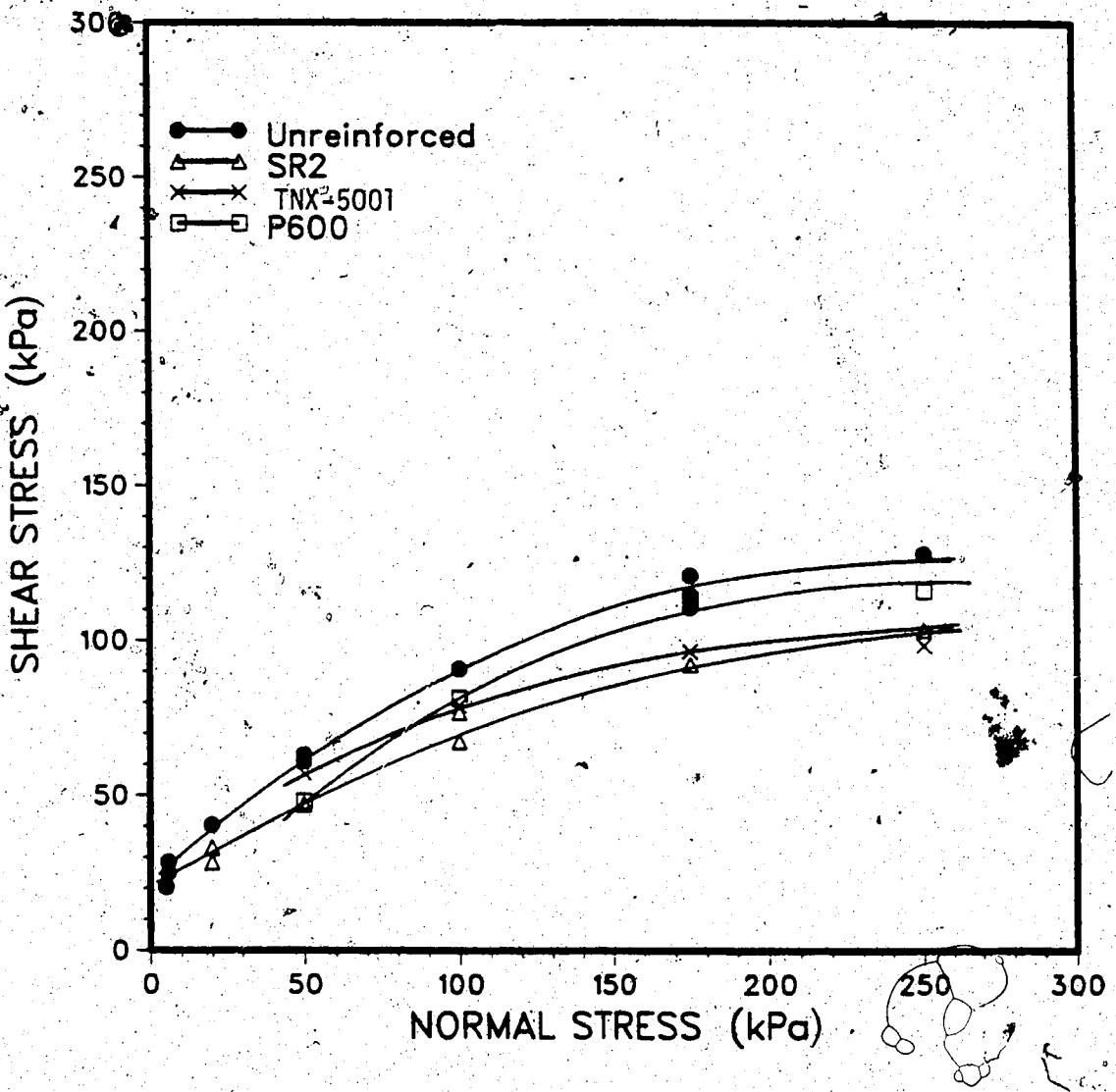

Figure 6.7 Undrained Shear Strength Envelopes of Reinforced

The geogrid TNX-5001 mobilizes slightly higher shear strength compared to SR2. Since the mechanism of the interaction is the same for the geogrids, the slightly higher strength may be attributed to a difference in geometry. As discussed previously SR2 and TNX-5001 have a similar ratio of the solid area of the reinforcement to the total area of the reinforcement (a=0.45, 0.42), but their aperture dimensions and thickness are quite different. It is possible that the slightly higher interfacial strength of TNX-5001 is attributed to the greater amount of soil shearing over soil in the larger apertures. The smooth and hard surface of TNX-5001 does not seem to have an effect on the shearing strength.

A comparison of the interfacial shear envelopes of the unreinforced clay and those reinforced with SS2, ParaGrid 50S, and P600 is made in Figure 6.8. The response of the reinforced clay is similar to that previously noted for TNX-5001 and SR2. The peak shear strength envelope for the unreinforced clay is greater than that for reinforced clay. SS2 has a slightly higher interfacial strength than ParaGrid 50S.

For ParaGrid 50S and SS2 it appears that aperture dimension has no influence on strength. Even though the area of the aperture in ParaGrid 50S is 5.23 times larger than SS2, the interface strength of ParaGrid 50S is less than SS2. The embossed surface of ParaGrid 50S also appears not to have an influence on the strength. SS2 has a smooth

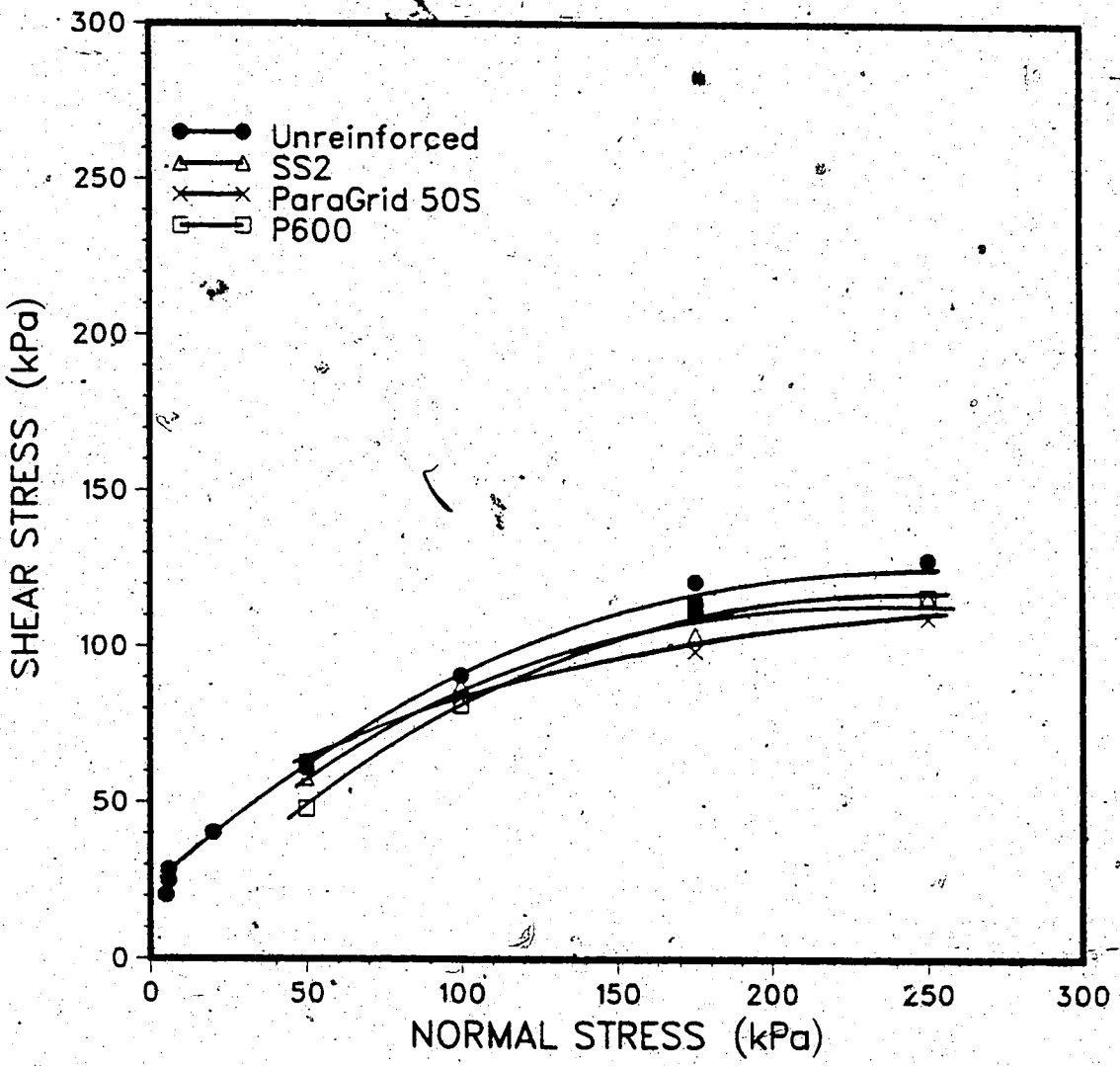

Figure 6.8 Undrained Shear Strength Envelopes of Reinforced

surface yet exhibits higher shear strength than ParaGrid 50S. The possible explanation is that when a is small, the total area of the reinforcement consists of openings. The interfacial strength is predominately from the shearing of soil particles in the apertures, thus the size of the opening has no major effect on the strength. Since a relatively small portion of the total reinforcement is solid, the contribution of the shear resistance generated from soil sliding on the solid surface is small. For this reason whether the solid surface of the geogrid is smooth or embossed has no effect on the shear strength.

For rough textured P600, the contribution of shear strength is predominately from the shearing of soil over the entire rough surface and penetration and lodging of soil particles in the openings between the yarns. Figures 6.7 and 6.8 indicate that this mode of shear resistance is superior to those of the geogrids. As discussed by Williams and Houlihan (1987) the interlocking of soil within the openings and the roughness of the surface of the geotextile may be sufficient enough to cause the shear stress to be transferred from the interface into the adjacent soil layer. They found the shear surface is developed at a distance of between 0.4 to 3.2 mm above the interface. Thus, the strength of the soil-geotextile matrix can approach the strength of the unreinforced soil.

It is evident from the comparison of the five envelopes that for a grid type of reinforcement, the ratio of the

solid area of the reinforcement to the total area of the reinforcement governs the interfacial interaction. When there is an extensive amount of soil to soil interaction through the apertures, the interfacial strength is independent of the aperture dimensions and surface texture. When the soil to soil interaction is limited, the interfacial strength is strongly dependent on the surface characteristics of the reinforcement. Thus, it appears that the type of reinforcement and its geometry influences the shear strength behavior.

6.5 Efficiency

For reinforced non-cohesive soils the efficiency (E) is commonly defined as $\tan \delta_{Tp}/\tan \phi_p$. For reinforced cohesive soils, Collis et al. (1984), Koerner, Martin, Koerner (1986), and Milligan (1987) have divided efficiency into two terms, one related to friction E_ϕ and the other to cohesion or adhesion E_c:

$$E_\phi = \frac{\tan \delta_{Tp}}{\tan \phi_u} \qquad [6.3]$$

and

$$E_c = \frac{c_{Tp}}{c_u} \qquad [6.4]$$

The literature review shows that E_ϕ ranges from 0.4 to 1.0 and E_c from 0.1 to 0.9 and vary with the applied normal stress, particle size, and geometry of the reinforcement

For the test results shown here, the curvature of the failure envelope indicates that the apparent angle of internal friction ϕ_u, the total angle of interfacial friction δ_{Tp}, the apparent cohesion c_u, and the interfacial cohesion c_{Tp} vary with applied normal stress. For this reason, efficiency is expressed in terms of total interfacial shear strength.

$$E = \frac{\tau_{Tp}}{\tau_p} \qquad [6.5]$$

The efficiency for each reinforced test is calculated and presented in Figure 6.9. Efficiency ranges from 0.74 to 1.0. Although the calculated E is slightly scattered, it appears that efficiency decreases with increasing normal stress.

As discussed previously a seems to have some influence on the interfacial shear strength. To study the effect of a, the results are plotted in the form of efficiency versus a. Figure 6.10 shows that when a is small there is more soil to soil interaction. The interfacial shear strength approaches that of the unreinforced soil and the efficiency is high. As a increases, the soil to soil contact decreases while the soil to polymer surface interaction increases. The interfacial shear strength becomes less than that for unreinforced soil. A low efficiency value results. As a approaches unity, that is, a solid sheet of reinforcement,

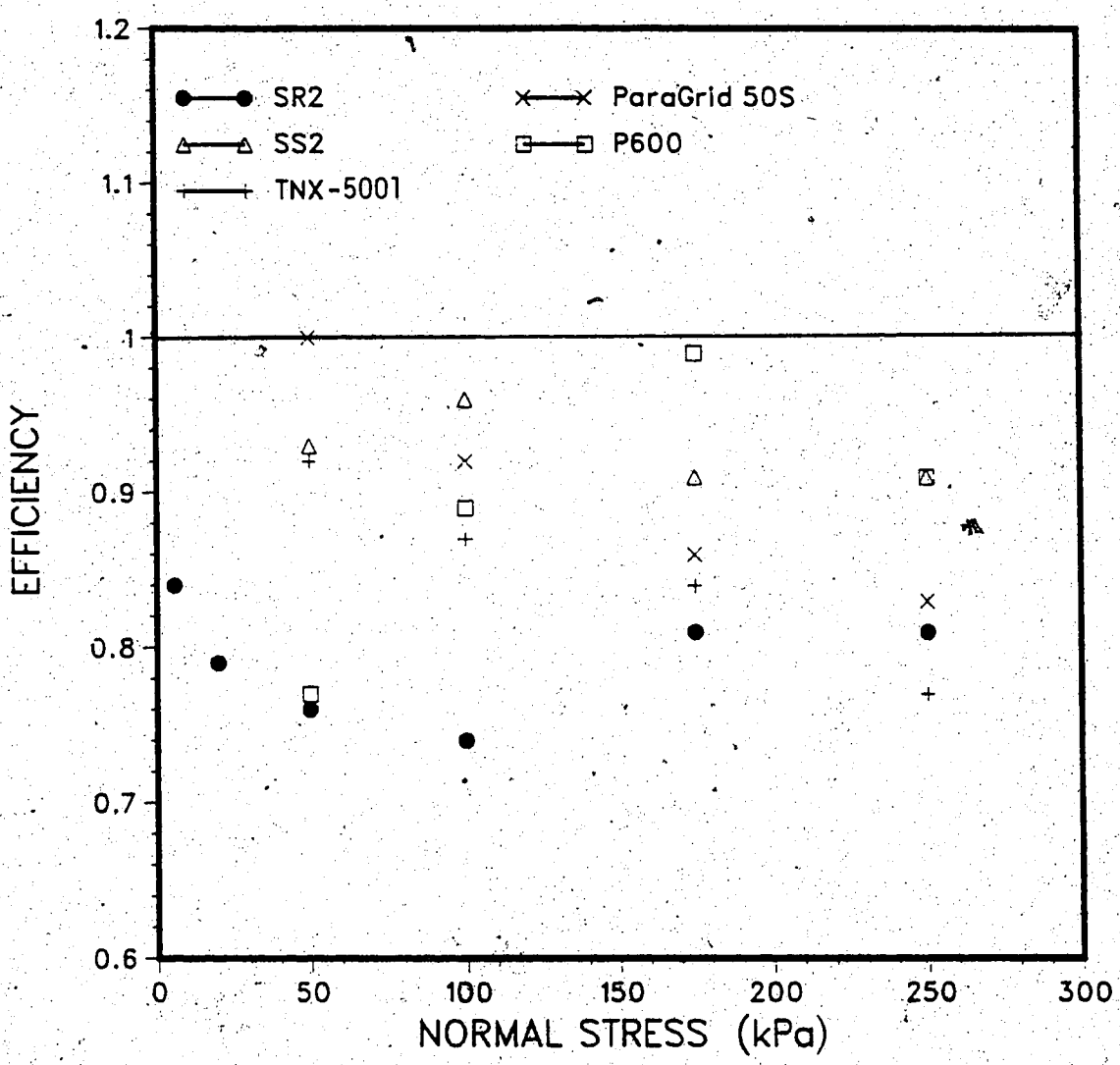

Figure 6.9 Efficiencies Of Silty Clay Reinforced by Geogrids and a Geotextile

the contact surface texture becomes important. Tables A.2 and A.4 show that for a sheet type of reinforcement efficiency ranges from 0.3 to 1.0. It varies with thickness and surface characteristic of the reinforcement. Figure 6.10 shows that with a rough contact surface, exemplified by P600, the interfacial shear strength can approach that of the soil, and the efficiency can be high.

The consolidated undrained shear test is performed to model the undrained shear stress behavior of a reinforced soil in the field. The drained condition associated with the effective shear strength was not included in the testing program. However, the test results of the reinforced sand have made it possible to estimate the drained efficiency of the reinforced silty clay. As shown by the results of the reinforced sand, drained efficiencies are similar to the undrained efficiencies of the reinforced clay. In addition, test results from Ingold and Jones (1981) also indicate that for kaolin clay reinforced with an inclined metal grid, the drained and undrained efficiencies are similar. Hence, the drained efficiencies of the four geogrids and one geotextile used in this research program would be similar to their undrained efficiencies. The drained efficiencies of these reinforcements are estimated to be between 0.84 and 0.93.

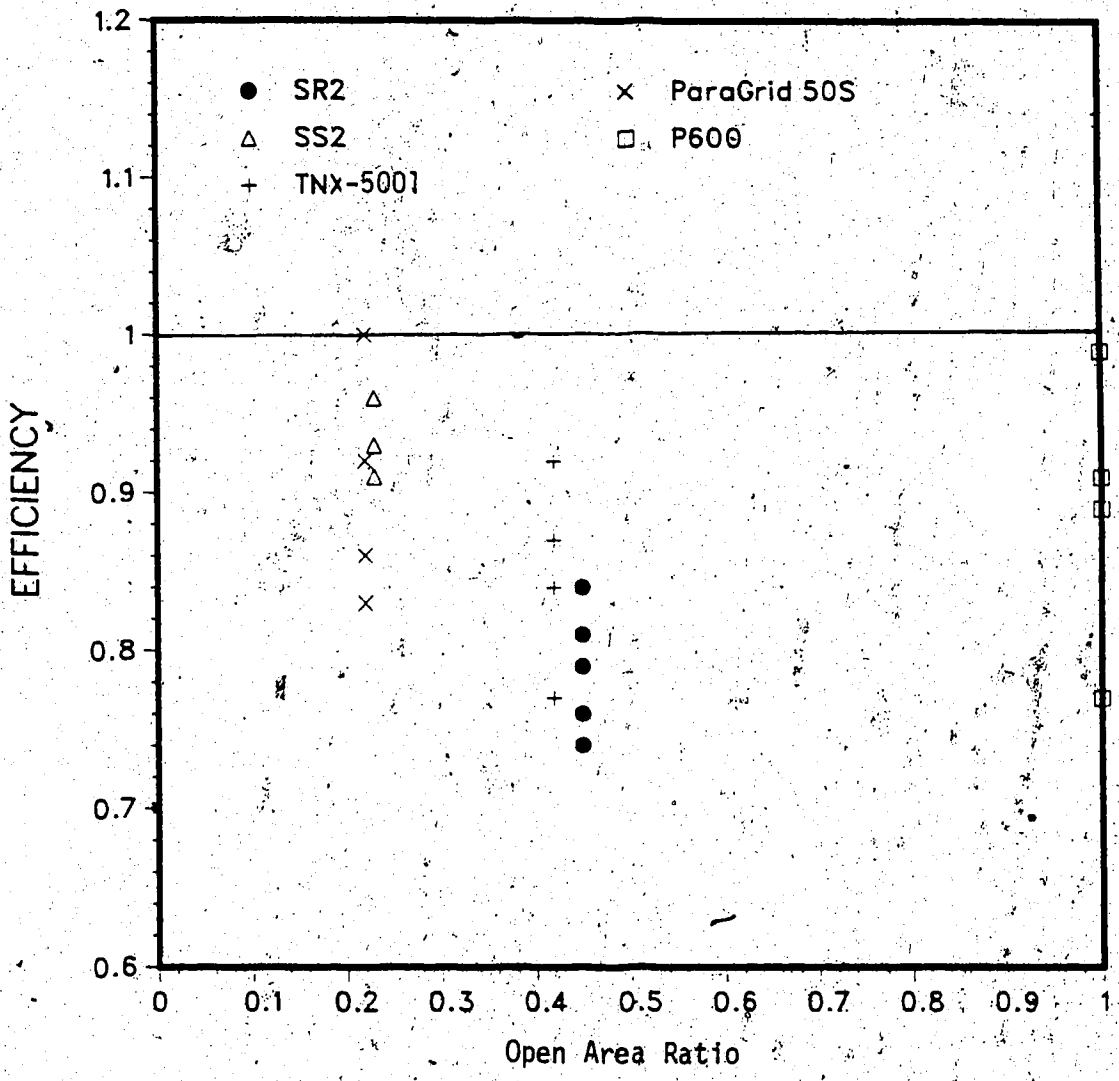

Figure 6.10 Influence of the Open Area Ratio on Undrained Efficiency

7. CONCLUSIONS AND RECOMMENDATIONS

7.1 Summary

The purpose of this research program was to determine the influence of the construction and geometry of four geogrids and one geotextile on the interfacial shear strength of a granular and a cohesive soil. In addition, a modification to a standard wide width direct shear box apparatus was presented and testing procedures were developed for this research. A total of 35 consolidated drained direct shear tests on one sand and five types of reinforcements were performed. The experimental results have been reported in Chapter 5. From these results the influence of the properties of the reinforcements were examined. The test results of 46 consolidated undrained shear tests on reinforced clay have been presented in Chapter 6. The effect of the reinforcement properties on a silty clay were discussed.

7.2 Conclusions

7.2.1 Reinforced Sand

The construction method of the reinforcement and therefore its geometry have some influence on the soil and reinforcement interaction. Geogrids which permit a greater degree of soil to soil interaction exhibit higher interfacial friction than woven geotextiles.

The interfacial friction between the densely compacted sands and the geogrids is close to the shear strength of the sand. Their efficiency is close to one. The high efficiency values of geogrids (0.95 ± 0.04) can be attributed to the extensive soil to soil interaction through the apertures. This implies that geogrids do not represent significant planes of weakness within a compacted granular fill. The aperture dimensions, the aperture shape, and an embossed surface have little effect on the mobilization of the interfacial friction when a geogrid has an open area ratio greater than 50%.

The interfacial friction of the densely compacted sand and geotextile is less than the shear strength of the sand. The lower efficiency (0.83 ± 0.06) of the geotextile indicates that it may represent a more potential sliding plane within a granular embankment. For geotextiles the surface roughness and the small openings created by the closely spaced yarns are essential in mobilizing the interfacial strength.

The residual total angles of interfacial friction of the geogrids (34.1° to 37.9°) are similar to that of the geotextile (34.1°). The residual efficiency is 0.92 ± 0.08. It appears that the percent of open area, the aperture shape, and the aperture dimensions have no apparent effect on the mobilization of the residual interfacial shear strength. The presence of the solid reinforcement has caused the reduction of the residual strength.

The dilation rate during shear is reduced by the presence of the reinforcement because the soil dilation is occurring predominantly in the apertures. The reduction is more pronounced with the geotextile because of its limited amount of soil to soil interaction and its planarity. The highest dilation rate is achieved by the geogrid with the combination of an embossed surface and a large opening size. Thus, the amount of soil dilation is a function of the percent of open area, the aperture dimension, and the surface roughness of the reinforcement. The reduction of the shear dilation of the reinforced sand may also be caused by the non-uniform normal stress distribution at the interface.

For a plane sheet of reinforcement the embossed surface appears not to have any effect on the peak total angle of interfacial friction of the solid reinforcement. The planarity and the rough surface texture of a sheet type of reinforcement appear to have some influence the residual interfacial strength.

7.2.2 Reinforced Clay

For geogrids, the ratio of the solid area of the reinforcement to the total area of the reinforcement, a, governs the interfacial interaction. When there is an extensive amount of soil to soil interaction through the apertures, the interfacial strength is independent of the aperture dimensions and surface texture. When the soil to soil interaction is limited ($a \simeq 1.0$), the interfacial

strength is strongly dependent on the surface characteristic of the reinforcement. For geotextiles, a rough surface can generate an adhesive shearing strength approaching that of clay. Thus, the construction method and the geometry of the reinforcement strongly influence the shear strength behaviour.

The interfacial shear strength of the reinforced clay was less than that of the unreinforced clay. The efficiency ranges between 0.74 and 1.00 varing with the construction and geometry of the reinforcement. The presence of the reinforcement has no effect on the strain-hardening behavior of the dynamically compacted silty clay or on the amount of the horizontal displacement to mobilize the peak strength.

7.2.3 Test Apparatus and Procedure

This study showed that the modified wide width direct shear apparatus was appropriate for determining the required material properties of a reinforced soil where interfacial sliding is a concern. The testing procedures developed for this research were suitable for assessing the influence of reinforcement properties on interfacial strength.

7.3 Summary of Literature Review

In soil reinforced with a geotextile or a geogrid, the interfacial friction between loosely compacted granular soil and reinforcement is similar to that of unreinforced soil. Its efficiency is therefore very close to one.

The interfacial friction between dense granular soil and reinforcement is less than that of the unreinforced soil. The reduction in efficiency may be related to the construction and geometry of the reinforcement.

The interfacial friction increases with increasing surface roughness independent of the type of soil and the type of reinforcement. A textured surface may provide better interlocking with the soil grains than a smooth surface, thus the efficiency increases.

In granular or cohesive soil reinforced with geogrids with the same planarity, the geogrid with the bigger opening dimensions has a higher interfacial friction. It appears that a greater amount of soil to soil interaction occurs in the larger opening which results in a high efficiency value.

For granular soil reinforced with woven geotextiles with a similar percent of open area, a thin and stiff geotextile mobilizes slightly higher frictional resistance than a thin and flexible geotextile. However, for the same percent of open area, a thick and flexible non-woven geotextile yields a higher friction angle than both a thin and flexible and a thin and stiff woven geotextile. It appears the thickness and the stiffness of geotextile have some influence on the interfacial friction.

Regardless of the type of soil and the type of polymer, the interfacial friction of geomembranes increase with increasing surface roughness. For materials with the same roughness, a thin and less stiff geomembrane mobilizes

greater strength than a thick and stiffer one.

7.4 Recommendations for Future Research

1. Although the modified large direct shear box was found suitable for measuring the required interfacial properties for a reinforced soil, the problem of boundary stress and the non-uniform stress distribution within the sample requires further study. The effect of normal stress distribution at the interface needs to be examined so that the measured interfacial friction and sample dilation may be interpreted more accurately. To measure the vertical stress distribution, small load cells may be embedded in the soil layer above the interface, in the apertures, and on the solid part of the reinforcement.
2. In addition to the five types of high strength geogrids and geotextile that were tested in this research program, the interfacial shear strength of geogrids and geotextiles which have various constructions and geometry need to be tested to verify the influence of the reinforcement properties that were found in this research.
3. Direct shear tests on various polymer sheets and soils need to be tested to determine the contribution of the interfacial shear strength of the solid reinforcement in the soil and reinforcement interaction.
4. Only the undrained shear stress behavior of the

reinforced silty clay was examined here. Therefore, the drained shear stress behavior of reinforced silty clay requires further study.

5. To solve the problem of tilting of the loading platen caused by the boundary stresses, the platen loading mechanism needs to be redesigned. Alternatively, an air bag which has been pressurzied with air or water might be used to applied the required normal stress more uniformily.

6. Strain gauges may be attached to the reinforcement to measure the strain that is necessary to cause the interfacial displacement.

REFERENCES

Akber, S. Z., Hammamji, Y., and Lafleur, J. 1985. Frictional Characteristics of Geomembranes, Geotextiles, and Geomembranes-Geotextile Composites. Proceedings, 2nd Canadian Symposium on Geotextiles and Geomembranes, Edmonton, September, pp. 209-217.

Bishop, A. W. 1950. Discussion: Proceedings of the Conference on Measurement of Shear Strength of Soils. Geotecnica, Vol. 2, No. 2, pp. 113-116.

Bolton, M. D. 1986. The Strength and Dilatancy Of Sands. Geotechnique, Vol. 36, No. 1, pp. 65-78.

Casagrande A., and Hirschfeld, R. C. 1960. First Progress Report on Investigation of Stress-Deformation and Strength Characteristics of Compacted Clays. Harvard Soil Mechanics Series, No. 61, May, 52p.

Christie, I. F. 1982. Economic and Technical Aspects of Embankments Reinforced with Fabric. Proceedings, 2nd International Conference of Geotextiles, Las Vegas, August, Vol. 3, pp. 659-664.

Collois, A., Delmas, P., Gourc, J. P. ,and Giroud, J. P. 1980. Experiments on Soil Reinforcement with Geotextiles. Preprint 80-177. The Use of Geotextiles for Soil Improvements. ASCE National Convention, Oregon. pp. 53-74.

DeGoutte, G., and Mathieu G. 1986. Experimental Research of Friction between Soil and Geomembranes or Geotextiles Using a 30 X 30 cm^2 Shear Box. Proceedings, 3rd International Conference on Geotextiles, Vienna, April, Vol. 3, pp. 791-796.

Giroud, J. P. 1984. Geotextiles and Geomembranes. Geotextiles and Geomembranes. Vol. 1, pp. 5-40.

Giroud, J. P., Arman A., Bell, J. R., Koerner, R. M., and Milligan V. 1985. Geotextiles in Geotechnical Engineering Practice and Research. Geotextiles and Geomembranes, Vol. 2, No. 3, pp. 185-239.

Haliburton, T. A., Anglin, C. C., and Lawmaster, J. D. 1978. Testing of Geotechnical Fabirc for Use and Reinforcement. Geotechnical Testing Journal, Vol, 1, Dec., pp. 203-212.

and Performance in Geotechnical Engineering, Calgary, June, pp. 227-237.

Hausmann, M. R., and Ring, G. J. 1980. Measurement of Soil/Reinforcement Interaction. Proceedings, 3rd Australian-New Zealand Conference on Geomechanics, Wellington, Vol. 1 pp. 149-153.

Ingold, T. S. 1980. **Reinforced Clay** Ph.D. Thesis, Department of Civil Engineering, University of Surrey, 252p.

Ingold, T. S. 1981. A Laboratory Simulation of Reinforced Clay Walls. Geotechnique, 31(3), pp. 399-412.

Ingold, T. S. 1982. Some Observations on the Laboratory Measurement of Soil-Geotextile Bond. Geotechnical Testing Journal, Vol. 5, No. 3/4, Sept./Dec., pp. 57-67.

Ingold, T. S. 1983. A Laboratory Investigation of Grid Reinforcements in Clay. Geotecnical Testing Journal, Vol. 6, No. 3, Sept., pp. 112-119.

Ingold, T. S. 1984. A Laboratory Investigation of Soil-Geotextiles Friction. Civil Engineering, London, Nov., pp. 21-28.

Jewell, R. A. 1980. **Some Effect of Reinforcement on the Mechanical Behavior of Soils.** Ph.D. Thesis, Cambridge University, Christ's College, March, pp. 11-31.

Jewell R. A. 1980. Some Factors which Influence the Shear Strength of Reinforced Sand. Proceedings, Symposium on Computer Applications to Geotechnical Problems in Highway Engineering. Cambridge, April, pp. 1-24.

Jewell, R. A., and Jones, C. J. F. P. 1981. Reinforcement of Clay Soils and Waste Materials Using Grids. Proceedings, 10th International Conference on Soil Mechanics and Foundation Engineering, Stockholm, Vol. 3, pp. 701-706.

Jewell, R. A., Milligan, G. W. E., Sarsby, R. W., and DuBois, D. 1984. Interaction Between Soil and Geogrids. Symposium on Polymer Grid Reinforcement in Civil Engineering, London, England, pp. 1.3.1-1.3.13.

Jewell, R. A., and Wroth, C. P. 1987. Direct Shear Tests on Reinforced Sand. Geotechnique, 37(1), pp. 53-68.

Koerner, R. M. 1986. **Designing with Geosynthetics.** Prentice-Hall: Englewood Cliffs, 424p.

No. 1, pp. 21-30.

Lafleur, J., Sall, M. S., and Ducharme, A. 1987. Frictional Characteristics of Geotextiles with Compacted Lateritic Gravels and Clays. Proceedings, Geosynthetics' 87 Conference, New Orleans, Feb., Vol. 1, pp. 205-215.

Lambe W. T., and Whitman, R. V. 1969. **Soil Mechancis**. John Wiley & Sons: New York, 553p.

Leach, J. A., Harpter, T. G., and Tape, R. T. 1987. Current Practice in the Use of Geosynthetics in the Heap Leach Industry. Proceedings, Geosynthetic ' 87 Conference, New Orleans, Feb., Vol. 2, pp. 365-370.

Marshall, C. B. 1983. The Interaction Between Polymer Geogrids and a Well Graded Granular Aggregate. Report No. Cl/G2/1, Bolton Institue of Higher Education, 10p.

Marshall, C. B. 1983. The Interaction Between Polymer Grids and a Fine Grained Granular Aggregate. Report No. CL/G3/1, Bolton Institute of Higher Education, 24p.

Martin, J. P., Koerner, R. M., and Whitty, J. E. 1982. Experimental Friction Evaluation of Slippage Between Geomembranes, Geotextiles, and Soils. Proceedings, International Conference on Geomembranes, Denver, U.S.A. pp. 191-196.

McGown, A. and Andrawes, K. Z. 1982. An Approach to Laboratory Testing of Geotextiles. Quarterly Journal of Engineer Geology, London, Vol. 15, pp. 177-185.

Milligan, G. W. E., and Palmeira, E. P. 1987. Prediction of Bond between Soil and Reinforcement. Proceedings, Prediction and Performance in Geotechnical Engineering, Calgary, June, pp. 147-153.

Mitchell, J. K. 1976. **Fundamentals of Soil Behavior**. John Wiley & Sons., Inc.: New York, 422p.

Miyamori, T., Iwai, s., and Makiuchi, K. 1986. Frictional Characteristics of Non-Woven Fabrics. Proceedings, 3rd International conference on Geotextiles, Vienna, Vol. 3, pp. 701-705.

Myles, B. 1982. Assessement of Soil Fabric Friction by Means of Shear. Proceedings, 2nd International Conference on Geotextiles, Las Vegas. Vol. 3, pp. 787-791.

Richards, E. A., and Scott, J. D. 1985. Soil Geotextile Interface Properties.Proceedings, 2nd Canadian Symposium on Geotextiles and Geomembranes, Edmonton, September, pp. 13-24.

Rowe, R. K., Ho, S. K., and Fisher, D. G. 1985. Determination of Soil-Geotextile Interface Strength Properties. Proceedings, Canadian Symposium on Geotextiles and Geomembranes, Edmonton, September, pp. 25-34.

Sarsby, R. W. 1983. The Interaction Between Pulverised Fuel Ash and Tensar SR2 Geogrids. Report No. NPWY/2/83, Bolton Institue of Higher Education, 16p.

Sarsby, R. W. 1985. The Influence of Aperture Size/Particle Size on the Efficiency of Grid Reinforcement. Proceedings, 2nd Canaidan Symposium on Geotextiles and Geomembranes, Edmonton, September, pp. 7-11.

Sarsby, R. W., and Marshall, C. 1983. A Method for Determing the Interactive Behavior of Polymer Grids and Granular Soils. Report No. BCS/G1/2A, Bolton Institue of Higher Education, 30p.

Saxena, S. K., and Wong, Y. T. 1984. Frictional Characteristics of a Geomembrane. Proceedings, International Conference on Geomembranes, Denver, Vol. 1, pp. 187-190.

Seed, H. B., Mitchell, J. K., and Chan, C. K. 1960. The Strength of Compacted Cohesive Soils. Proceedings, ASCE Research Conference on Shear Strength of Cohesive Soils, University of Colorado, June, pp. 887-964.

Snaith, M. S., Bell, A. L., and DuBois, D. D. 1979. Embankment Construction from Marginal Material. Proceedings, International Conference on Soil Reinforcement: Reinforced Earth and Other Techniques, Paris, March, Vol. 1, pp. 175-180.

Southern Waterway Authority, Kent River and Water Division. 1982. Shear Box Tests on Tensar SR2 Embedded in London Clay. Bolton Institute of Technology, 15p.

Wernick, E. 1977. Stresses and Strains on the Surface of Anchors. Revue Francaise de Geotechnique, No. 3, pp. 113-119.

Williams, N. D., and Houlihan, M. F. 1987. Evaluation of Interface Friction Properties Between Geosynthetics and Soils. Proceedings, Geosynthetic' 87 Conference, New Orleans, Feb., Vol. 2, pp. 616-627.

APPENDIX A: Soil-Geosynthetic Interfacial Shear Strength

Table A.1 Granular Soil-Geotextile/Geogrid Interfacial Shear Strength

Reference	Shear Test Description	Soil Description					Reinforcement Description	Interfacial Shear Strength	Efficiency
		Type	γ_d (g/cm^3)	C_u (%)	ϕ (°)	c kPa		δ (°)	
Akhter and Hadmanji (1985)	15.2 cm^2 Partially fixed shear test Static compaction Shear rate = 0.1 mm/s	Granular well graded subangular particles					Non woven, needle punched geotextiles		
		1. Soil passing 3/4" sieve, retained on 3/8" sieve			42.0		338 g/cm^2 585 g/cm^2 792 g/cm^2	30.7 30.0 30.0	0.66 0.64 0.64
		2. Soil passing 1/4" sieve, retained on #4 sieve			41.0		338 g/cm^2 585 g/cm^2 792 g/cm^2	29.6 28.2 28.4	0.65 0.62 0.62
		3. Soil passing #4 sieve, retained on #10 sieve			40.6		338 g/cm^2 585 g/cm^2 792 g/cm^2	28.9 28.1 27.7	0.64 0.62 0.61
		4. Soil passing #10 sieve, retained on #20 sieve			40.3		338 g/cm^2 585 g/cm^2 792 g/cm^2	29.3 27.9 27.6	0.66 0.61 0.62
Collin et al. (1980)	40 cm x 25 cm Partially fixed shear test Shear rate = 0.1 mm/s	1. Crushed gravel particle size 5 to 20 mm	1.45		53.0		Texunion, woven split film, opening size 1 mm	53.0	1.00
							Nets 1. Nortene 5548 opening size 7 mm	52.0	0.98
							2. Nortene 5550 opening size 28 mm	54.0	1.02
							3. Nortene 5515 opening size 28 mm	57.0	1.16
		2. Ballast stones	1.46		63.0		Texunion, woven split film, opening size 1 mm	50.0	0.61
DeGoutte and Mathieu (1986)	30 cm^2 Fixed shear test Static compaction Normal stress 200 to 1200 kPa	Sand D_{60}/D_{10} = 2.0 D_{50} = 0.3 mm	1.60	5.2	39.0		Geotextile	16.0	0.90
	3 cm^2 Fixed shear test Static compaction Normal stress 300 to 600 kPa	Sand D_{60}/D_{10} = 2.0 D_{50} = 0.3 mm	1.60	5.2	39.0		Geotextile	34.0	0.83
Ingold (1980, 1982, 1983, 1984)	6 cm^2 Fixed shear test Shear rate = 2%/min Normal stress 50 to 200 kPa Consolidated Drained	Boreham Woodpit Sand C_u = 2.8 G = 2.64 ρ_d = 1.91 g/cm^3	1.88		34.0		Nets 1. Netlon CE111 Oval mesh 5x7 mm^2 Thickness 2.9 mm	27.5	0.78
							2. Netlon CE121 Oval mesh 6x7 mm^2 Thickness 3.3 mm	32.0	0.93
							3. Netlon CE131 Oval mesh 25x30 mm^2 Thickness 5.2 mm	33.5	0.98
							4. Netlon CE161 Diamond mesh 10 mm pitch Thickness 4.0 mm	34.0	1.00
							5. Netlon 1168 Diamond mesh 6.5 mm pitch Thickness 4.0 mm	34.0	1.00
							6. Netlon FBM5 Rectilinear grid Opening size 11x60mm^2 Thickness 4.0mm	34.0	1.00
							Non Woven 1. Terram 1000 Melt bonded Thickness 0.7 mm	31.0	0.89
							2. Terram 2000 Melt bonded Thickness 1.0 mm	31.0	0.89
							Composite 1. Terram RF/12 Knitted and woven	31.0	0.89

Table [illegible] Continue

Reference	Shear Test Description	Soil Description					Reinforcement Description	Interfacial Shear Strength	Efficiency
		Type	ρ_d (g/cm^3)	w (%)	ϕ (°)	c kPa		δ (°)	
Ingold (1980, 1982, 1983, 1984)	30 cm^2 Partially fixed shear test Shear rate = 1 mm/min Normal stress 50 to 200 kPa	Boreham Woodpit Sand C_u = 2.8 G = 2.64 ρ_d = 1.91 g/cm^3	1.87		35.0		Non woven, melt bonded 240 g/m^2	25.0 to 30.0	0.67 to 0.82
							Knitted/woven, rough surface 320 g/m^2	35.0	1.00
							Geogrid	33.0	0.92
	30 cm^2 Fixed shear test Shear rate = 1 mm/min Normal stress 50 to 200 kPa	Boreham Woodpit Sand C_u = 2.8 G = 2.64 ρ_d = 1.91 g/cm^3	1.87		35.0		Non woven, melt bonded 240 g/m^2	27.0 to 32.0	0.71 to 0.89
							Knitted/woven, rough surface 320 g/m^2	31.0	0.86
							Geogrid	29.0	0.79
Koerner (1986) Martin, Koerner, and Whitty (1982)	10.0 cm^2 Fixed shear test Shear rate = 0.127 mm/min	1. Concrete Sand D_{50} = 0.20 mm C_u^d = 2.6 D_d = 0.9 Angular shaped particles			30.0		Polyfilter X Woven monofilament Stiff, thin High % open area	26.0	0.84
							Mirafi 500X Woven split film Thin, flexible High % open area	24.0	0.77
							DuPoint 140 Non woven heat set Flexible, thin Low % open area	26.0	0.84
							CZ 600 Non woven needled punched Thick, flexible High % open area	30.0	1.00
		2. Mica Schist Silty Sand D_{10} = 0.057 mm C_u = 5.1			26.0		Mirafi 500X	23.0	0.87
							CZ 600	25.0	0.96
		3. Ottawa Sand D_{10} = 0.42 mm C_u = 1.9 Rounded particles			28.0		Mirafi 500X	24.0	0.84
							CZ 600	26.0	0.92
Marshall (1983, 1983)	30 cm^2 Partially fixed shear test Vibratory hammar compaction Shear rate = 0.2 mm/min Normal stress 50 to 200 kPa	1. Crushed Limestone G = 2.65 ρ_d = 2.30 g/cm^3 w_{opt} = 6.5 %	2.08		53.0		Tensar SR2 Opening size 106 mm x 22.9 mm	51.0	0.93
		2. Crushed Limestone G = 2.65 ρ_d = 2.17 g/cm^3 w_{opt} = 8.5 %	1.99		40.5		Tensar SR2	36.5	0.87

Table A.1 Continue

Reference	Shear Test Description	Soil Description: Type	ρ_d (g/cm³)	w (%)	ϕ (°)	c kPa	Reinforcement Description	Interfacial Shear Strength δ (°)	Efficiency
Rowe, Ho, Fisher (1985)	10 cm² Partially fixed shear test No compaction	Silty Sand D_{50} = 0.2 mm			32.0		Geotextile 1. Permealiner M1195 Woven, 225 g/m² 0.4 mm thick	32.0	1.00
							2. Mirafi P600 X Woven, 207 g/m² 0.4 mm thick	32.0	1.00
							3. Mirafi P500 Woven, 167 g/m² 0.4 mm thick	33.0	1.04
							4. Geolon 1250 Woven, 730 g/m² 2.26 mm thick	35.0	1.12
							5. Terrafix 370RS Composite, non woven 475 g/m², 0.9 mm thick	36.0	1.16
							6. Terrafix 1200R Woven, 1019 g/m² 4.5 mm thick	36.0	1.16
							7. Tensar SR2 Open mesh, 938 g/m² 3.0 mm thick	30.0	0.92
Saraby (1983)	30 cm² Partially fixed shear test Vibratory hammar compaction Shear rate = 0.6mm/min Normal stress 50 to 200 kPa	Pulverized Fuel A h	1.10	27.4	35.0		Tensar SR2	29.5	0.81
Saraby and Marshall (1987)	30 cm² Partially fixed shear test Vibratory hammar Shear rate = 0.6 mm/min Normal stress 50 to 200 kPa	1. Crushed Limestone ρ_d = 2.13 g/cm³ w_{opt} = 7.5 %	1.91		58.8		Tensar SR2	58.3	1.00
		2. Bolton Crushed Stone ρ_d = 2.06 g/cm³ w_{opt} = 7.8%	1.84		55.6		Tensar SR2	55.0	1.00
Williams and Houlihan (1987)	30.5 cm² Partially fixed or free shear test Shear rate = 0.3 mm/min Normal stress 0 to 100 kPa	1. Ottawa Sand C_u = 1.3 D_d = 0.95 Well rounded particles	1.57		38.0		Typar 3401 Non woven heat bonded Smooth surface 0.38 mm thick	25.0	0.60
							Trevira 1155 Non woven	28.0	0.68
							Nicolon 900-M Woven, rough surface	35.0	0.90
		2. Concrete Sand D_d = 0.95 Subrounded to subangular particles	1.51		36.0		Typar 3401	27.0	0.60
							Trevira 1155	28.0	0.68
							Nicolon 900-M	35.0	0.90
		3. Saprolite C_u = 2.0 ρ_d = 1.62 g/cm³ w_{opt} = 12.0% Subangular to angular, medium to fine sand with 0.5 to 1% mica	1.58	12.0	36.0		Typar 3401	29.0	0.80
							Trevira 1155	30.0	0.79
							Nicolon 900-M	31.0	0.83

Table A.2 Cohesive Soil-Geotextile/Geogrid Interfacial Shear Strength

Reference	Shear Test Description	Soil Description: Type	γ_d (g/cm³)	w (%)	ϕ (°)	c kPa	Reinforcement Description	Interfacial Shear Strength: δ (°)	c_a kPa	Efficiency: E_ϕ	E_c
DeGoutte and Mathieu (1986)	30 cm² Fixed shear test Static compaction Normal stress 200 to 1200 kPa	Sandy Clay w_p = 13.0% Particle size 23% finer than 80 μm 7% finer than 2 μm	1.84	12.5	33.5	50.0	Geotextile	19.0		1.22	
Ingold (1980, 1983)	6.0 cm² Fixed shear test Static compaction Shear rate = 2%/min Normal stress 50 to 200 kPa	Kaolin Clay	1.87	34.0	24.0	0.0	Nets 1. Netlon CE111 Oval mesh 5x7 mm² Thickness 2.9 mm	14.5		0.58	
							2. Netlon CE121 Oval mesh 6x7 mm² Thickness 3.3 mm	16.5		0.67	
							3. Netlon CE131 Oval mesh 25x30 mm² Thickness 5.2 mm	17.0		0.69	
							4. Netlon CE161 Diamond mesh 10 mm pitch Thickness 4.0 mm	19.0		0.77	
							Non woven 1. Terram 1000 Melt bonded Thickness 0.7 mm	20.0		0.83	
							2. Terram 2000 Melt bonded Thickness 1.0 mm	20.0		0.83	
Lafleur, Sall, and Ducharme (1987)	5.0 cm² Partially fixed shear test Shear rate = 0.024 mm/min Normal stress = 50 to 150 kPa	Plastic clay w_L = 56% w_p = 26% I_p = 30%		25.0	35.0	8.0	Woven MP-500 Stiff, 0.4 mm thick	22.0		0.58	
							Non woven PF-700 1.7 mm thick	37.0		1.08	
							Non woven TX-7643 2.3 mm thick	39.0		1.16	
				40.0	32.0	6.0	Woven MP-500	21.0		0.61	
							Non woven PF-700	37.0		1.04	
							Non woven TX-7643	34.0		1.08	
				60.0			Woven MP-500	15.0		0.48	
							Non woven PF-700	29.0		1.00	
							Non woven TX-7643	28.0		0.96	
Southern Water Authority (1982)	30.0 cm² Partially fixed shear test Dynamic compaction Shear rate = 3.0 mm/min	1. Brown plastic clay w_L = 82% I_p = 42.9%		37.2	12.9		Tensar SR2	9.2		0.71	
		2. Brown Sandy Clay w_L = 40.5% I_p = 1.9%		37.4	18.9		Tensar SR2	16.2		0.85	
Williams and Houlihan (1987)	30.5 cm² Partially fixed or free shear test Shear rate = 0.3 mm/min Normal stress 0 to 100 kPa	1. Ottawa sand and 5% Bentonite w_p = 16%, I_p = 20% e = 0.7, S = 43% ρ_d = 1.76 g/cm³ w_{opt} = 9%	1.70	10.0	36.0		Typar 3401 Non woven heat bonded Smooth surface 0.38 mm thick	22.0	0.6	0.56	
							Trevira 1155 Non woven	27.0	1.4	0.70	
							Nicolon 900-H Woven, rough surface	31.0	0.1	0.83	
		2. Ottawa Sand and 10% Bentonite w_p = 20%, I_p = 27%	1.87	13.3	36.0		Typar 3401	22.0	0.6	0.56	
							Trevira 1155	27.0	1.4	0.70	
							Nicolon 900-H	34.0	0.1	0.93	
		3. Gulf Coast Clay w_p = 28%, I_p = 14% e = 0.74, S = 63% ρ_d = 1.84 g/cm³ w_{opt} = 15.5%	1.81	15.5	20.0	57.0	Typar 3401	39.0	1.3	2.22	0.03
							Trevira 1155	45.0	1.8	2.75	0.03
							Nicolon 900-H	43.8	2.0	2.57	0.04
		4. Glacial Till w_p = 17%, I_p = 0%	2.17	7.5	36.0	31.0	Typar 3401	33.0	0.4	0.89	0.01
							Trevira 1155	37.0	0.5	1.04	0.02

Table A.3 Granular Soil-Geomembrane Interfacial Shear Strength

Reference	Shear Test Description	Soil Description					Reinforcement Description	Interfacial Shear Strength	Efficiency
		Type	ρ_d	w	ϕ	c		δ	
			(g/cm^3)	(%)	(°)	kPa		(°)	
Akber and Kammanji (1985)	15.2 cm^2 Partially fixed shear test Static compaction Shear rate = 0.1 mm/s	Granular well graded subangular particles							
		1. Soil passing 3/4" sieve, retained on 3/8" sieve			42.0		1. PVC-2 1.68 mm thick, rough surface	33.4	0.74
							2. PVC-4 0.75 mm thick, flexible and smooth surface	30.5	0.65
							3. EPDM 1.13 mm thick, flexible and rough surface	33.7	0.74
							4. HDPE 1.5 mm thick, stiff and smooth surface	24.9	0.52
							5. BPX-1 3.88 mm thick, flexible but surface	36.4	0.82
							6. BPX-1 3.88 mm thick flexible but smooth surface	34.2	0.75
							7. NPT 3.75 mm thick stiff and smooth surface	41.0	0.97
							8. NPT 3.75 mm thick stiff and rough surface	43.1	1.04
		2. Soil passing 3/8" sieve, retained on #4 sieve			41.0		1. PVC-2	33.6	0.76
							2. PVC-4	28.1	0.61
							3. EPDM	31.3	0.70
							4. HDPE	23.2	0.49
							5. BPX-1 (smooth)	36.0	0.84
							6. BPX-L (rough)	34.7	0.80
							7. NPT (smooth)	40.0	0.97
							8. NPT (rough)	41.0	1.00
		3. Soil passing #4 sieve, retained on #10 sieve			40.6		1. PVC-2	30.7	0.69
							2. PVC-4	28.5	0.63
							3. EPDM	30.5	0.69
							4. HDPE	22.2	0.48
							5. BPX-1 (smooth)	35.6	0.84
							6. BPX-1 (rough)	36.0	0.85
							7. NPT (smooth)	38.5	0.93
							8. NPT (rough)	38.2	0.92
		4. Soil passing #10 sieve, retained on #20 sieve			40.3		1. PVC-2	30.4	0.69
							2. PVC-2	25.0	0.55
							3. EPDM	33.4	0.78
							4. HDPE	22.1	0.48
							5. BPX-1 (smooth)	34.2	0.80
							6. BPX-1 (rough)	38.1	0.92
							7. NPT (smooth)	35.8	0.85
							8. NPT (rough)	35.0	0.83
DeGoutte and Mathieu (1986)	30 cm^2 Fixed shear test Static compaction Normal stress 200 to 1200 kPa	Sand D_{60}/D_{10} = 2.0 D_{50} = 0.3 mm			39.0		PVC	36.5	0.91

Table A.3 Continue

Reference	Shear Test Description	Soil Description: Type	γ_d (g/cm^3)	w (%)	ϕ (°)	c kPa	Reinforcement Description	Interfacial Shear Strength δ (°)	Efficiency $\frac{\delta}{\phi}$
Koerner (1986) Martin, Koerner, and Whitty (1984)	10.0 cm^2 Fixed shear test Shear rate = 0.127 mm/min	1. Concrete Sand D_{50} = 0.20 mm C_u = 2.6 D_d = 0.9 Angular shaped particles			30.0		1. EPDM 0.75 mm thick, flexible and smooth surface	24.0	0.77
							2. HDPE 0.5 mm thick, stiff and smooth surface	18.0	0.56
							3. PVC 0.75 mm thick, medium stiff and rough surface	27.0	0.88
							4. PVC 0.75 mm thick, medium stiff and smooth surface	25.0	0.81
		2. Ottawa Sand D_{10} = 0.42 mm C_u = 1.9 Rounded particles			28.0		1. EPDM 2. HDPE	20.0 18.0	0.68 0.61
		3. Mica Schist Silty Sand D_{10} = 0.057 mm C_u = 5.1			26.0		1. EPDM 2. HDPE 3. PVC (rough) 4. PVC (smooth)	24.0 17.0 25.0 21.0	0.91 0.63 0.96 0.79
Leach, Harpe, and [illegible]		Sand					PVC (rough) PVC (smooth) HDPE	25.0 - 27.0 21.0 - 25.0 17.0 - 27.0	
	27.9 cm^2 Partially fixed shear test Shear rate = .76 mm/min Normal stress 68.9 to 206.7 kPa	1. Ottawa Sand G = 2.66	1.88				HDPE	21.7	
		2. Low grade Limestone Ballast	2.01				HDPE	53.0	
Williams and Houlihan (1987)	30.5 cm^2 Partially fixed or free shear test Shear rate = .3 mm/min Normal stress 0 to 100 kPa	1. Ottawa Sand C_u = 1.3 D_d = 0.95 Well rounded particles	1.57		38.0		HDPE 1.5 mm thick and smooth surface	19.0	0.44
							PVC 0.75 mm thick and smooth surface	26.0	0.62
		2. Concrete Sand D_d = 0.95 Subrounded to subangular particles	1.51		36.0		HDPE PVC	27.0 33.0	0.70 0.89
		3. Saprolite C_u = 2.0 ρ_d = 1.62 g/cm^3 $w_{d\ opt}$ = 12.0% Subangular to angular, medium to fine sand with 0.5 to 1% mica	1.58	12.0	36.0		HDPE PVC	21.0 28.0	0.53 0.73

Table A.4 Cohesive Soil-Geomembrane Interfacial Shear Strength

Reference	Shear Test Description	Soil Description: Type	ρ_d (g/cm³)	w (%)	ϕ (°)	c kPa	Reinforcement Description	Interfacial Shear Strength: δ (°)	c_a kPa	Efficiency: E_ϕ	E_c
DeGoutte and Mathieu (1986)	30 cm² Fixed shear test Static compaction Normal stress 200 to 1200 kPa	Sandy Clay 7% finer than 2 micron	1.84	12.5	33.5	50.0	PVC	35.0		1.06	
Koerner, Martin, and Koerner (1986)	10.2 cm² Fixed shear test Shear rate = 0.06 mm/min	1. Delaware River Clayey Silt w_L = 28%, I_p = 8% ρ_d = 1.81 g/cm³ w_{opt} = 13.5%	1.52	13.5	38.0	9.0	PVC	39.0	8.5	1.00	0.94
							CPE	40.0	8.0	1.00	0.89
							EPDM	33.0	5.0	0.87	0.55
							HDPE	26.0	5.0	0.68	0.88
							Embossed HDPE	35.0	9.0	0.92	1.00
		2. Sandy Silty Clay w_L = 46%, I_p = 29% ρ_d = 1.94 g/cm³ w_{opt} = 11.8%	1.63	11.8	34.0	12.0	PVC	23.0	3.7	0.69	0.31
							CPE	24.0	3.2	0.71	0.27
							EPDM	23.0	5.0	0.67	0.42
							Embossed HDPE	29.0	11.0	0.85	0.92
		3. Kaolinite Clay w_L = 57%, I_p = 27% ρ_d = 1.39 g/cm³ w_{opt} = 31.0%	1.39	30.8	30.0	20.0	PVC	16.0	14.0	0.53	0.70
							CPE	17.0	13.0	0.52	0.65
							EPDM	23.0	8.0	0.77	0.70
							HDPE	15.0	14.0	0.50	0.70
							Embossed HDPE	27.0	18.0	0.90	0.90
		4. Clayey Sand w_L = 87%, I_p = 72% ρ_d = 1.81 g/cm³ w_{opt} = 15.0%	1.73	16.2	24.0	25.0	PVC	24.0	8.0	1.00	0.28
							CPE	23.0	8.0	0.96	0.32
							EPDM	20.0	7.5	0.83	0.30
							HDPE	21.0	3.0	0.88	0.12
							Embossed HDPE	26.0	15.0	1.00	0.60
		5. Sandy Clay w_L = 87%, I_p = 72% ρ_d = 1.81 g/cm³ w_{opt} = 17.0%	1.72	18.2	28.0	22.0	PVC	17.0	12.0	0.77	0.43
							CPE	19.0	10.0	0.86	0.36
							EPDM	18.0	9.0	0.82	0.32
							HDPE	15.0	14.0	0.68	0.50
							Embossed HDPE	25.0	16.0	1.00	0.57
Leach, Harpe, and Tape (1987)		Clay					PVC (rough)	26.2			
							PVC (smooth)	25.0			
							HDPE	13.0			
Saxena and Wong (1984)	27.9 cm² Partially fixed shear test Shear rate = 0.76 mm/min Normal stress 68.9 to 206.7 kPa	Sandy Clay	1.76	16.0	12.6	7.6	HDPE	13.9	7.5	1.10	0.99
Williams and Houlihan (1987)	30.5 cm² Partially fixed or free shear test Shear rate = 0.3 mm/min Normal stress 0 to 100 kPa	1. Ottawa Sand and 5% Bentonite w_o = 16%, I_p = 20% e = 0.7, S = 41% ρ_d = 1.76 g/cm³ w_{opt} = 9%	1.70	10.0	36.0		HDPE 1.5 mm thick and smooth surface	14.0	0.6	0.34	
							PVC 0.75 mm thick and smooth surface	19.0	0.8	0.47	
		2. Ottawa Sand and 10% Bentonite w_p = 20%, I_p = 27%	1.87	13.3	36.0		HDPE	17.0	0.6	0.42	
							PVC	19.0	0.7	0.47	
		3. Gulf Coast Clay w_p = 28%, I_p = 14% e = 0.74, S = 63% ρ_d = 1.84 g/cm³	1.81	15.5	20.0	57.0	HDPE	25.0	1.0	1.28	0.02
							PVC	23.0	1.6	1.17	0.03
		4. Glacial Till w_p = 17%, I_p = 0%	2.17	7.5	36.0	31.0	HDPE	22.0	0.7	0.56	0.03
							PVC	25.0	1.0	0.64	0.03

APPENDIX B: Calibration and Compliance of Direct Shear Apparatus

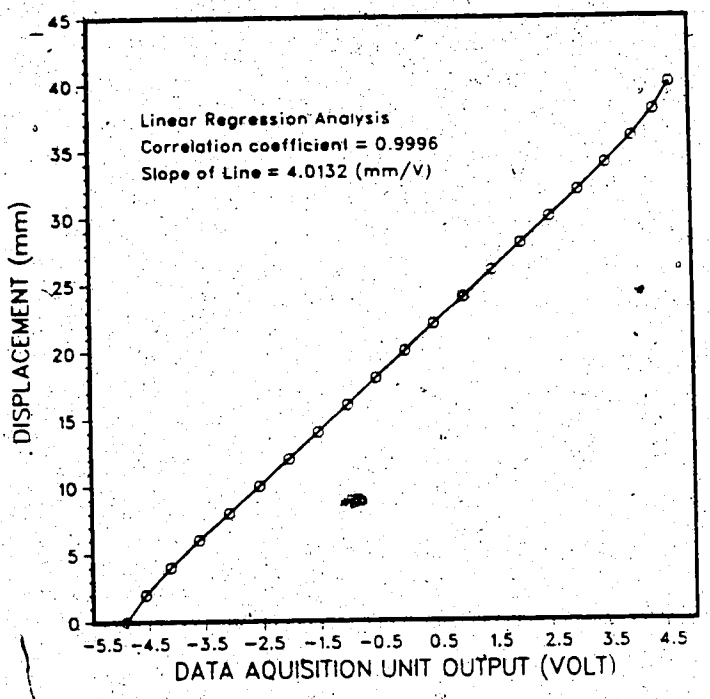

Figure B.1 Calibration Curve for Linear Variable Differential Transformer No. 1

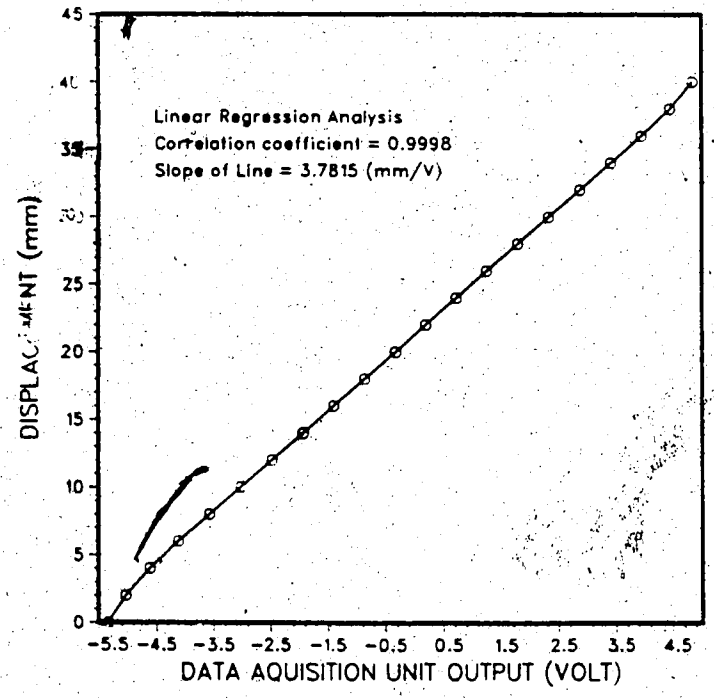

Figure B.2 Calibration Curve for Linear Variable Differential Transformer No. 2

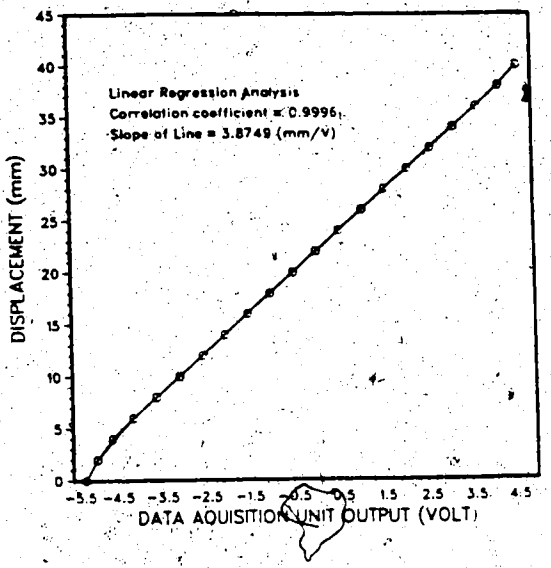

Figure B.3 Calibration Curve for Linear Variable Differential Transformer No. 3

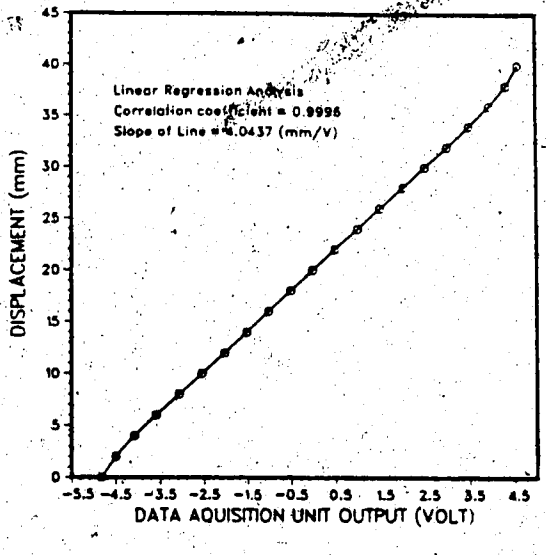

Figure B.4 Calibration Curve for Linear Variable

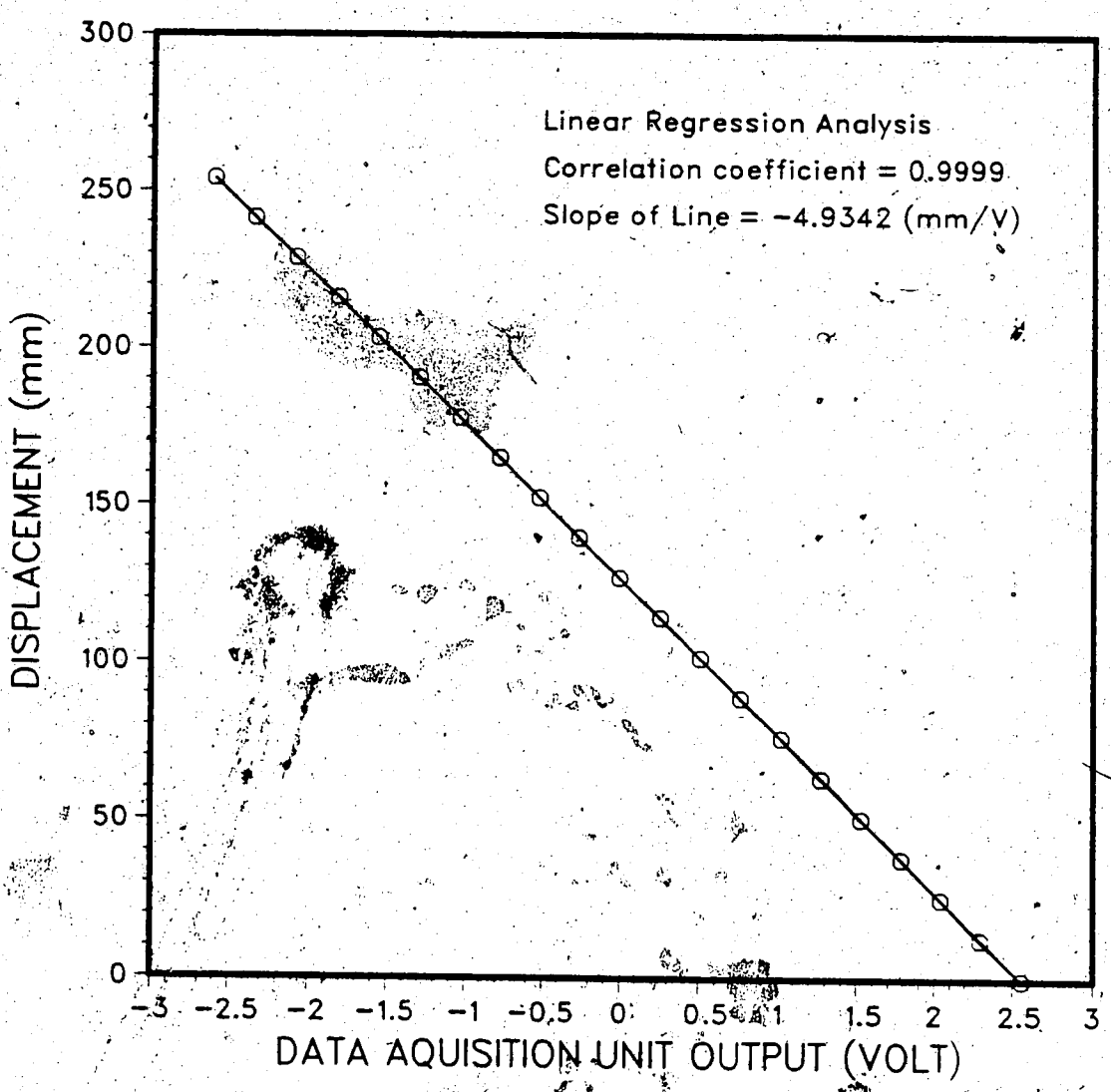

Figure B.5 Calibration Curve for Linear Variable Differential Transformer for Measuring Horizontal

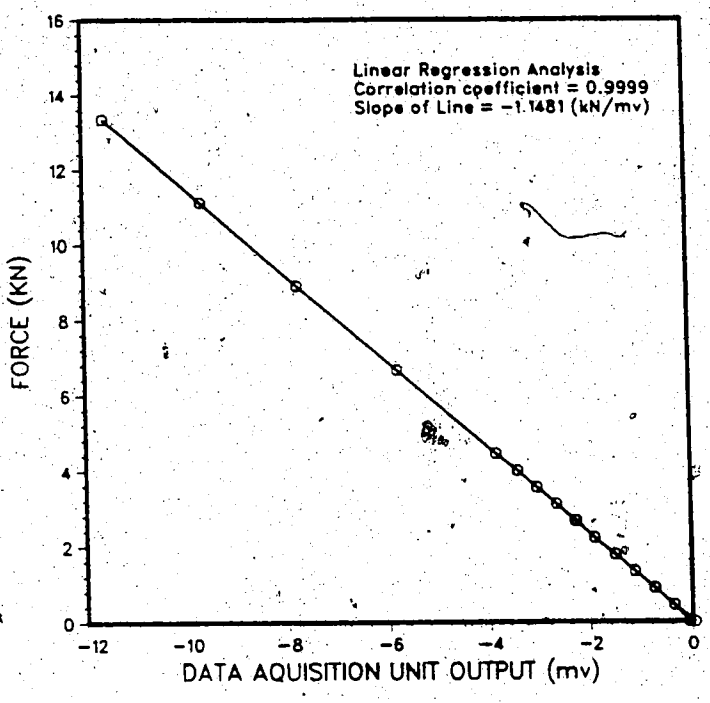

Figure B.6 Calibration Curve for Load Cell

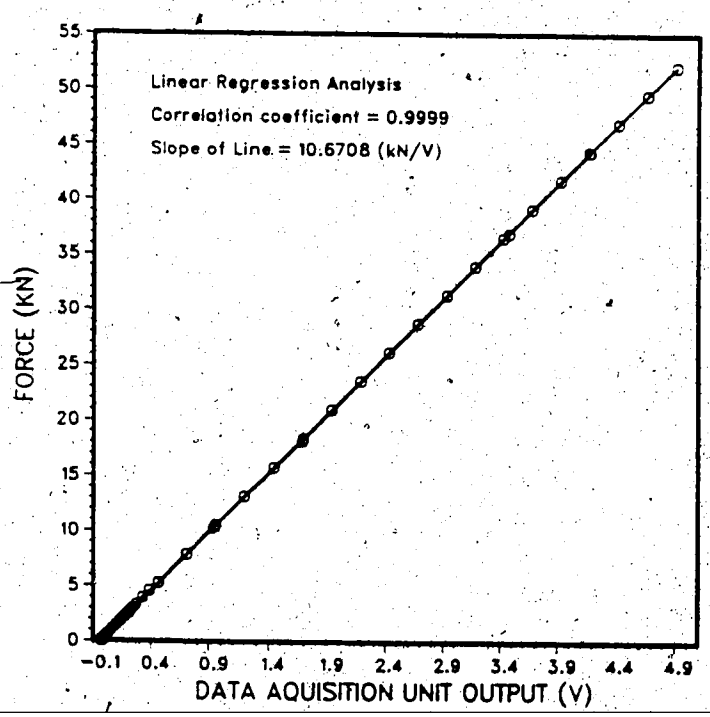

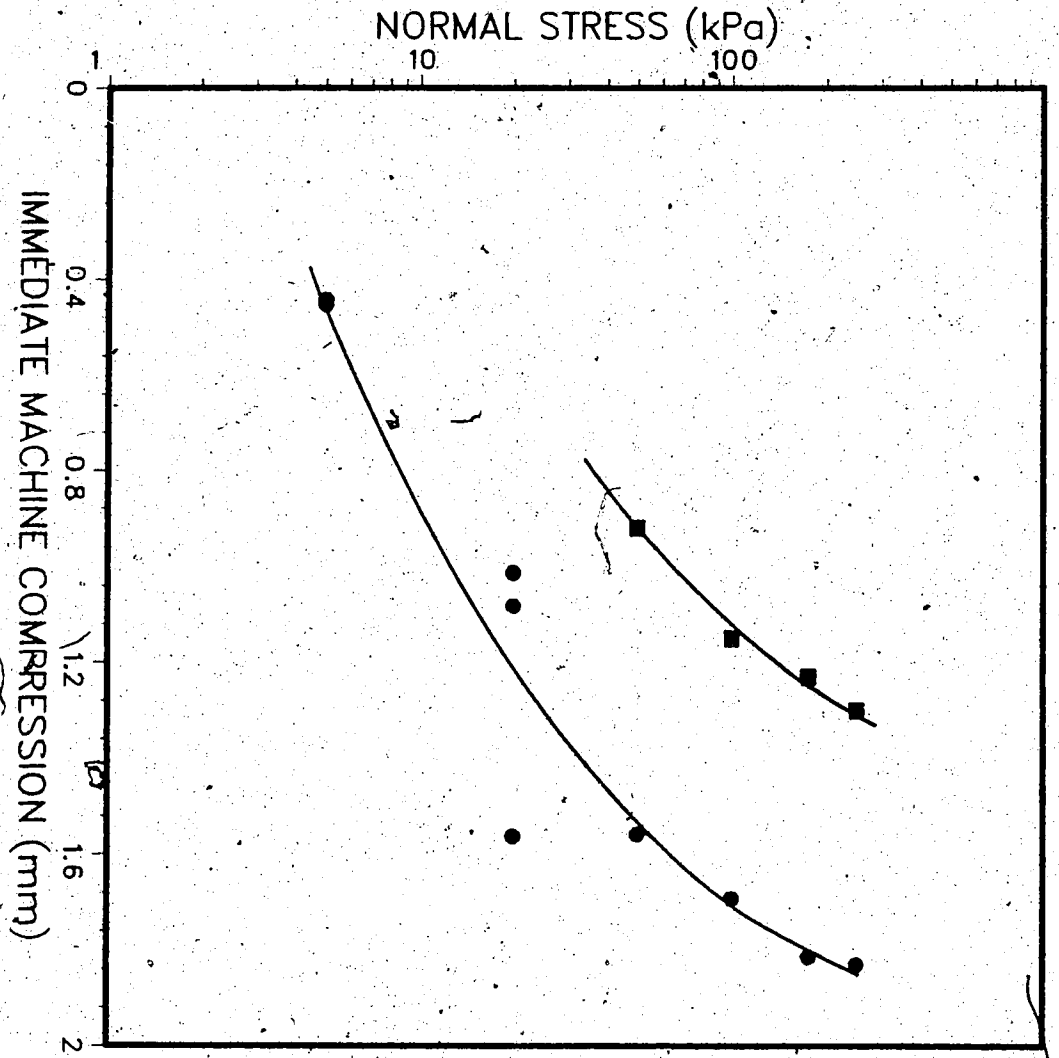
NORMAL STRESS (kPa)
1
10
100
0
0.4
0.8
1.2
1.6
2
IMMEDIATE MACHINE COMPRESSION (mm)

APPENDIX C: Reinforced Sand Test Results

Table C.1 Data of Sand

Test No.	1	2	3	4	5	6
Initial						
w %	0.72	0.72	0.72	0.72	0.58	0.58
ρ_w (g/cm^3)	1.75	1.79	1.79	1.78	1.77	1.78
ρ_d (g/cm^3)	1.74	1.77	1.77	1.77	1.76	1.77
e	0.52	0.48	0.48	0.49	0.50	0.49
D_d (%)	72.30	79.20	79.20	78.50	76.50	78.00
S (%)	3.70	3.90	3.90	3.90	3.10	3.10
After						
ρ_w (g/cm^3)	1.77	1.85	1.85	1.82	1.77	1.78
ρ_d (g/cm^3)	1.76	1.83	1.84	1.80	1.76	1.77
e	0.50	0.44	0.43	0.46	0.50	0.49
D_d (%)	75.90	89.60	90.80	84.00	76.50	78.00
Compacted Height (cm)	9.82	9.63	9.58	9.64	9.55	9.89
Δh (mm)	0.93	2.67	1.04	1.48	0.12	-1.37
Normal Stress (kPa)	175.0	250.0	100.0	50.0	175.0	20.0
Maximum Shear Stress (kPa)	161.2	234.5	99.6	50.8	164.4	25.5
Displacement to Peak (mm)	9.70	11.20	10.10	8.50	12.80	9.72
Residual Shear Stress (kPa)	139.6	191.2	79.0	40.1	39.1	20.5
Remarks:						

Table C.2 Data of Sand Reinforced with SR2

Test No.	1	2	3	4	5	6
Initial						
w %	0.61	0.61	0.47	0.47	0.47	0.53
ρ_w (g/cm^3)	1.77	1.77	1.78	1.76	1.76	1.78
ρ_d (g/cm^3)	1.76	1.76	1.77	1.76	1.75	1.78
e	0.50	0.50	0.49	0.50	0.50	0.48
D_d (%)	75.70	76.20	78.40	75.70	75.30	79.60
S (%)	3.20	3.20	2.50	2.50	2.50	2.90
After						
ρ_w (g/cm^3)	1.77	1.77	1.79	1.75	1.77	1.79
ρ_d (g/cm^3)	1.76	1.76	1.78	1.75	1.76	1.79
e	0.50	0.49	0.48	0.51	0.49	0.48
D_d (%)	76.90	77.40	79.60	73.80	77.10	81.00
Compacted Height (cm)	9.96	9.82	9.78	9.88	9.89	10.21
Δh (mm)	0.39	0.20	0.31	-0.58	0.54	0.27
Normal Stress (kPa)	175.0	250.0	100.0	50.0	100.0	50.0
Maximum Shear Stress (kPa)	157.9	215.5	93.5	53.6	92.5	50.9
Displacement to Peak (mm)	10.10	10.50	7.10	7.40	7.50	8.90
Residual Shear Stress (kPa)	109.0	176.7	73.5	41.4	73.5	40.4
Remarks:						

Table C.3 Data of Sand Reinforced with SS2

Test No.	1	2	3	4	5
Initial					
w %	0.66	0.66	0.67	0.47	0.47
ρ_w (g/cm^3)	1.81	1.79	1.77	1.76	1.74
ρ_d (g/cm^3)	1.80	1.78	1.76	1.76	1.73
e	0.46	0.47	0.50	0.50	0.52
D_d (%)	84.00	82.00	77.00	77.00	72.00
S (%)	3.70	3.70	3.50	3.50	2.40
After					
ρ_w (g/cm^3)	1.82	1.84	1.79	1.78	1.74
ρ_d (g/cm^3)	1.81	1.83	1.78	1.77	1.73
e	0.45	0.44	0.48	0.49	0.52
D_d (%)	87.20	88.70	79.90	78.60	72.40
Compacted Height (cm)	9.55	9.61	9.75	9.79	9.91
Δh (mm)	1.19	2.45	0.97	0.36	0.05
Normal Stress (kPa)	175.0	250.0	100.0	50.0	100.0
Maximum Shear Stress (kPa)	148.4	222.0	88.6	47.6	89.9
Displacement to Peak (mm)	10.60	12.40	9.00	9.00	10.30
Residual Shear Stress (kPa)	134.1	203.3	74.9	37.4	74.2
Remarks:					

Table C.4 Data of Sand Reinforced with TNX-5001

Test No.	1	2	3	4
Initial				
w %	0.75	0.75	0.80	0.80
ρ_w (g/cm^3)	1.79	1.79	1.80	1.79
ρ_d (g/cm^3)	1.77	1.78	1.79	1.77
e	0.48	0.48	0.47	0.49
D_d (%)	80.20	79.40	82.10	79.10
S (%)	4.10	4.10	4.50	4.30
After				
ρ_w (g/cm^3)	1.81	1.81	1.82	1.79
ρ_d (g/cm^3)	1.79	1.79	1.81	1.78
e	0.47	0.47	0.46	0.48
D_d (%)	83.00	83.30	85.40	80.00
Compacted Height (cm)	9.67	9.68	9.62	9.72
Δh (mm)	1.11	1.13	1.00	0.36
Normal Stress (kPa)	184.0	250.0	100.0	50.0
Maximum Shear Stress (kPa)	166.9	216.2	91.8	46.7
Displacement to Peak (mm)	11.40	11.40	10.80	6.00
Residual Shear Stress (kPa)	147.2	191.4	79.5	39.7
Remarks:				

Table C.5 Data of Sand Reinforced with ParaGrid 50S

Test No.	1	2	3	4
Initial				
w %	0.61	0.61	0.61	0.61
ρ_w (g/cm^3)	1.77	1.79	1.79	1.78
ρ_d (g/cm^3)	1.76	1.77	1.78	1.77
e	0.50	0.49	0.48	0.49
D_d (%)	76.90	79.00	80.50	78.10
S (%)	3.20	3.30	3.40	3.30
After				
ρ_w (g/cm^3)	1.78	1.79	1.80	1.79
ρ_d (g/cm^3)	1.76	1.77	1.79	1.77
e	0.49	0.48	0.47	0.49
D_d (%)	77.90	79.70	82.00	79.10
Compacted Height (cm)	9.80	9.74	9.69	9.78
Δh (mm)	0.10	0.05	0.40	-1.30
Normal Stress (kPa)	175.0	250.0	100.0	50.0
Maximum Shear Stress (kPa)	163.0	224.0	99.0	57.6
Displacement to Peak (mm)	12.70	11.10	10.50	8.70
Residual Shear Stress (kPa)	137.2	183.0	79.7	48.4
Remarks:				

Table C.6 Data of Sand Reinforced with P600

Test No.	1	2	3	4	5
Initial					
w %	0.64	0.64	0.64	0.64	0.64
ρ_w (g/cm^3)	1.77	1.77	1.76	1.77	1.78
ρ_d (g/cm^3)	1.76	1.76	1.75	1.76	1.77
e	0.50	0.50	0.50	0.50	0.49
D_d (%)	76.00	76.00	75.10	76.50	78.00
S (%)	3.40	3.40	3.30	3.40	3.40
After					
ρ_w (g/cm^3)	1.77	1.77	1.76	1.81	1.81
ρ_d (g/cm^3)	1.76	1.76	1.75	1.80	1.80
e	0.50	0.50	0.50	0.47	0.47
D_d (%)	77.00	76.00	75.10	82.00	82.00
Compacted Height (cm)	9.71	9.73	9.78	9.74	9.68
Δh (mm)	0.14	0.06	0.01	0.40	0.30
Normal Stress (kPa)	175.0	250.0	100.0	50.0	100.0
Maximum Shear Stress (kPa)	126.7	189.9	73.9	43.8	133.0
Displacement to Peak (mm)	8.10	7.30	6.70	5.50	6.40
Residual Shear Stress (kPa)	134.1	203.3	74.9	37.4	74.2
Remarks:					

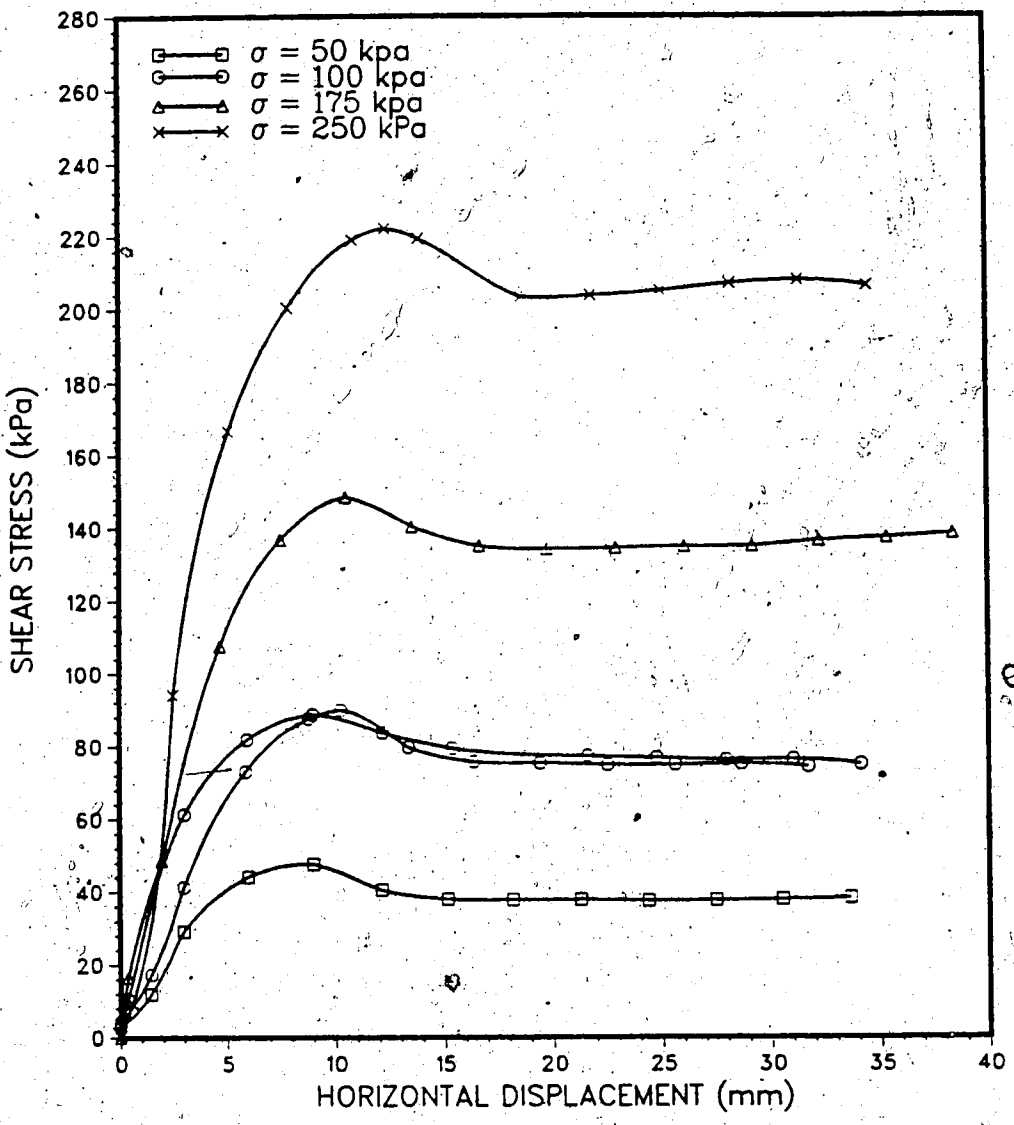
σ = 50 kpa
σ = 100 kpa
σ = 175 kpa
σ = 250 kPa
SHEAR STRESS (kPa)
HORIZONTAL DISPLACEMENT (mm)
0
20
40
60
80
100
120
140
160
180
200
220
240
260
280
0
5
10
15
20
25
30
35
40

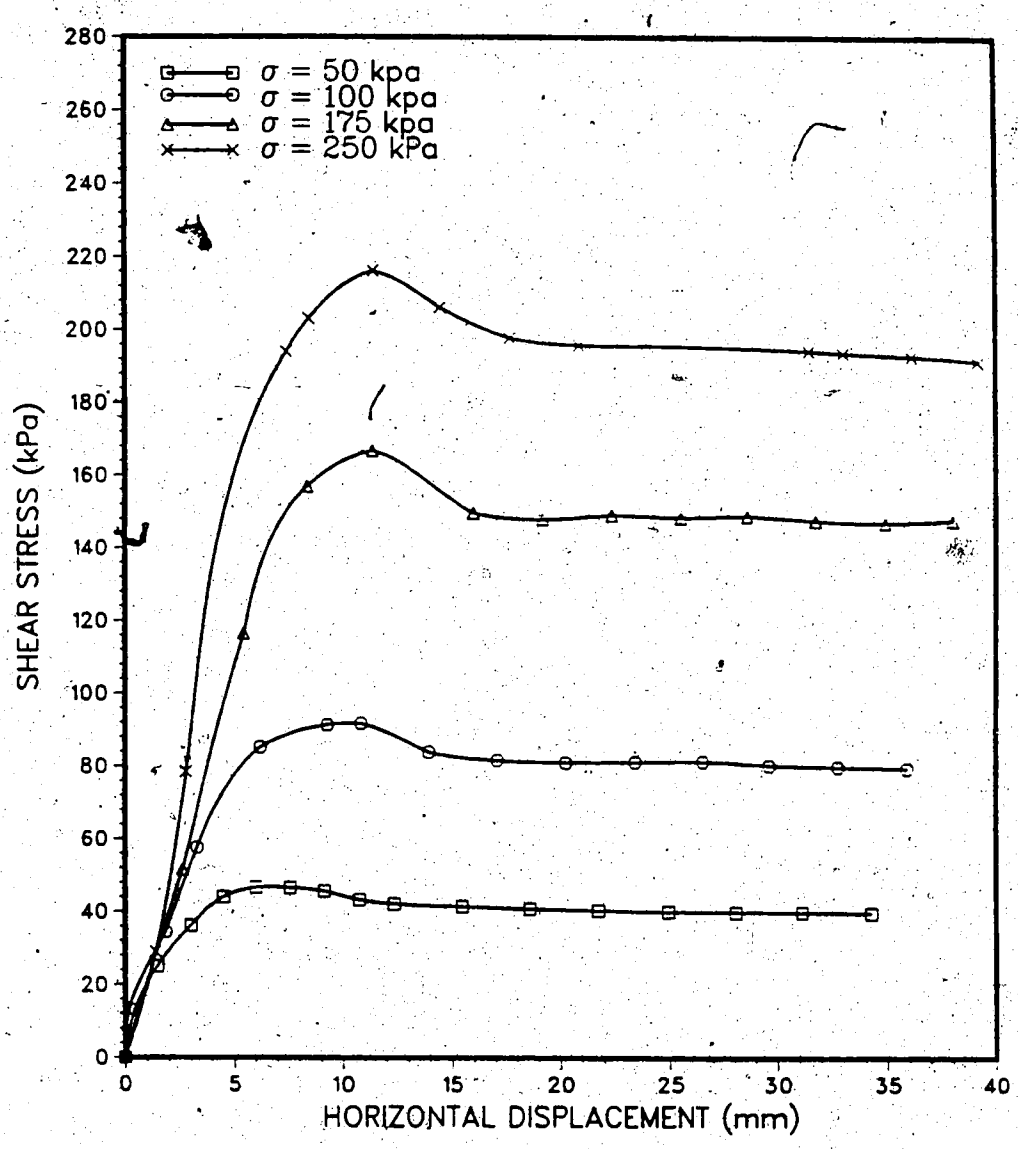
σ = 50 kpa
σ = 100 kpa
σ = 175 kpa
σ = 250 kPa
SHEAR STRESS (kPa)
HORIZONTAL DISPLACEMENT (mm)
0
20
40
60
80
100
120
140
160
180
200
220
240
260
280
0
5
10
15
20
25
30
35
40

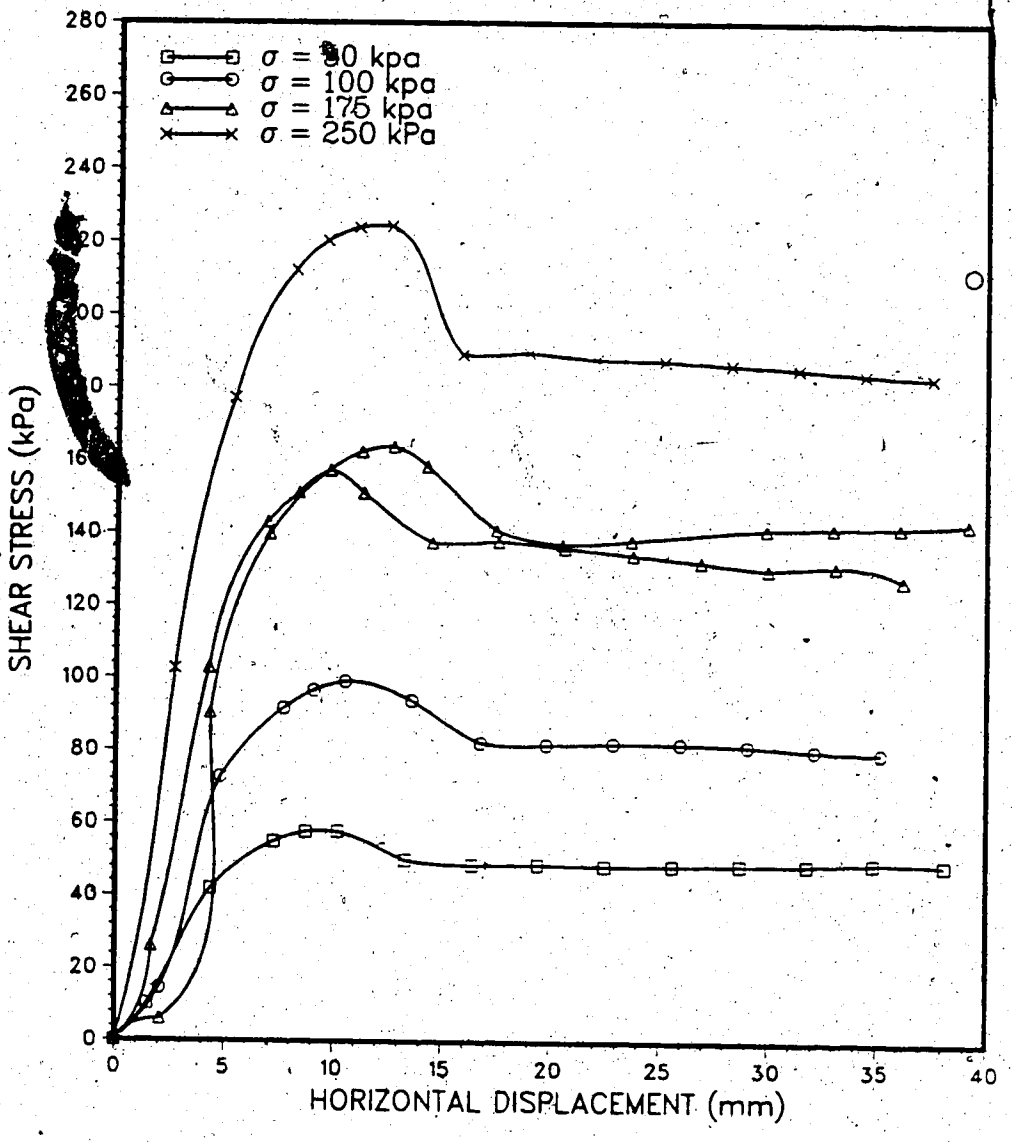
σ = 80 kpa
σ = 100 kpa
σ = 175 kpa
σ = 250 kPa
SHEAR STRESS (kPa)
HORIZONTAL DISPLACEMENT (mm)
0
20
40
60
80
100
120
140
160
240
260
280
0
5
10
15
20
25
30
35
40

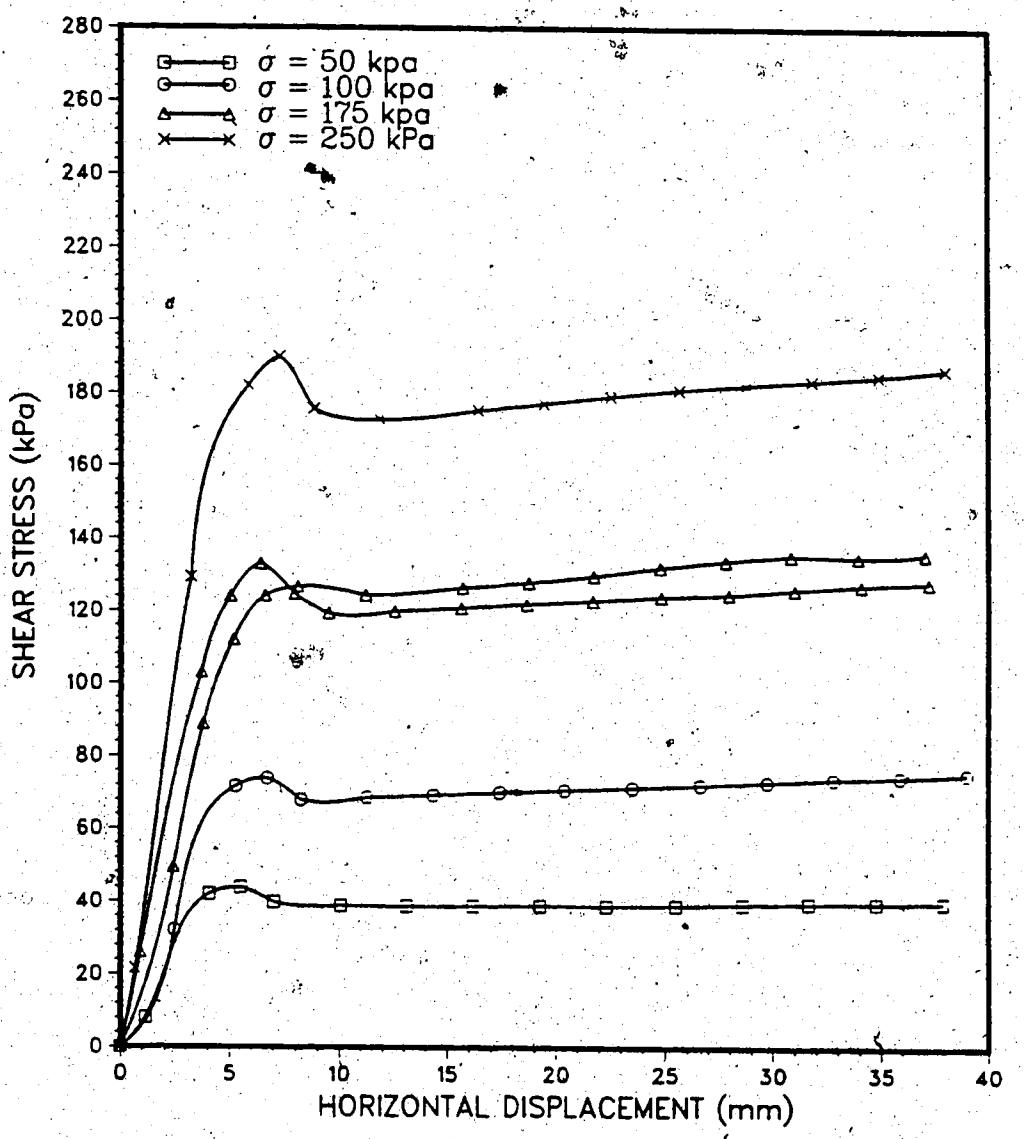
σ = 50 kpa
σ = 100 kpa
σ = 175 kpa
σ = 250 kPa
SHEAR STRESS (kPa)
HORIZONTAL DISPLACEMENT (mm)
0
20
40
60
80
100
120
140
160
180
200
220
240
260
280
0
5
10
15
20
25
30
35
40

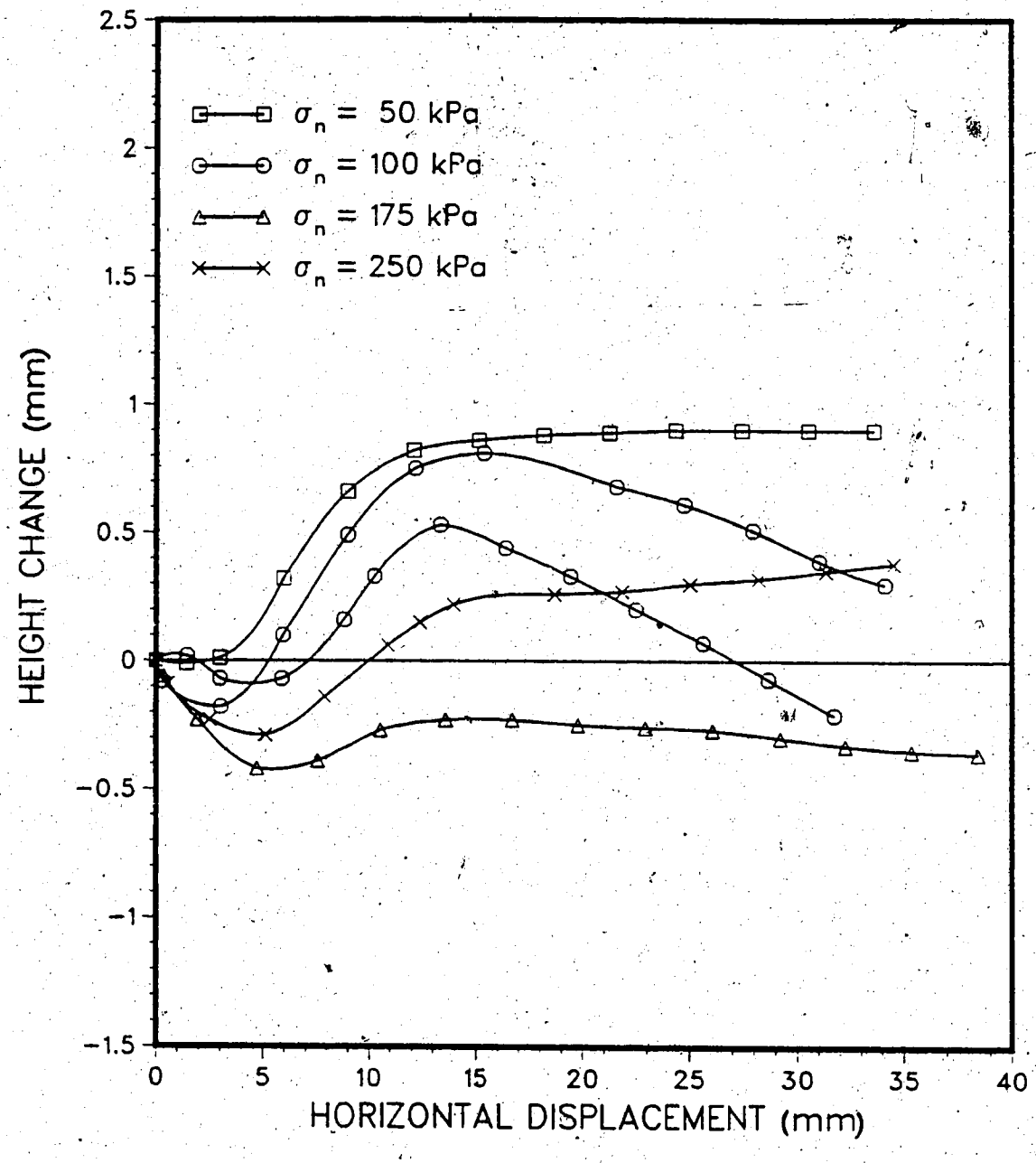
σ_n = 50 kPa
σ_n = 100 kPa
σ_n = 175 kPa
σ_n = 250 kPa
HEIGHT CHANGE (mm)
HORIZONTAL DISPLACEMENT (mm)
2.5
2
1.5
1
0.5
0
−0.5
−1
−1.5
0
5
10
15
20
25
30
35
40

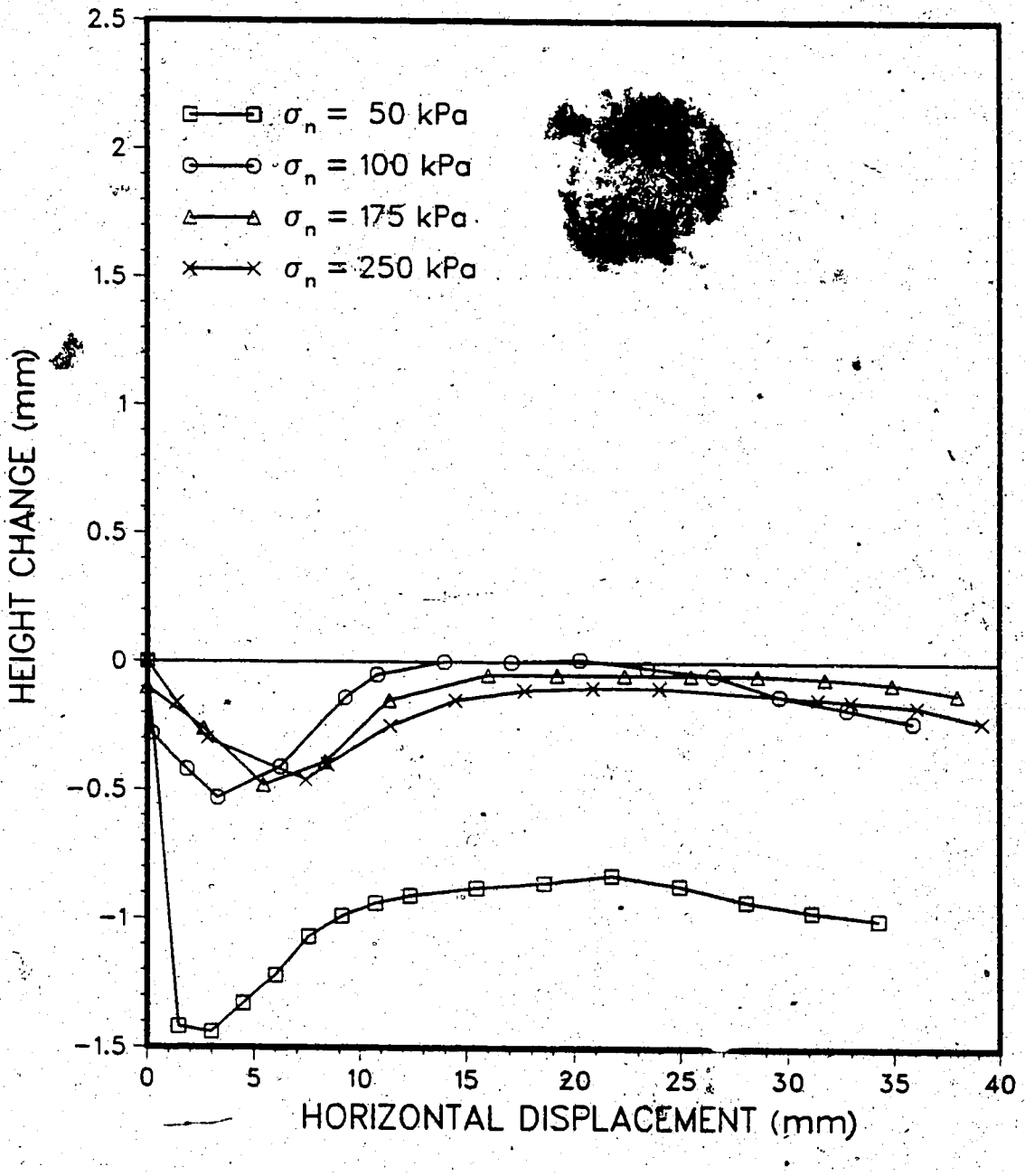
σ_n = 50 kPa
σ_n = 100 kPa
σ_n = 175 kPa
σ_n = 250 kPa
HEIGHT CHANGE (mm)
HORIZONTAL DISPLACEMENT (mm)
2.5
2
1.5
1
0.5
0
−0.5
−1
−1.5
0
5
10
15
20
25
30
35
40

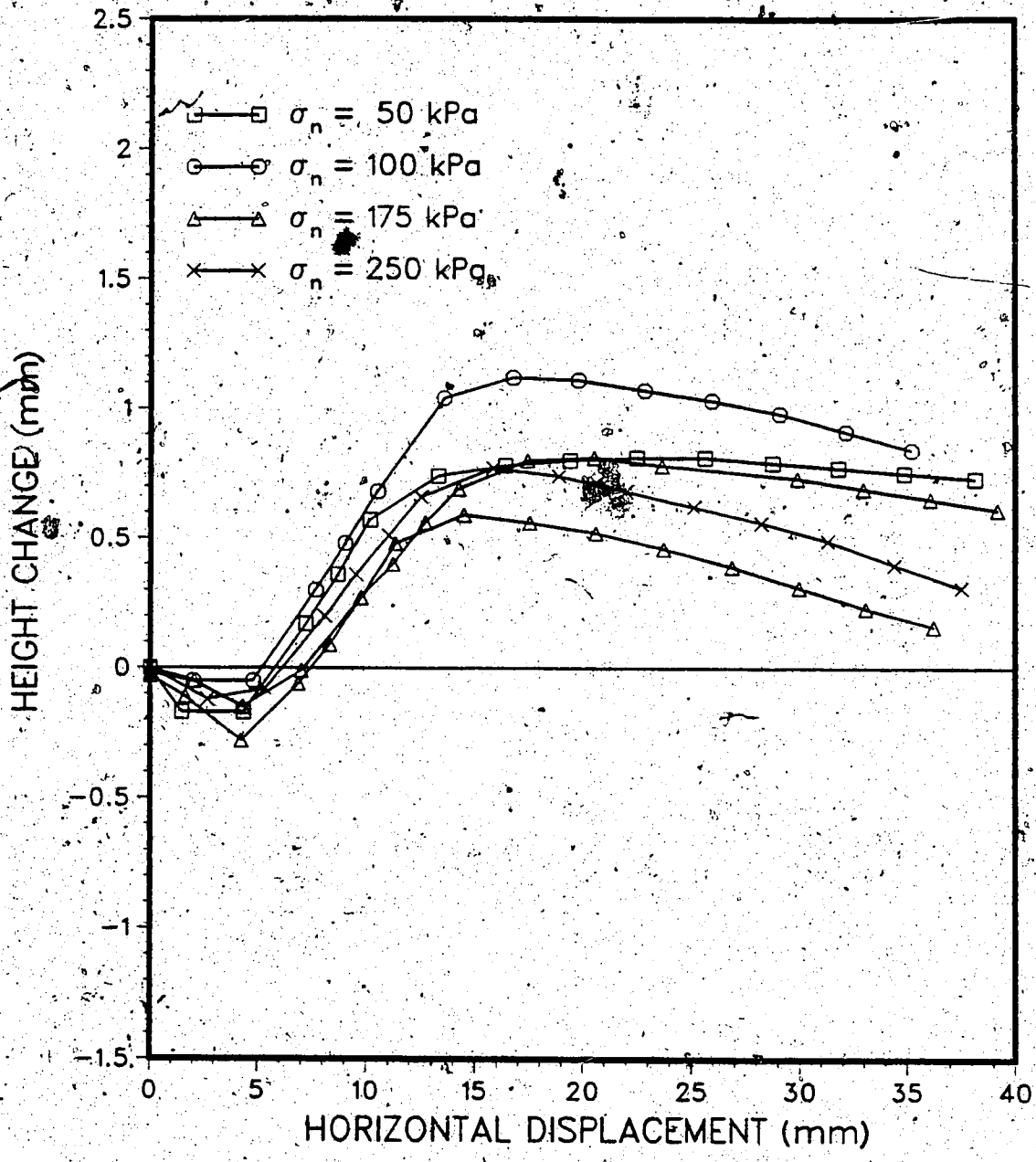

Figure C.7 Horizontal and Vertical Displacement Curves for Sand Reinforced with ParaGrid 50S

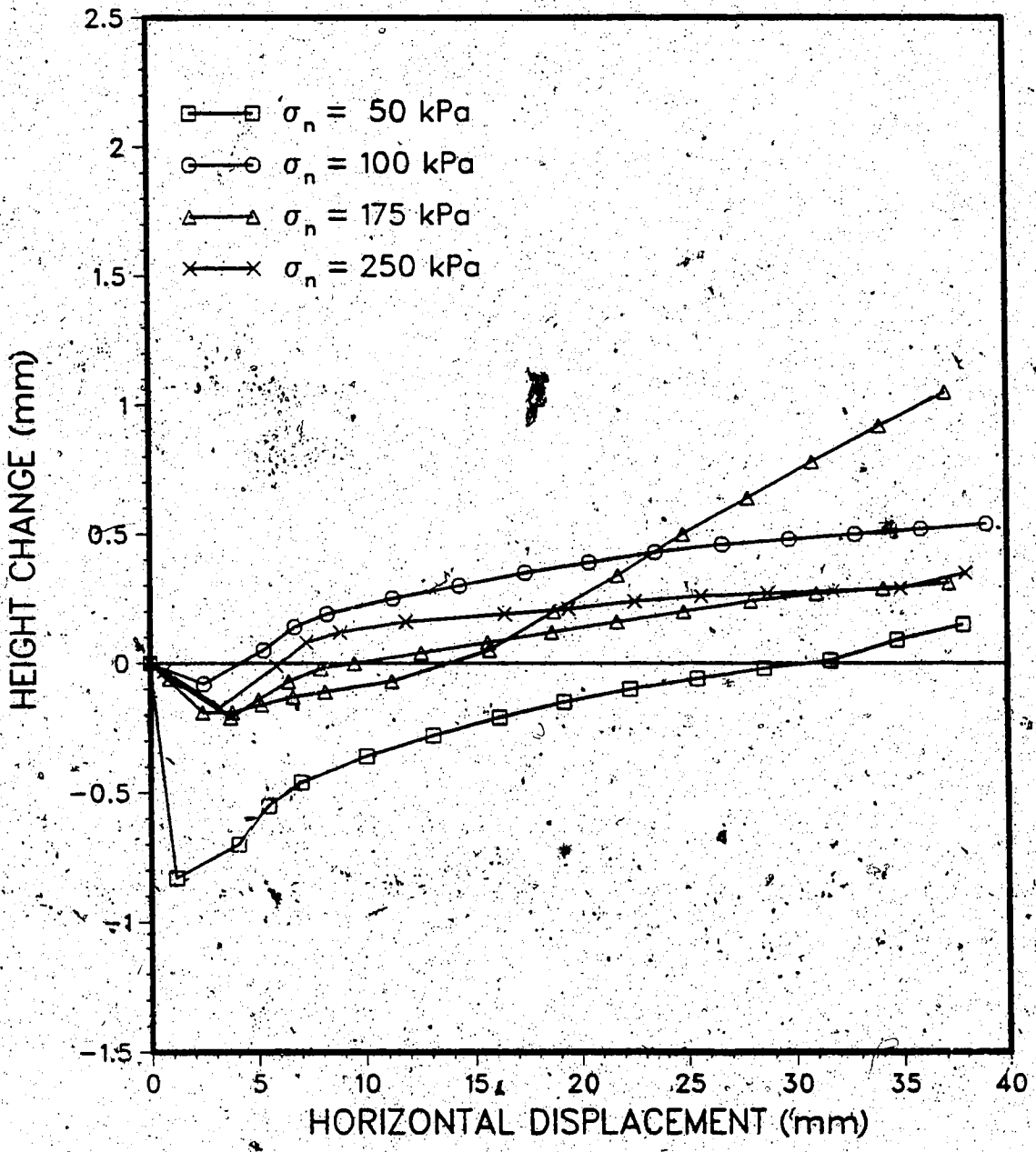

Figure C.8 Horizontal and Vertical Displacement Curves for Sand Reinforced with P600

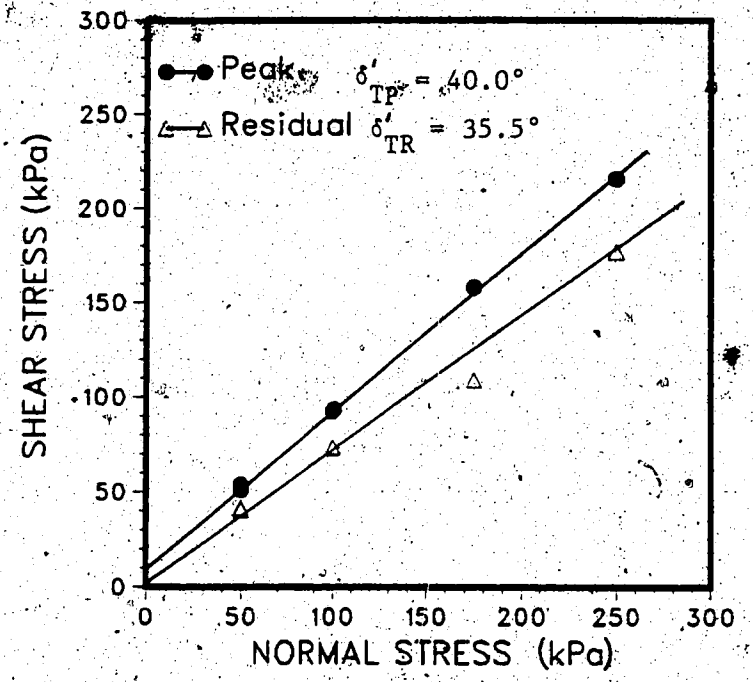

Figure C.9 Peak and Residual Strength Envelopes for Sand Reinforced with SR2

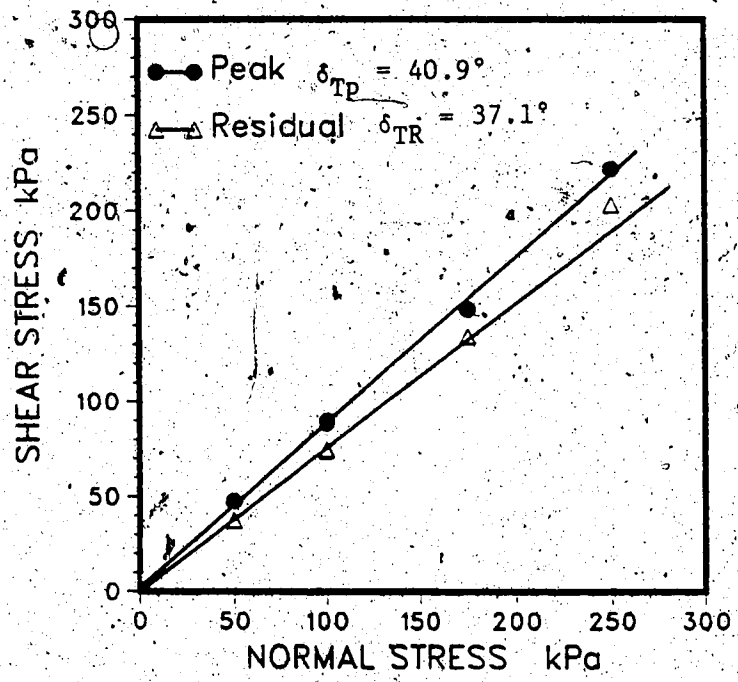

Figure C.10 Peak and Residual Strength Envelopes for Sand Reinforced with SS2

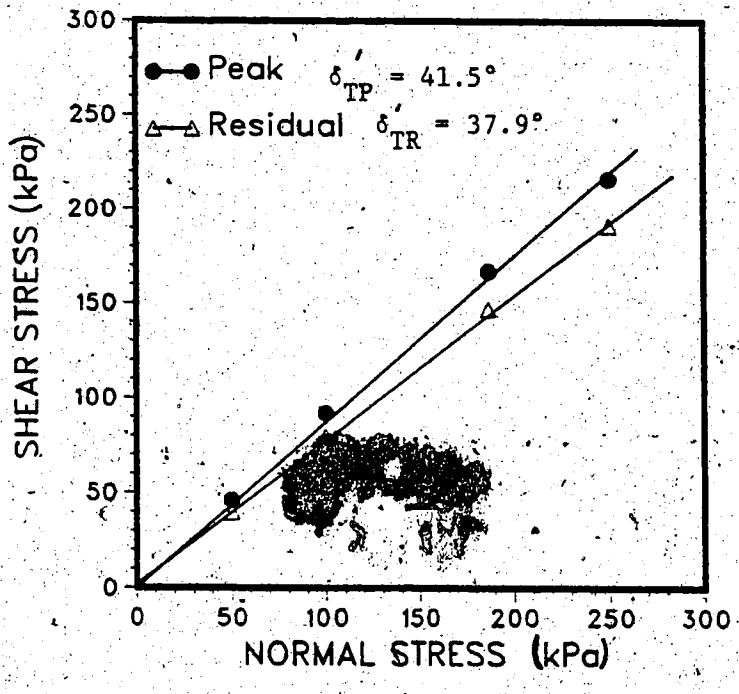

Figure C.11 Peak and Residual Strength Envelopes for Sand Reinforced with TNX-5001

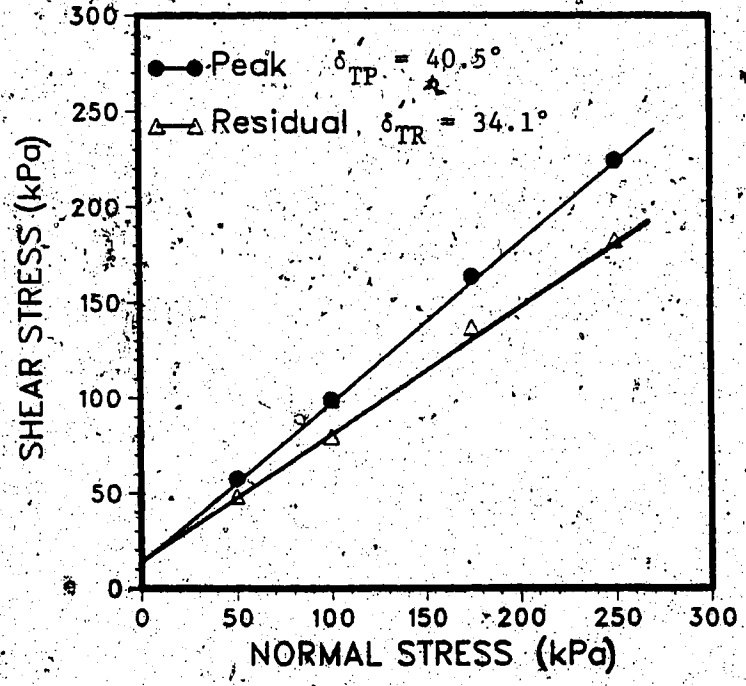

Figure C.12 Peak and Residual Strength Envelopes for Sand Reinforced with ParaGrid 50S

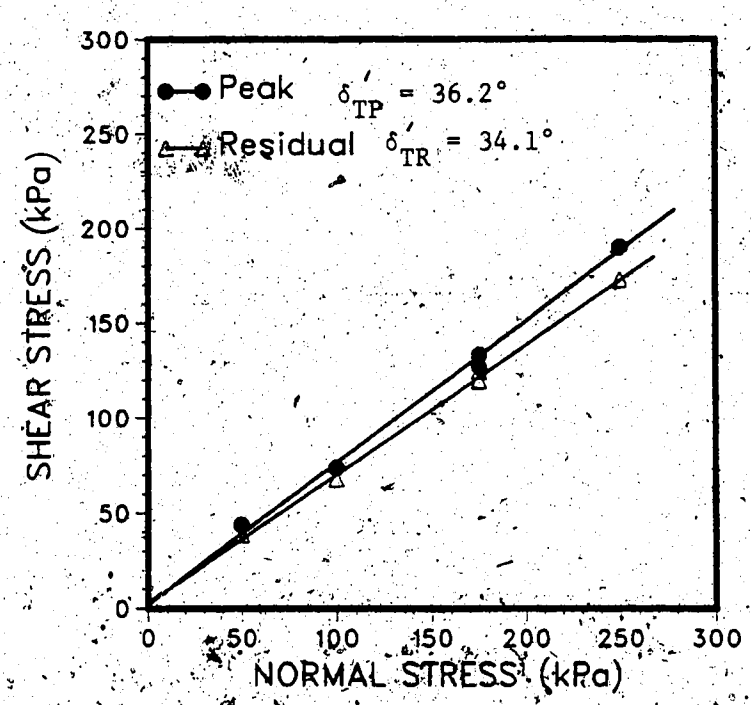

Figure C.13 Peak and Residual Strength Envelopes for Sand Reinforced with P600

APPENDIX D: Reinforced Silty Clay Test Results

Table D.1 Data of Silty Clay

Test No.	1	2	3	4	5	6	7	8	9	10	11	12
Initial												
w %	23.56	23.30	22.90	23.14	23.02	23.57	23.32	23.44	22.69	23.73	24.50	23.92
ρ_w (g/cm^3)	2.17	2.03	2.08	2.08	2.07	2.12	2.09	2.06	2.08	2.08	2.06	2.10
ρ_d (g/cm^3)	1.76	1.65	1.69	1.69	1.68	1.71	1.69	1.67	1.69	1.68	1.66	1.69
e	0.55	0.66	0.61	0.62	0.63	0.59	0.61	0.63	0.61	0.63	0.65	0.61
S (%)	117.0	97.0	102.0	103.0	100.0	108.0	104.0	101.0	97.3	98.70	102.0	103.0
After												
w %	22.89	22.41	22.25	22.34	23.29	22.87	23.05	22.19	22.69	23.73	24.50	23.92
ρ_w (g/cm^3)	2.29	2.16	2.22	2.18	2.13	2.12	2.13	2.19	2.08	2.08	2.06	2.10
ρ_d (g/cm^3)	1.86	1.76	1.81	1.79	1.73	1.73	1.73	1.77	1.69	1.68	1.66	1.69
e	0.46	0.55	0.50	0.53	0.58	0.56	0.58	0.54	0.61	0.63	0.65	0.61
S (%)	135.0	111.0	120.0	115.0	110.0	110.0	109.0	112.0	100.0	103.0	103.0	107.0
Compacted Height (cm)	8.77	10.67	10.11	10.70	10.47	10.23	10.92	11.26	11.08	11.22	11.27	11.16
Δh (mm)	4.62	6.10	6.17	5.02	3.27	-	8.2	6.66	2.00	2.09	1.19	1.75
Normal Stress (kPa)	175.0	175.0	175.0	175.0	100.0	5.8	50.0	250.0	5.8	50.0	5.0	20.0
Maximum Shear Stress (kPa)	114.3	110.7	121.0	114.5	90.8	28.4	63.0	128.0	24.9	61.0	20.4	39.3
Displacement to Peak (mm)	38.9	39.1	34.7	39.0	36.0	8.3	17.6	38.0	6.6	40.8	7.7	6.2
Compression (mm)												
Immediate	2.79	4.61	4.69	3.26	2.39	-	1.84	5.36	-	0.88	1.19	1.18
Consolidation	1.83	1.49	1.49	1.76	0.89	-	0.37	1.30	-	1.21	-	0.57
Cv (10^{-7} m^2/s)	2.1	18.0	110.0	80.0	74.0	-	0.3	2.1	-	0.4	-	2.9
Remarks:												

Table D.2 Data of Silty Clay Reinforced with SR2

Test No.	1	2	3	4	5	6	7	8
Initial								
w %	23.77	23.44	22.36	22.83	23.52	22.06	23.02	22.07
ρ_w (g/cm^3)	2.06	2.06	2.07	2.05	2.08	2.05	2.10	2.05
ρ_d (g/cm^3)	1.67	1.67	1.69	1.67	1.68	1.68	1.71	1.68
e	0.64	0.64	0.61	0.63	0.62	0.63	0.60	0.63
S (%)	101.0	100.0	100.0	98.0	104.0	96.0	106.0	96.0
After								
w %	21.38	22.17	23.70	22.82	22.90	23.50	23.02	23.22
ρ_w (g/cm^3)	2.19	2.18	2.10	2.12	2.15	2.19	2.10	2.10
ρ_d (g/cm^3)	1.81	1.78	1.70	1.73	1.75	1.78	1.70	1.71
e	0.51	0.53	0.61	0.58	0.56	0.54	0.60	0.60
S (%)	114.0	114.0	107.0	107.0	111.0	110.0	106.0	106.0
Compacted Height (cm)	9.45	9.73	9.92	9.86	9.74	9.08	9.63	9.87
Δh (mm)	5.46	5.41	1.44	3.38	3.13	5.70	-	2.40
Normal Stress (kPa)	175.0	250.0	20.0	100.0	50.0	100.0	5.0	20.0
Maximum Shear Stress (kPa)	92.2	103.6	28.4	76.8	47.1	67.4	23.9	33.1
Displacement to Peak (mm)	38.0	36.5	5.0	17.9	10.4	18.6	5.2	4.3
Compression (mm)								
Immediate	4.14	3.42	0.41	2.61	2.29	4.93		2.12
Consolidation	1.33	1.99	1.03	-	0.84	0.77	-	0.28
Cv (10^{-7} m^2/s)	1.6	0.8	9.9	—	3.9	2.8	-	5.0
Remarks:								

Table D.3 Data of Silty Clay Reinforced with SS2

Test No.	1	2	3	4	5
Initial					
w %	23.44	23.62	22.53	22.36	22.84
ρ_w (g/cm^3)	2.09	2.08	2.05	2.07	2.09
ρ_d (g/cm^3)	1.69	1.68	1.67	1.69	1.70
e	0.61	0.62	0.63	0.62	0.61
S (%)	104.0	103.0	97.0	99.0	102.0
After					
w %	21.95	22.35	21.86	22.58	23.03
ρ_w (g/cm^3)	2.24	2.22	2.20	2.13	2.16
ρ_d (g/cm^3)	1.84	1.80	1.81	1.74	1.76
e	0.48	0.50	0.51	0.57	0.55
S (%)	124.0	121.0	117.0	108.0	114.0
Compacted Height (cm)	9.83	9.56	9.02	9.82	9.68
Δ h (mm)	6.93	6.14	6.40	2.98	3.36
Normal Stress (kPa)	175.0	250.0	250.0	100.0	50.0
Maximum Shear Stress (kPa)	104.2	116.2	125.0	87.6	57.8
Displacement to Peak (mm)	41.4	40.9	41.3	40.6	39.6
Compression (mm)					
Immediate	5.74	4.07	4.44	1.66	3.09
Consolidation	1.19	2.07	2.00	1.32	0.27
Cv (10^{-7} m^2/s)	0.9	0.7	0.6	0.9	0.2
Remarks:					

Table D.4 Data of Silty Clay Reinforced with TNX-5001

Test No.	1	2	3	4	5	6
Initial						
w %	23.52	23.17	22.43	23.25	23.41	23.29
ρ_w (g/cm^3)	2.09	2.09	2.08	2.05	2.04	2.04
ρ_d (g/cm^3)	1.69	1.69	1.70	1.67	1.65	1.66
e	0.61	0.62	0.61	0.64	0.65	0.65
S (%)	105.0	103.0	100.0	99.0	98.0	98.0
After						
w %	22.54	21.87	21.17	23.46	22.56	23.23
ρ_w (g/cm^3)	2.13	2.18	2.14	2.09	2.22	2.14
ρ_d (g/cm^3)	1.74	1.79	1.77	1.69	1.82	1.73
e	0.57	0.53	0.55	0.61	0.51	0.57
S (%)	108.0	113.0	106.0	104.0	122.0	110.0
Compacted Height (cm)	9.79	9.72	9.78	9.87	9.11	9.06
Δh (mm)	4.63	4.12	2.31	1.89	7.37	6.74
Normal Stress (kPa)	175.0	250.0	100.0	50.0	250.0	250.0
Maximum Shear Stress (kPa)	96.5	114.5	78.9	57.2	118.0	98.5
Displacement to Peak (mm)	37.2	39.1	17.5	21.5	42.5	36.3
Compression (mm)						
Immediate	3.19	2.57	2.31	1.07	5.39	3.98
Consolidation	1.44	1.55	0.53	0.82	1.98	2.76
Cv (10^{-7} m^2/s)	2.2	3.3	1.3	1.3	3.3	4.1
Remarks:						

Table D.5 Data of Silty Clay Reinforced with ParaGrid 50S

Test No.	1	2	3	4
Initial				
w %	24.03	23.72	24.43	24.17
ρ_w (g/cm^3)	2.02	2.05	2.05	2.03
ρ_d (g/cm^3)	1.63	1.66	1.65	1.64
e	0.68	0.65	0.66	0.67
S (%)	97.0	100.0	102.0	99.0
After				
w %	21.30	23.35	23.98	23.75
ρ_w (g/cm^3)	2.06	2.19	2.13	2.07
ρ_d (g/cm^3)	1.70	1.78	1.71	1.67
e	0.62	0.54	0.59	0.63
S (%)	93.0	119.0	111.0	103.0
Compacted Height (cm)	9.63	9.55	9.71	9.80
Δh (mm)	3.84	6.05	3.55	1.84
Normal Stress (kPa)	175.0	250.0	100.0	50.0
Maximum Shear Stress (kPa)	98.7	109.3	83.8	63.1
Displacement to Peak (mm)	37.5	38.5	37.7	19.8
Compression (mm)				
Immediate	2.13	3.62	2.54	1.40
Consolidation	1.71	2.44	1.01	0.44
Cv (10^{-7} m^2/s)	0.3	0.4	1.7	2.4
Remarks:				

Table D.6 Data of Silty Clay Reinforced with P600

Test No.	1	2	3	4	5
Initial					
w %	22.76	22.72	22.60	23.95	23.77
ρ_w (g/cm^3)	2.06	2.11	2.04	2.06	2.06
ρ_d (g/cm^3)	1.68	2.11	2.04	2.06	2.06
e	0.62	0.59	0.64	0.64	0.64
S (%)	100.0	105.0	97.0	102.0	101.0
After					
w %	22.36	22.18	22.87	22.02	24.25
ρ_w (g/cm^3)	2.14	2.23	2.09	2.16	2.10
ρ_d (g/cm^3)	1.75	1.82	1.70	1.77	1.69
e	0.56	0.50	0.60	0.54	0.61
S (%)	109.0	121.0	103.0	111.0	108.0
Compacted Height (cm)	9.76	9.60	9.96	9.80	9.77
Δ h (mm)	3.62	5.02	2.67	7.13	1.94
Normal Stress (kPa)	175.0	250.0	100.0	250.0	50.0
Maximum Shear Stress (kPa)	113.6	132.1	81.3	116.2	48.0
Displacement to Peak (mm)	40.8	40.2	29.6	38.4	23.7
Compression (mm)					
Immediate	2.46	2.88	1.89	4.43	0.89
Consolidation	1.17	2.14	0.78	2.70	1.05
Cv (10^{-7} m^2/s)	0.9	1.1	1.5	0.8	3.3
Remarks::					

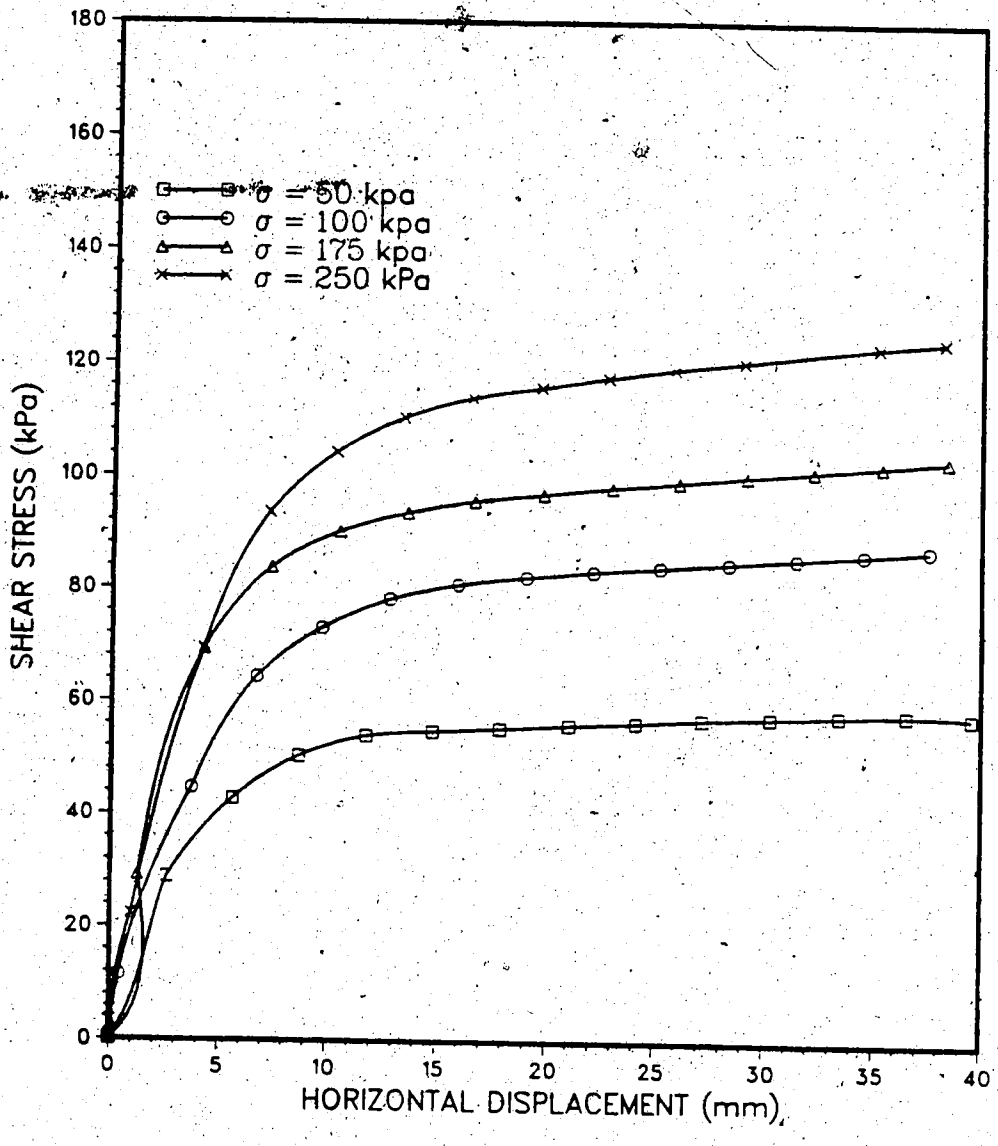

Figure D.1 Shear Stress-Deformation Curves for Clay Reinforced with SS2

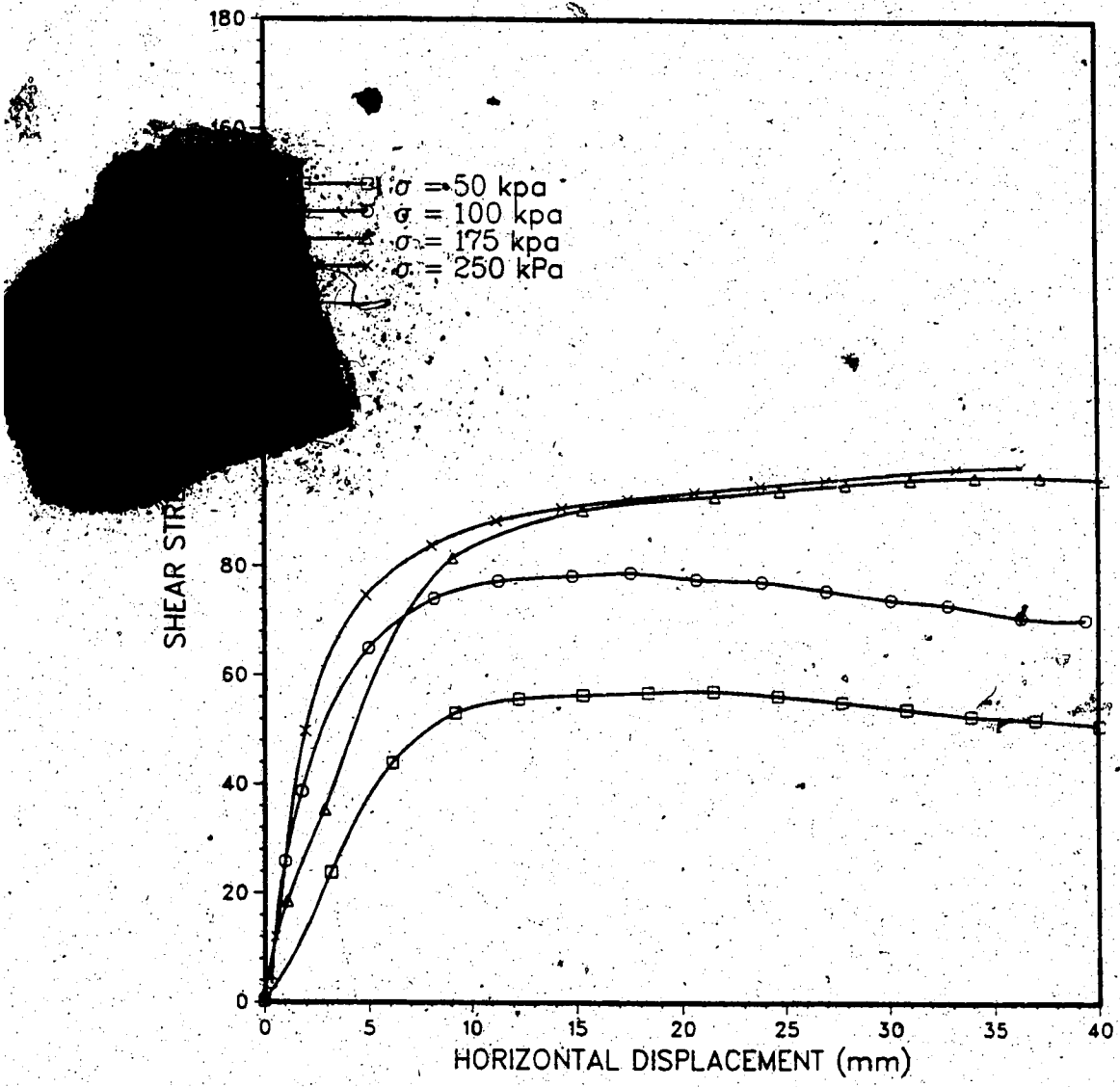

Figure D.2 Shear Stress-Deformation Curves for Clay Reinforced with TNX-5001

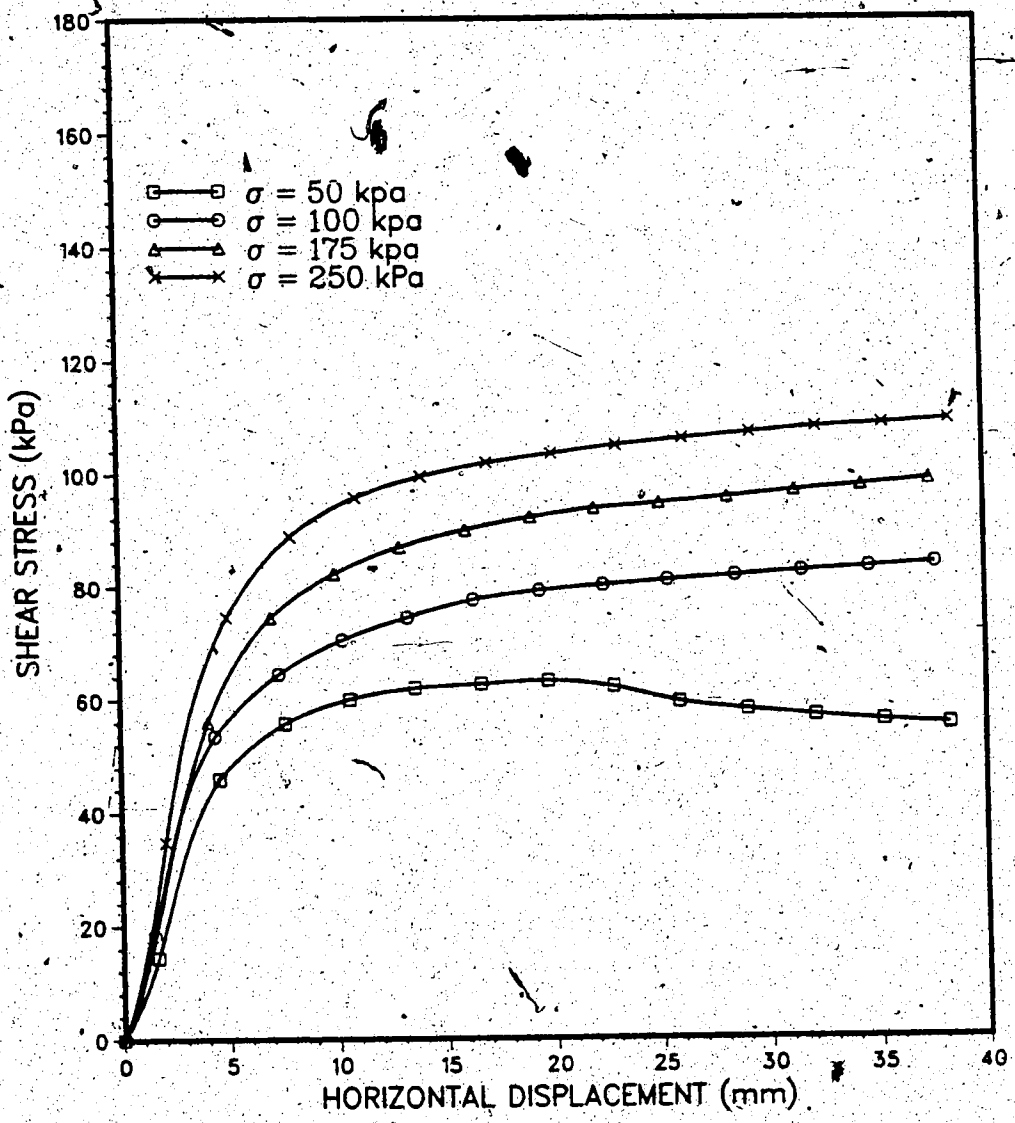

Figure D.3 Shear Stress-Deformation Curves for Clay Reinforced with ParaGrid 50S

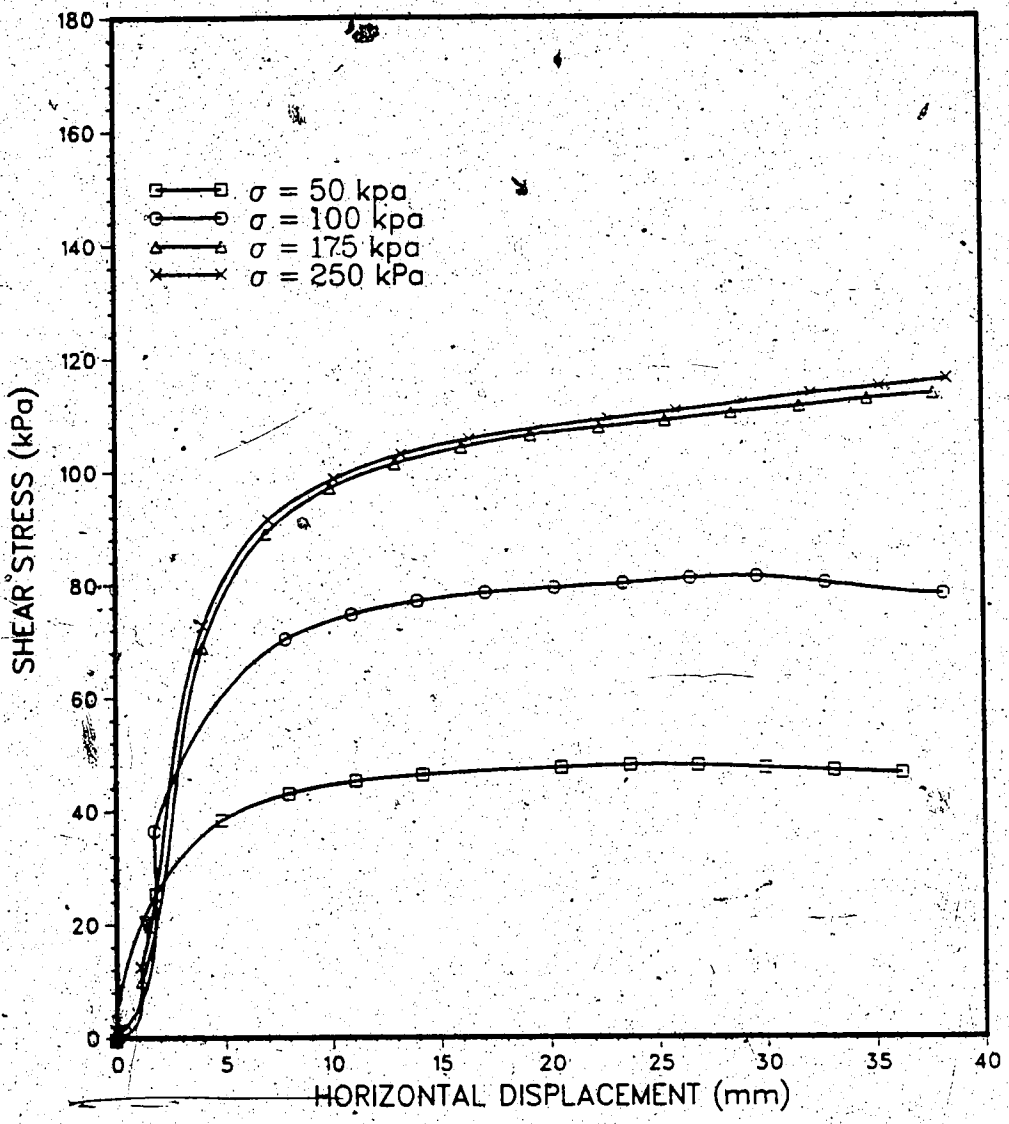

Figure D.4 Shear Stress-Deformation Curves for Clay Reinforced with P600

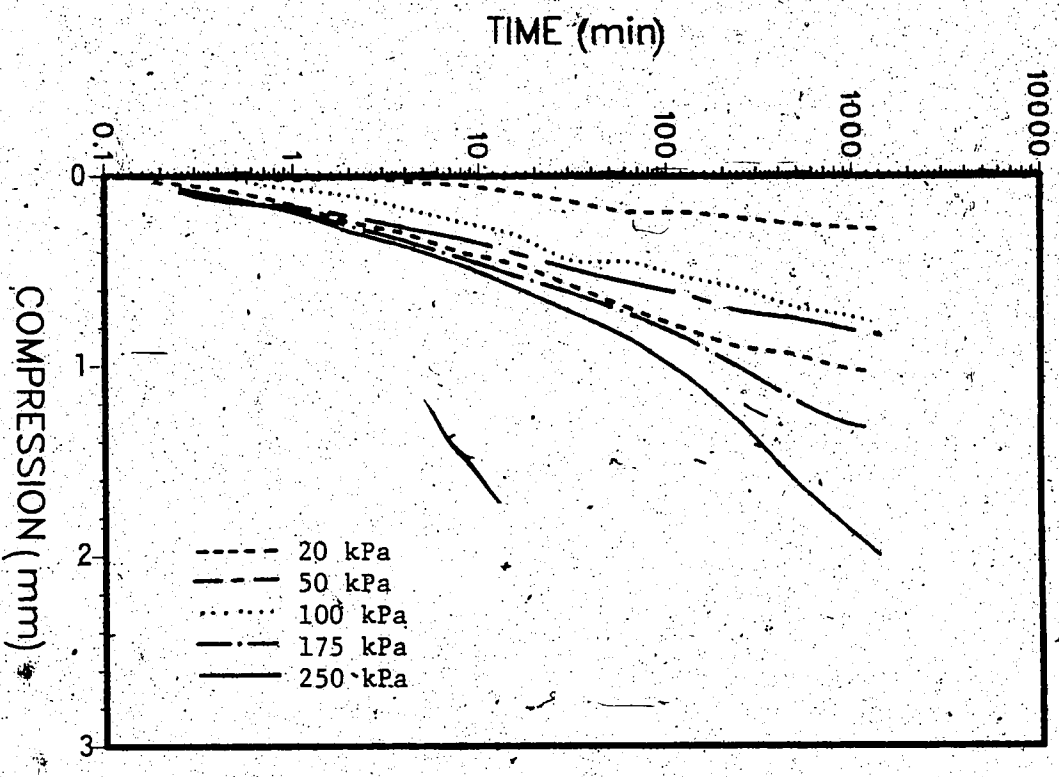

Figure D.5 Consolidation Curves for Clay Reinforced with SR2

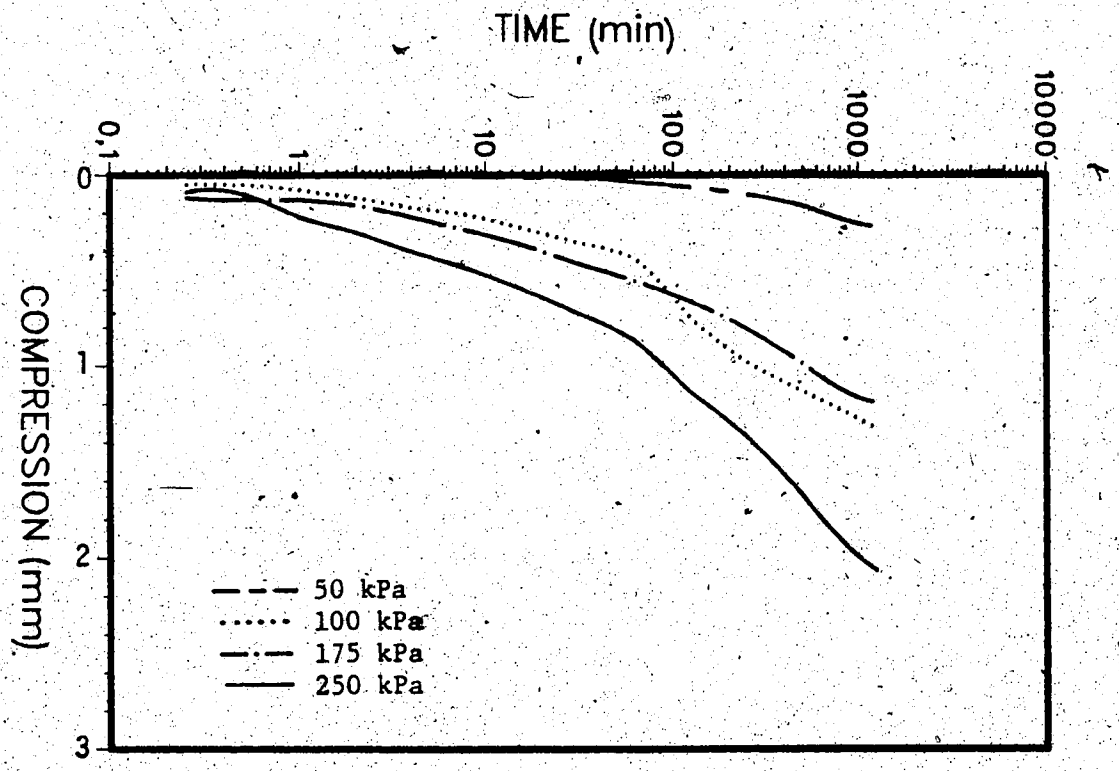

Figure D.6 Consolidation Curves for Clay Reinforced with SS2

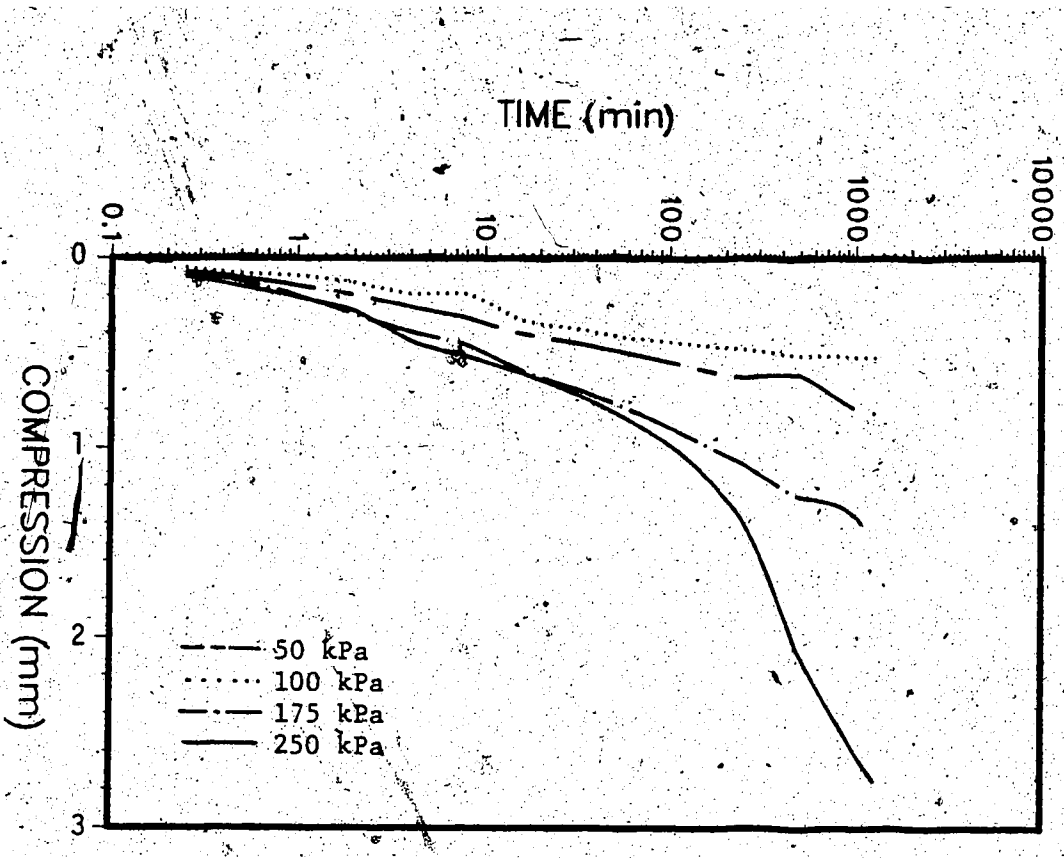

Figure D.7 Consolidation Curves for Clay Reinforced with TNX-500.1

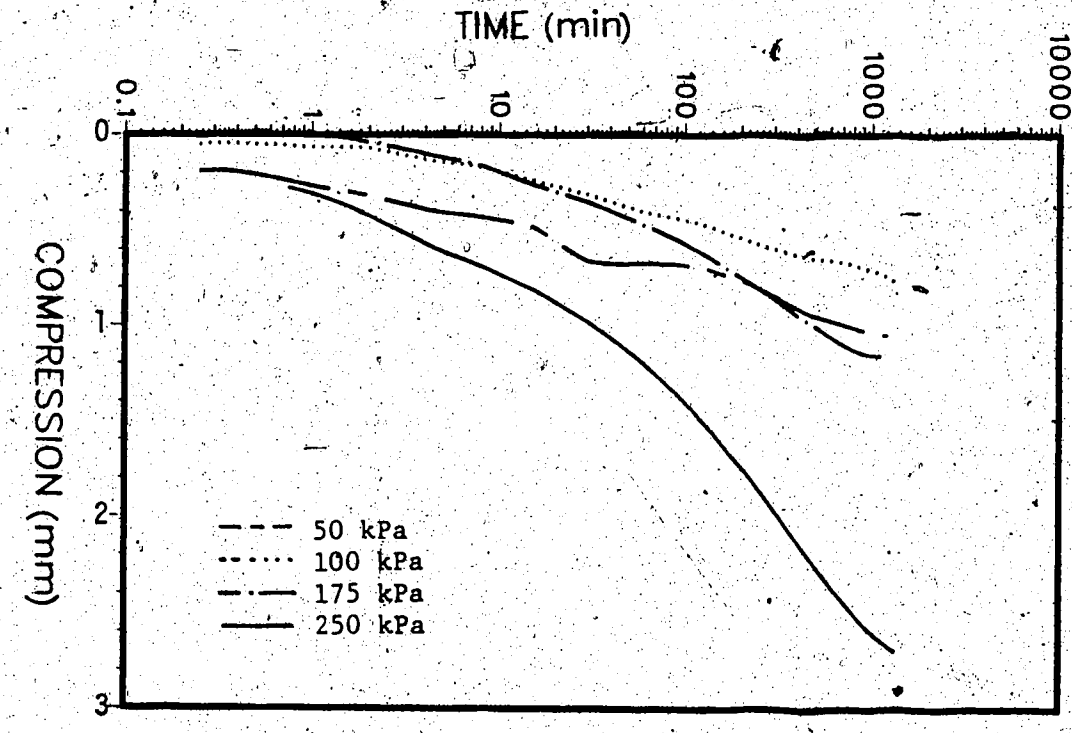

Figure D.8 Consolidation Curves for Clay Reinforced with P600